The Heat Treatment of Medium Carbon Steels in the Ferrite plus Austenite Range

A Thesis submitted for the degree of

Doctor of Philosophy

in the

University of London

by

Saeed Saboury-Sichani
M.Sc., DIC

Department of Metallurgy and Materials Science
Royal School of Mines
Imperial College of Science and Technology
London SW7

March 1983

Abstract

An investigation is reported of the application of intercritical (i.e. within the ferrite+austenite range) heat treatments to two grades of medium carbon commercial steels, namely En24 and En8, with the aim of identifying the optimum heat treatment parameters to obtain maximum resistance to crack propagation.

Studies involving structural observations and hardness measurements have been made of the kinetics and mechanisms of austenite formation within the critical range. Austenite formation occurs very rapidly, leading to high hardness values on quenching to produce martensite. An important feature is the formation of lamellar aggregates of ferrite+austenite with associated high areas of interphase boundaries.

En24 and En8 Charpy specimens were conventionally austenitized at 835°C and 850°C respectively; they were then given intercritical treatments involving furnace heating to 735, 750 and 765°C, and holding for 30 minutes followed by oil quenching. After these treatments, specimens were tempered at various temperatures up to ~650°C. Charpy tests were made at room temperature. For En24 steel, intercritically heated at 765°C and then tempered to hardness values between 450 and 550Hv an improved combination of strength and toughness was achieved. This improvement is associated with a decreased susceptibility to intergranular decohesion (temper embrittlement). At hardness levels less than 450Hv, the intercritically heat treated material exhibits similar toughness to the conventionally heat treated material. In the case of En8 steel, no enhancement was achieved in the combined mechanical properties as a result of intercritical treatment.

Contents

List of Tables

List of Plates

List of Figures

Chapter 1

Introduction

Steels are generally heat treated in one of two ways, by austenitizing followed by quenching and tempering or by slow cooling. There are indications from published research that enhancement of properties, particularly fracture toughness, might be substantially improved by the application of novel heat treatment procedures such as quenching from within the (α + γ) range. This approach involving the ferrite plus martensite structures has been studied to a relatively small extent in medium carbon steels, e.g. Ref.1; however, the low carbon steels have been the subject of extensive work during the last decade, e.g. Ref.117.

The main factors contributing to the properties of two phase structures are considered to be morphology, properties and volume fraction of phases. From the Fe-C equilibrium phase diagram, it is evident that when an iron-carbon alloy is held at a temperature between A_1 and A_3, the alloy will separate into austenite with a high carbon content and ferrite containing very little carbon. The carbon concentration in each phase decreases and the volume fraction of the γ-phase increases as the "intercritical" annealing temperature is increased. Upon cooling, the austenite transformation products depend on its composition and the rate of cooling. If austenite contains only carbon and is water quenched, it transforms to dislocated and/or twinned martensite depending on its carbon content.

Over thirty years ago, Nehrenberg studied the formation and growth of austenite in the two phase (α + γ) region in steels [1]. According to his work, when a 0.25% C-Mn-Si-Ni-Mo steel in the spheroidized condition was heated above the Ae_1 temperature, the newly formed austenite did not envelop the carbide particles and grow in an equiaxed fashion, but instead acicular shaped grains of austenite were formed; also the "excess" ferrite present after heating between A_1 and A_3 was acicular in form, thus giving a lamellar nature to the microstructure. Detailed studies were made by light microscopy of a number of steels including '4340' (close in composition to En24). The results obtained showed that the morphology of austenite formed from spheroidized ferrite+carbide structures depended on the route by which the spheroidized structure had been produced. When the spheroidization had been achieved by a process involving isothermal transformation of austenite, then on subsequent heating above A_1, the austenite morphology that developed was essentially equiaxed and the ferrite was "blocky". In contrast, when the spheroidization had been produced by the tempering of martensite, the austenite and ferrite morphologies obtained on heating above A_1 were acicular, giving an overall lamellar structure. The acicular/lamellar structures were also produced when the prior structures were martensite (or tempered martensite) or bainite. These features were observed for compositions ranging from hypo- to hyper-eutectoid and

covering both plain carbon and alloy steels. The effects were explained by the fact that the austenite growth, in its early stages, is confined within the boundaries of the ferrite grains. Thus, when the initial ferrite grains are equiaxed, as in structures produced by a high temperature transformation, then the austenite grains are equiaxed. In the martensitic (or tempered martensitic) or bainitic structures the acicular ferrite structures lead to acicular austenite grains.

The "dual-phase" steels produced by annealing of low carbon steels in the ferrite+austenite range are important in sheet form for their combination of high strength and formability. The microstructure of these steels consists of small isolated islands of martensite distributed in a fine-grained ferrite matrix. The volume fraction of islands of martensite is usually between 10 and 30 percent [117].

Considering mechanical properties of dual-phase steels, Marder [118] found a linear relationship between the amount of martensite and both tensile strength and uniform elongation in a 0.1%C, 1.5%Mn, 0.2%Mo, 0.1%V steel for martensite volume fractions up to 65 percent . No microcracking was observed in spite of the previous work predicting microcracking of martensite above 0.2 volume fraction, and fracture in tension was observed to be caused by void formation at small inclusions or at ferrite/martensite interfaces. In an earlier investigation on the mechanical properties of steels containing 0.06-0.52 percent carbon and 1.5 percent manganese, Davies [119] found that the strength of a dual-phase structure was dependent on the ferrite grain size and the volume fraction of martensite and was independent of the composition and strength of martensite. Extrapolating the 0.2 percent flow stress of specimens containing varying amounts of martensite to 100 percent martensite, gave a strength indicative of a 0.4 percent carbon martensite tested in tension. Upon this basis Davies suggested the possibility of autotempering in the higher carbon martensite so that only 0.4 carbon remained in solution independent of the initial carbon content of the austenite. Another possibility considered was that martensite had a lower strength when formed in a relatively soft ferrite matrix than that obtained upon quenching a fully austenitic structure.

Relating the properties to the microstructure in dual-phase steels, it is believed that a fine fibrous martensite, on the one hand, offers more effective barriers to the motion of dislocations and simultaneously, on the other hand, provides more efficient composite strengthening for a fixed volume fraction of martensite [108]. The poor elongation ductility of the coarse dual-phase structures, obtained by direct quenching of an Fe, 0.1%C, 2%Si from the γ region into the two phase ($\alpha + \gamma$) range, was attributed to the initiation of cleavage cracks in the ferrite phase where maximum localised stress concentration took place [106]. In the finer fibrous or globular structures, however, fracture occurred by void nucleation and coalescence after large amounts of plastic deformation, which resulted in a significant improvement in elongation ductility without much sacrifice in strength. This study showed that direct quenching of austenite into the two

phase range, resulted in the nucleation and growth of ferrite at the prior austenite grain boundaries and into the austenite respectively. The resulting structure thus depended on the austenite grain size and after quenching, a relatively coarse equiaxed martensite surrounded by ferrite was produced. Alternatively, if a hypoeutectoid ferrite-pearlite mixture was heated directly to the two phase region, austenite nucleated at the carbide/ferrite interfaces and formed as fine globular grains along the ferrite boundaries.

Regarding the structure of martensite produced as a result of quenching ($\alpha + \gamma$) structures, it was suggested that the carbon content at which the martensite substructure changes from dislocated lath to twinned plate can be higher than the limit known for that in fully martensitic structures (i.e ~0.4 pct C), because transformation strains can be accommodated by slip in the surrounding ferrite [122].

Wada and Doane [116] reported an investigation of the influence of intercritical heat treatment on the temper embrittlement of a steel containing 0.25C, 3.5Ni, 1.7Cr, 0.5Mo, 0.1V (wt%) with deliberate additions of P, Sn or Sb. Martensitic and bainitic samples were heated to an intercritical temperature of 750°C (about 60°C below A_3) for times up to 40 hours and were then cooled to give either martensitic or bainitic structures. The samples were tempered to produce the desired hardness, followed by water quenching or a step cooling sequence. Embrittlement induced by step cooling after final tempering was significantly reduced by the intercritical treatment as compared to the embrittlement associated with conventional heat treatment.

In spite of an enormous amount of work published on the heat treatment of low carbon steels in the ferrite+austenite range in recent years [117-122], relatively few papers appear to have been published on the intercritical heat treatment of medium carbon steels. In the present investigation the effect of such treatments was studied on the structure and mechanical properties of two grades of medium carbon commercial steels, namely En8 and En24. The initial condition prior to intercritical annealing was either as-quenched or quenched-and-tempered. Both grades of steels were annealed at different intercritical temperatures with 15°C intervals for various times followed by quenching into oil or water. Through employing different heating media and specimens of varying dimensions, the effect of heating rate to intercritical range was investigated. After quenching the intercritically treated material, Charpy specimens were tempered at temperatures ranging from 100 to 650°C with 50°C intervals followed by water quenching. Based on similar hardness levels between 450 and 550Hv, En24 steel intercritically heat treated at 765°C, showed an enhanced resistance to fracture at room temperature as compared to the conventionally treated material. The improvement in toughness was observed to be associated with a reduced susceptibility to tempered martensite embrittlement as a consequence of the intercritical treatment.

Chapter 2

Previous Work

2.1 Formation of austenite

Formation of the face-centered cubic solid solution of carbon in γ iron (austenite) has been the subject of extensive work and a comprehensive survey has been presented by Paxton [9]. However, the works concerning the partial transformation of medium carbon steels in the ($\alpha + \gamma$) region are relatively limited.

A significant paper on austenite growth was published by Nehrenberg [1] in 1950 with the aim of determining the conditions responsible for the mode of austenite growth as a result of up-quenching ferrite-carbide aggregates. Nehrenberg found that a relationship existed between the prior structure and the manner in which austenite grew during heating above the Ae_1 temperature. When the prior structure produced by a high temperature transformation was pearlite or spheroidite, the austenite grew in an equiaxed manner and if partially transformed, the excess ferrite was blocky. On the other hand, when the prior structure was martensite, tempered martensite or bainite, the austenite which formed was acicular in shape and in the case of partial transformation, a lamellar pattern consisting of acicular grains of austenite and ferrite was produced. According to Nehrenberg the relationship between the prior structure and the way in which austenite grew, was independent of the composition of steel and was found to hold for steels in general. He concluded that austenite nucleation occurred at ferrite-ferrite boundaries, probably at points where carbides were located, but the subsequent growth of austenite bore no relation to the shape or distribution of carbides. The new austenite did not grow freely in a symmetrical manner around carbides, as assumed in Bain's work [2], but was confined within the boundaries of the ferrite grain in which it happened to start its growth. Nehrenberg suggested that the preferential growth of austenite in some of the ferrite grains during the early stages of formation, might be due to the difference in crystallographic orientation between the grains. One orientation of ferrite might have been more favourable for the growth of austenite than another and the new austenite assumed the shape of the acicular ferrite grains in which its growth started.

According to Baeyertz [3] and Kula and Cohen [4], acicular austenite grains formed in the Ae_1 - Ae_3 range, can be stabilized at higher temperatures within this range, by preventing the migration of ferrite lath boundaries. This can be achieved by precipitating relatively large carbide particles on these boundaries.

The influence of the initial structure on the rate of formation of austenite was studied by Roberts and Mehl [5]. According to these authors, the transformation occurred more rapidly when the starting structure was finer. Hultgren [6] in 1929 demonstrated the presence of concentration gradients remaining in the austenite after the carbide particles had been dissolved. He showed that as a result of heating ferrite-carbide aggregates above Ae_1, the transformation of the matrix to austenite occurred rapidly whereas the dissolution of carbides in the austenite proceeded very sluggishly. He suggested that the low rate of dissolution might be caused by the presence of alloying elements, in particular those elements that associated mainly with cementite, as these would have to diffuse into the austenite as the cementite dissolved. He showed that elements originally segregated to cementite, were still located close to the same position after dissolution of the cementite. Hillert [7] developed the idea by pointing out that a growing austenite phase would inherit the alloy content of the matrix while it was still in metastable chemical equilibrium with the matrix at the interface. This was said to be accomplished by the presence of a local change in alloy content in the matrix just ahead of the growing phase.

Molinder [8] studied the formation of austenite and solution of cementite in a 1.27 pct C, 0.19 pct Cr steel at different temperatures above Ae_1. His starting structure was ferrite with rounded grains of cementite, i.e. soft-annealed. By studying the progressive increase in the carbon content of austenite as a function of time, Molinder came to the conclusion that the determining factor in the rate of cementite dissolution was not the carbon diffusion rate in the austenite but the *disintegration* speed of cementite. In his presentation, Molinder divided the course of transformation into three periods:

a- Formation of embryos for austenite nuclei
b- Transformation of ferrite to austenite with rapid dissolution of cementite
c- Further slow dissolution of cementite with approach to equilibrium.

During the first period, it was suggested that the carbon content of the ferrite in contact with cementite approached the equilibrium content for each temperature. This period was said to be so quickly completed that it was not possible to observe it directly at the higher temperatures. During the second period, the formation of austenite started from cementite particles. The austenite which formed first contained a low carbon content which increased with the time as the amount of austenite also increased. This period terminated when the last part of the ferrite disappeared. According to Molinder's results, the duration of the second period decreased as the transformation temperature increased, (Table 2.1). This longer transformation time at the lower temperatures produced a closer to equilibrium condition at the termination of the second period for both the carbon content of austenite and the volume percent of undissolved cementite particles. Table 2.1 compares the equilibrium values for the above variants

with those reported by Molinder, at the end of the second period, for different temperatures. The noticeable fact in Table 2.1 was that at the end of the second period the carbon content of austenite was ~ 0.6 pct and was independent of the transformation time and temperature.

Temperature °C	Time to complete 2nd period's	Volume % of phases at the end of 2nd period		Austenite Carbon Content %		Vol% Cementite	
		α	γ	End of 2nd period	Equilibrium	End of 2nd period	Equilibrium
750	1000	0	88	0.60	0.67	12	9.8
775	30	0	88	0.57	0.73	12	9.0
800	1	0	88.5	0.60	0.80	11.5	8.2
850	0.3	0	88	0.58	0.93	12	6.2

Table 2.1- Extracted from Molinder's results [8]

In the final period, a gradual dissolution of carbide in the austenite took place and after a relatively long time the carbon content of the austenite approached the equilibrium value. The rate of carbide dissolution in this period was observed to be much lower than that in the second period and it took, for example, 10^5s for the process to approach equilibrium at 750°C. From thermodynamic considerations, Molinder concluded that the rate controlling step for the dissolution of cementite was not the rate of carbon diffusion in austenite, but probably a factor termed *the rate of disintegration* of cementite. His calculation implied that before equilibrium was attained, the rate of disintegration of cementite was insufficient to maintain the equilibrium carbon content of austenite at the phase boundaries (interface controlled process).

Subsequent works have disputed Molinder's interpretation, since the effect of Cr content on the rate of carbon diffusion in austenite was not considered in his study [12].

Paxton [9] confirmed that in conventional heating for austenitizing, the carbides acted as nuclei over a range of temperatures above Ae_1. Possible geometries for austenite nucleation are as presented in Fig. 2.1, the most favourable situations being c, d and e, with the latter two being most common.

Judd and Paxton [10] studied the effect of 0.5 pct Mn, as an alloying element, and also the location of carbides, on the rate of dissolution of cementite. They used spheroidized low carbon steels, made from zone-refined

Fe, up-quenched to temperatures above Ae_1. The effect of impurities was also studied in a commercial steel with a similar composition. The authors compared their experimental results with an analytical model in which the carbon diffusion in austenite was assumed to be the rate controlling step for the cementite dissolution process. For the zone-refined Fe-C specimens they found an excellent correlation between the experimental data for the growth of austenite from a cementite-ferrite aggregate and the calculated predictions. However, the experimental results for the substitutionally alloyed material (i.e. containing Mn) did not fit the model at the lower solution temperatures. The authors explained this discrepancy in terms of the effect of deliberate alloying elements on the boundary conditions for carbon diffusion. Moreover, they expressed their doubts about the validity of using models based on boundary conditions defined by binary phase diagrams for transformations in more complex systems. In fact Molinder's work [8] can be considered as evidence to support this idea, since the carbide dissolution rate reported in his Cr containing alloy, was about an order of magnitude below the rate predicted by a mathematical model for carbon diffusion using binary phase concentrations for boundary conditions.

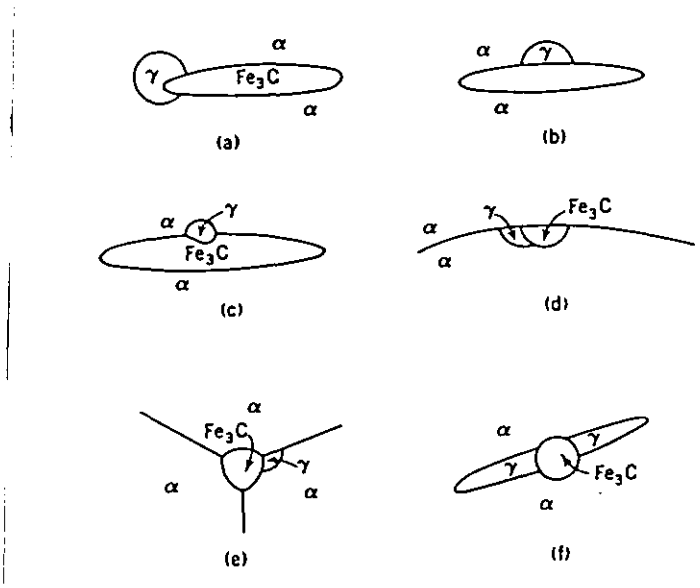

Fig. 2.1- Some possible nucleation geometries for austenite at the ferrite-cementite interface (after Paxton, Ref.9)

According to Judd and Paxton [10] the austenite incubation nucleation period was longer and the nucleation rate was lower in the substitutionally alloyed material as compared to those for the zone-refined Fe-C alloy. The Mn additions affected both carbide stability and diffusion fluxes in the system. Furthermore, even when the calculations were adjusted for the differences in austenite nucleation incubation period and nucleation rate, they reported a discrepancy with the experimental results for the alloy steel treated at lower temperatures (750 and 762.5°C). This difference

constituted the basis upon which the authors expressed their doubts about the validity of their proposed model for the Fe-Mn-C alloy. Since the calculated curves for the alloyed material approached the experimental results at higher temperatures, (775 and 787.5°C), the divergence was explained in terms of the effect of a change in the boundary conditions on the rate-controlling process rather than an alteration in the kinetic rate-controlling step due to the addition of 0.5 pct Mn to the Fe-C alloy. The effect was thought to be a result of Mn segregation between the carbide and the matrix in the ratio of about 10:1 respectively. They postulated that after a very small amount of carbide dissolution, the local Mn concentration led to a decrease in the carbon concentration gradient in the austenite and hence to a decrease in carbon flux through the austenite resulting in a smaller austenite growth rate. This effect became less pronounced as the dissolution temperature increased because of the increase in the austenite carbon solubility range, C_2-C_1, (Fig. 2.2).

The ferrite-ferrite grain boundaries, and especially grain boundary triple points were observed to enhance the nucleation of austenite at a cementite-ferrite interface. Carbides in grain boundaries were observed to nucleate austenite nodules after incubation periods that were only a fraction of those for carbides in the matrix away from α - α grain boundaries. The austenite nucleation rate at grain boundary carbides was three to eight times greater than that for carbides in the matrix. This was thought to be due to a surface energy contribution to the bulk free energy for nucleation when a small α - α grain boundary is replaced by a nucleus. It was suggested that the nucleation incubation period was necessary to raise the carbon concentration in the ferrite to its saturation level (Fig. 2.2, dashed line). The carbon concentration in ferrite at the cementite/ferrite interface would be comparatively high because the equilibrium carbon concentration in ferrite in Fe-C alloys increases steeply with increasing temperature above 500°C. Thus the ferrite/cementite interface would be a potent nucleation site for austenite.

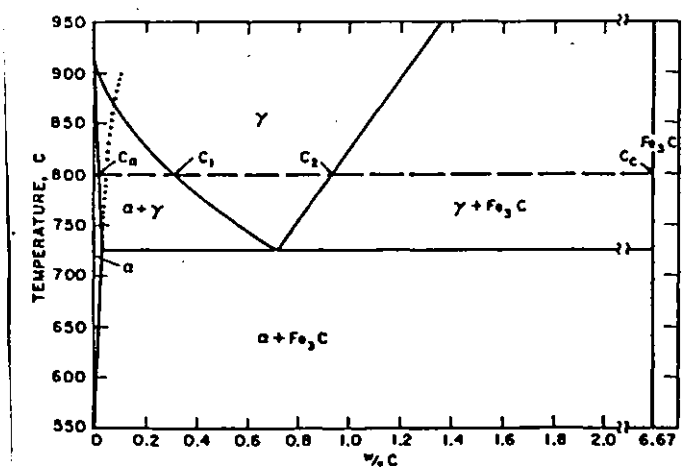

Fig. 2.2. Iron-rich, low-temperature region of Fe-Fe_3C diagram

Speich and Szirmae [11] studying the formation of austenite from ferrite

and ferrite-carbide aggregates in a number of Fe-C and plain carbon steels, confirmed that nucleation of austenite in spheroidite occurred at junctions between carbides and ferrite grain boundaries. The carbide was subsequently enveloped by the austenite and continued dissolution of the carbide occurred by carbon diffusion through the austenite envelope.

Hillert *et al* [12] examined the effect of alloying elements on the rate of dissolution of carbides and growth rate of austenite. They compared their data and that from earlier work with quantitative theoretical predictions based on a model for complete diffusion control. The authors considered five different mechanisms of dissolution of cementite, assuming local equilibrium at all phase interfaces. They disputed any idea of the austenite growth and cementite dissolution being interface-controlled. Their results supported the local equilibrium model and they concluded that, similar to the pure Fe-C systems, the growth of austenite in the presence of alloying elements was governed by the rate of carbon diffusion, provided the effect of the alloying elements on the process was accounted for.

D'yachenko and Fedorov [13] used an X-ray diffraction method to study the recrystallization of austenite in a O.6 pct C steel on heating above Ae_1. According to their work, the $(111)_\gamma$ // $(110)_\alpha$ orientation relationship was maintained as a result of slowly heating (2°C/min) the pre-quenched structure. However, in annealed specimens, and rapid heating (50°C/min) of as-quenched specimens, the phase transformation was accompanied by grain refinement and the austenite nuclei that formed did not reveal any of the general features of an orientation relationship.

Transmission electron microscopy was utilized in 1976 to investigate the partial transformation of a low carbon-low alloy steel and a medium carbon, 9 pct Ni steel from martensitic structures in the Ae_1 - Ae_3 temperature range [14]. Ferrite lath boundaries and cementite particles were found to be effective nucleation sites for the formation of acicular austenite. Through the mutual crystallographic inter-relation between ferrite, cementite and austenite, it was shown that only one of the austenite variants could be produced. Consequently the acicular austenite grains formed within a single prior austenite grain were identically orientated to each other. The authors showed that on further heating the acicular austenite grains above Ae_3, a coarse austenite grain similar to that of the prior coarse austenite structure was produced. According to the mechanism proposed, the acicular austenite regions grew in width either via the coalescence of commonly orientated austenite grains or by *spreading* through the recovering ferrite lath. It was considered that the formation of new nuclei involved a greater activation energy than that involved in the continuous growth of the identically orientated grains. No indication of recrystallization was observed in the ferrite laths upon heating the structure to lower temperatures within the Ae_1 - Ae_3 range but the laths recovered and grew to coarse ferrite grains at the lower temperatures in this range. Fine equiaxed polygonal austenite was also observed to form on the prior austenite boundaries while within the grains elongated austenite formed along the ferrite laths. In the low carbon

steel partially transformed to austenite, twinned martensite formed on quenching, thus implying a high carbon content in the martensite, which would require carbon partitioning to the transformed regions. The authors dispute the proposed diffusionless formation of austenite from martensitic structures heated slowly over Ae_1 temperature [15] because of the lack of a large enough non-equilibrium overheating. They suggested that the process was diffusion controlled. The observation of twinned martensite, in a similar investigation [16] on low carbon steels, substantiates the evidence that carbon diffusion occurred along the ferrite lath interfaces, where the diffusion is much enhanced, during the formation of austenite laths. The preferential formation of austenite laths at the ferrite lath interfaces is said to arise out of small misfit between the $\{ 110 \}_\alpha$ lath interfaces and the $\{ 111 \}_\gamma$ austenite plane. In referring to an earlier investigation [17] on a 9 pct Ni steel, the authors [16] suggest that the diffusion process involved the diffusion of substitutional as well as interstitial atoms. It has been demonstrated by chemical analysis of extracted austenite, that the austenite laths which formed at 550°C from 9 pct Ni steel martensite were markedly enriched in the substitutional atoms such as Mn and Ni [17]. Watanabe *et al* [16] suggest that Ni atoms build up in the ferrite at the cementite/ferrite interface, (as Ni has a low solubility in cementite), and subsequently diffuse into the austenite. An interesting in-situ observation of austenite formation in a Fe-C eutectoid steel and two commercial steels was published in 1977 [18]. In the eutectoid steel, the carbide particles were observed to dissolve in the ferrite matrix when the migrating austenite interface approached them at 740°C. In the material containing ~ 0.5 pct Mn and ~ 0.7 pct C heated to the same temperature, cementite particles were frequently engulfed by the migrating austenite boundary and further dissolution of cementite occurred mainly in austenite. From a record of the structural changes in the 0.5 pct Mn steel at this temperature, the average migration rate of the α/γ boundary was evaluated to be about 3×10^{-5} cm/s, which was an order of magnitude lower than that predicted theoretically for a binary Fe-C alloy by the mechanism described as type III by Hillert *et al* [12]. Using a local equilibrium model, the effect of Mn was shown to be strong enough to practically prevent the dissolution of cementite in ferrite, (unless the temperature was very high), but weaker once the particle was surrounded by austenite [12]. The migration rate of an austenite/ferrite boundary along an elongated carbide particle in the commercial steel was observed to be more than ten times that before contact with the particle [18]. The migration rate of curved interfaces was suggested to be controlled by the rate of carbon diffusion, and the effect of Mn on the reaction was shown to be compatible with the local equilibrium model [12]. Movement of dislocations around particles has been observed during the dissolution process of carbides in both ferrite and austenite [18].

Plichta and Aaronson [19] studied the effect of some alloying elements on the morphology of austenite formed from martensite in low carbon steels after heating to intercritical temperatures. In this work the authors suggested that the nucleation and growth of austenite at boundaries between

martensite needles and migration of these boundaries into lower energy configurations were competitive processes. A rapid rate of nucleation of austenite at the original martensite lath boundaries would strongly inhibit the motion of the boundaries. Addition of alloying elements such as Mn, Ni and Cu would lower the temperature range of the no-partition Ae_3 compared to the Fe-C system, which would result in a higher driving force for the nucleation and growth of austenite. Consequently the amount of martensite lath boundary migration would be restricted, thus resulting in an acicular growth of austenite along the faces of parallel martensite laths. On the other hand, elements like Mo would decrease the driving force for nucleation and growth of austenite, as do carbide-forming elements like Cr, through the *solute drag-effect* upon growth [20] retarding the reaction kinetics for growth. Thus boundary migration would occur to produce approximately equiaxed austenite grains.

Gilmour *et al* [21], in their study of a portion of the Fe-C-Mn phase diagram, indicated that as a result of isothermally heating an Fe-3.55 at pct Mn-0.5 at pct C steel in the ($\alpha + \gamma$) region, the austenite first formed as relatively long, closely spaced plate-like precipitates which tended to break up into larger, more equiaxed precipitates after further annealing. After a few days annealing, the plate-like precipitates showed considerable Mn partitioning and were thought to be approaching equilibrium.

Low carbon-low alloy steels with acicular structures formed two types of austenite as a result of an intercritical treatment just above Ae_1, [22] : globular and acicular. The globular austenite grains were formed in tempered martensite by the diffusional reverse transformation. This process always accompanied the dissolution of cementite and the growth rate of austenite was controlled by the diffusion of carbon in austenite. An empirical equation was presented as :

$$R = K\, t^{1/2} \qquad (2.1)$$

where R is the radius of globular austenite, K is the growth parameter and t is the intercritical transformation time. The smaller value of K found for tempered martensite, compared to that for martensitic or bainitic structures, was suggested to be caused by segregation of Mn in cementite, thus inhibiting its dissolution. The acicular austenite, on the other hand, formed in a lengthwise direction parallel to the martensite lath boundaries and this process did not accompany the dissolution of cementite. Most of the acicular grains had nearly the same orientation and it was concluded that they were formed by a reverse martensitic transformation obeying the Kurdjumov-Sachs orientation relationship between austenite and martensite.

The formation of austenite in 1.5 pct Mn low carbon steels was studied at 725°C (an intercritical temperature) from spheroidized Fe_3C-ferrite structures [23]. A relatively low heating rate ($\sim$ 1°C/s) was attained at temperatures close to the set temperature by furnace heating the samples. An increase in the carbon content of the material from 0.01 to 0.22 pct

resulted in an increase in both the distribution of Fe_3C precipitates, and the extent of banding in the starting structure. Thus, as the amount of austenite increased with holding time at 725°C, the appearance of banding became more pronounced and the final austenite that formed in 0.22 pct C steel exhibited a banded morphology reflecting the original banded structure of spheroidized Fe_3C. The sigmoidal shape of the percent γ vs $Ln\ t$ curves indicated the nucleation and growth nature of the reaction. The maximum amount of austenite took about 400 min to form and this period appeared to be independent of carbon content of the alloy and consequently of the amount of austenite eventually formed. Optical micrographs showed that the austenite preferentially nucleated at Fe_3C particles located on ferrite-ferrite grain boundaries and the nucleation countinued throughout the relatively long isothermal holding time. The austenite grains grew both into the ferrite grains and along the ferrite boundaries. It was suggested that the difference in diffusion coefficients perpendicular and parallel to the ferrite grain boundaries resulted in a much slower growth of austenite into the grains compared to the growth rate along the grain boundaries. It was reported that the growth perpendicular to the grain boundaries virtually ceased after 10 minutes. Extensive grain growth of ferrite was detected only in the steel with the lowest carbon content (i.e. 0.01 pct) during isothermal holding at 725°C. In the higher carbon steels, the presence of larger amounts of Fe_3C on the grain boundaries was believed to be responsible for retarding ferrite grain growth at this temperature.

2.2 Structure and Properties of Ferrous Martensites

2.2.1 Introduction

Martensite in steels is the name given to the body centered tetragonal structure formed when the face centred cubic solid solution of carbon in γ iron (austenite) is rapidly cooled. A martensitic transformation is usually characterized by the change in shape of the transformed regions and a high growth velocity. The phases produced by a martensitic transformation frequently have substructures which cannot be obtained in any other way. Martensite may be regarded as a supersaturated solution of carbon in α iron, in which the symmetry is distorted from cubic to tetragonal. This arises when the interstitial carbon atoms are confined by the transformation mechanism to one of the three possible sets of octahedral sites of the body centred cubic structure. This distinguishes martensite from supersaturated ferrite which forms during rapid cooling from a temperature in the α range of stability. All interstitial sites in ferrite have equal probability of occupation, so the structure remains cubic. The observation of cubic martensite, however, has been reported [24] in alloys containing 0.08 and 0.12 pct carbon, revealing an identical crystal structure to ferrite but with a different morphology.

The theory of martensitic transformation strengthening in steels is considered to be complex due to the simultaneous contribution of different mechanisms.

It has been deduced that the main effect of carbon in strengthening martensite is indirect [25], through its influence on the substructure, rather than in giving solid solution or precipitation hardening. The substructure, however, is not the only source of great strength. Other factors include the intrinsic lattice resistance to dislocation motion, interstitial solid solution hardening, rearrangement of interstitial solutes (like cluster formation and precipitation), grain size hardening, work hardening and substitutional solution hardening. An accurate assessment of the relative importance of the factors mentioned is complex, since they interact with one another.

2.2.2 Structure of Martensite

According to Thomas [26] and Krauss and Marder [27], there are two major types of martensite, i.e. lath and plate, which form in iron base alloys as a result of the shear type diffusionless martensitic transformation of high temperature stable solid solution austenite. These two types of martensite differ in their formation, fine structure, unit shape and microstructure.

The structure of lath martensite can be characterized by its substructure of tangled dislocations within the laths [28], the laths being units which are planar and long in one direction. Fine twins have also been observed in some lath structures [28,29].

The substructure of plate martensite is made up of fine twins [28] and/or dislocation arrays contained in the plates [30]. The microstructure of lath martensite is characterized by the association of many parallel laths of approximately the same size. Adjacent parallel laths may be separated by either low- or high-angle boundaries [31-33], which may be twin related [32,33] to make up a packet. The width of the laths range from 0.1 to several microns, with the most frequent occurring width being between 0.1 and 0.2 microns [34]. Several packets may be found in a single austenite grain [35].

In contrast, units of plate martensite are non-parallel and vary significantly in size. The plates which are the first to form tend to span their parent austenite grains and effectively partition the austenite, thus limiting the size of plates that subsequently form. These new plates offer both nucleation sites and barriers to plate growth [27]. The effect of this partitioning is to produce a large range of plate sizes in this type of martensite.

In studying the twinned martensite in Fe-Ni alloys, Thomas revealed that the twins in plate martensite may themselves be twinned. He believed that double twinning was characteristic of the martensitic transformation [26], i.e. not the result of plastic deformation after transformation. Double twinning was also reported to occur in lath martensite [36]. According to Thomas [26] the martensitic structure resembled that in shock-loaded materials [37]. As the shock pressure is increased, twins are formed when the dislocation density attains some critical value in f.c.c. metals [38]. By

analogy, it is postulated [26] that twins observed in martensite laths may have been induced because the limiting dislocation density had already been attained, thus implying that slip shears always precede twin shears.

Lai *et al* [39] evaluated the effect of austenitizing temperature on the mechanical properties of as-quenched 4340 steel (similar in composition to En24). They reported a decrease in the amount of twinning when the austenitizing temperature was raised from 870°C to 1200°C. This increase also resulted in a relatively large increase in the volume fraction of retained austenite. They also described the microstructure of 4340 martensite as a mixture of lath and plate martensites. The laths generally exhibited a high dislocation density, while the observation of a few twinned laths was also reported. The plate martensite in the specimens austenitized at 870°C was twinned and showed no autotempering whereas the dislocated martensite was autotempered and epsilon carbide was precipitated during quenching.

In their study of as-quenched 4340 steel, Bhadeshia and Edmonds [40] reported a lath structure martensite with the lath width being of the order of 0.25 μm. Retained austenite was absent within the lath packets and the authors concluded that the lath packet was the fundamental transformation unit. Short time (5 min) austenitizing at 1100°C produced relatively small (100μm) austenite grains and most of the martensite plates were observed to nucleate at austenite grain boundaries. Longer time (130 min) austenitizing at a higher temperature (1200°C) produced a larger austenite grain size (1100 μm) and it was suggested that most of the martensite plates nucleated within the austenite grains. The nucleation of the lath packets at prior austenite grain boundaries was associated with higher transformation temperatures within the M_s-M_f range. On decreasing the austenitizing temperature the morphology became more " strain-energy-controlled ", causing an increase in the aspect ratio of the martensite plate. It was suggested that the nucleation of plates within the austenite grain was associated with an even more stringent strain energy control of morphology at the lowest transformation temperatures.

Kelly and Nutting [28] showed that increasing carbon and nickel and subsequently lowering of M_s temperature increased the possibility of transformation twinning. Subsequent work on the effects of other alloying elements, including cobalt which does not have much influence on M_s temperature, has shown that all of the principal alloying elements C, Ni, Mn, Cr, Mo and Co increase the tendency to twinning [41-43].

Thomas suggested that the transformation structure depends on the relative values of the critical resolved shear stress for slip and twinning over the M_s-M_f transformation range [26]. Thus the lower the M_s-M_f temperatures and the stronger the steel, then the inhomogeneous shear component of transformation strain would be twinning rather than slip. With higher M_s temperatures (>300°C) the structure is principally dislocated. The same author concludes that M_s temperature alone is not the controlling parameter determining the martensitic sub-structure. The strength of martensite (and

austenite from which it forms) is suggested to be the single most important factor which determines whether martensite is dislocated, twinned or both.

2.2.3 Structure-Property Relationships

The high hardness of martensite in steels was originally attributed mainly to the solid solution carbon in iron and to the small size of the martensite crystals. Christian, in a general review on the strength of martensite [44], refers to a number of mechanisms, namely the combination of a high defect density with fine, uniformly distributed precipitates of alloy carbides, intermetallic compounds and iron carbides, as the most effective contributors to the room temperature strength of martensite. The importance of solid solution hardening is also emphasized in freshly quenched steels with low M_s temperatures; however this effect is considered to be difficult to distinguish from clustering and precipitation contributions. The lattice resistance to dislocation motion, according to the author, becomes a major factor at low temperatures.

According to Winchell and Cohen [45], if martensite were regarded as a supersaturated solution of carbon, much of its strength would be due to solid solution hardening. Kelly and Kehoe [25] are of the opinion that the relationship between the strength of lath martensite and the square root of carbon content is not due to interstitial solid solution hardening. Instead, they suggest that the strength is related to a carbon-dependent dislocation density. Two main points are presented supporting their idea. First, they refer to the fact that the solid solution theories predict that the slope of the plot of strength vs $c^{0.5}$ should be temperature dependent. However, the available data contradicts this prediction showing a constant slope over the temperature range 77° to 273°K [46,47]. The second supporting evidence to their interpretation are reports indicating that all the carbon in lath martensite is not in true solid solution, even when precipitation is carefully avoided during quenching [48-51]. They show that in a series of high purity Fe-C fast quenched (>30,000°C/s) alloys the martensitic specimens retained less than 0.01 pct carbon in true solid solution, and the amount of carbon in solution was appoximately constant for all compositions between 0.01 and 0.1 pct carbon. Furthermore, the martensitic specimens were considerably stronger, even with less carbon in solution, when compared with ferritic samples of the same alloy. This indicated that an additional strengthening mechanism was operative in the case of martensite. The grain size hardening was shown to have an indirect effect, resulting from changes in dislocation density with grain size [52,53]. This was supported by Kelly and Kehoe [25] who indicated that for the specimens with approximately the same amount of carbon in solution, the strength was linearly related to the square root of the dislocation density ρ, irrespective of structure or grain size. The slopes of the strength vs $\rho^{0.5}$ were also independent of temperature and showed a linear relationship between σ and $\rho^{0.5}$. The dislocation density was also found to be linearly related to the total carbon content of martensite, which was consistent with earlier work, indicating that carbon

increases the dislocation storage rate in cold worked ferrite [54]. This led to an apparent relationship between strength and $c^{0.5}$. However, in the case of ferrite with relatively large amounts of carbon in solution (up to 0.04 pct), the authors give evidence for true solid solution hardening.

In considering grain size, the grain diameter is not a well defined concept in a martensitic structure, but empirically it might be expected that the yield strength should increase as the mean size of the martensite plate decrease. In three grades of commercial martensitic steels, including AISI 4340, Grange [55] showed a Hall-Petch relationship between the prior austenite grain size and the strength of martensite tempered at 205°C. The smaller martensite average plate size, produced by quenching the smaller austenite grains, was believed to be associated with the increase in the yield strength of steels. The contribution by substitutional alloy elements to solid solution hardening of carbon martensite is complex and is believed to be relatively small [44]. However, these elements can indirectly influence the strength of martensite through their effect on the grain size and M_s temperature.

On the relative importance of carbon solution hardening and precipitation strengthening, most earlier work considers that the latter makes the major contribution but that solution strengthing is also significant[44]. However, in analysing the strength of an AISI 4340 steel, which was determined to be about 225 Kg mm^{-2}, Leslie *et al* [56] estimated that about 120 Kg mm^{-2} was due to clústering and precipitation and about 42 Kg mm^{-2} was contributed by solution hardening.

The arrays of fine transformation twins, which usually characterise plate martensite, can contribute to strengthening through their resistance to the passage of either dislocations or twins. In a qualitative account, Kelly and Nutting [28,57] explained an increase of strength with carbon content up to a saturation level, in terms of an increasing population of twinned plates.

The dislocated untwinned martensitic structure can be considered as a structure produced by heavy deformation and its contribution to strength can roughly be compared to that of severe work hardening. The dislocated lath structure is typical of low carbon martensites and yields high toughness with moderate to high tensile strength. On the other hand, the presence of a high twin density in a martensitic structural steel is associated with low fracture toughness and high yield strengths. In twinned martensite, cementite can precipitate preferentially along the twin boundaries, so very long continuous carbides can form. These carbides act as strong barriers for the movement of dislocations and so induce high stress concentrations which may lead to crack nucleation. Gillbert *et al* [58] reported the observation of such twin-induced cracks. Martensite in the twinned areas tends to deform by twinning rather than slip and plastic deformation is restricted in this mode [59]. This can result in low toughness. Internal twinning itself increases the strength of metals and in steels it is additive to the strengthening from carbon in solution; however, at the same strength level

the twinned martensite has a lower fracture toughness than dislocated martensite [41], or, for the same carbon content, fracture toughness decreases with increasing twinning [43].

The formation of the units of plate martensite at angles to one another, results in accommodation effects at sites of impingement. Marder *et al* [60] showed that microcracking in plate martensite in Fe-C alloys is directly related to an increase in the carbon content of the alloy and is not affected by quenching medium or prior austenite grain size. The nucleation of cracks can also occur at defects formed by the dynamic interaction of growing martensite plates with austenite boundaries causing *delayed fracture* [61] when the martensite is under static loads lower than the dynamic yield stress. High internal stresses, created during the martensitic transformation, can produce microcracks at sites like the intersection of two martensite plates or a martensite plate and a grain boundary or the twin intersections. Quench cracking is usually associated with acicular martensitic structures in plain carbon steels with a carbon content of 0.75 pct and above; however microcracks of 1-6 μm were observed in a 0.46 pct carbon steel [62] on quenching.

2.2.4 Tempering of Martensite

2.2.4.1 Introduction

Tempering of martensite occurs in several well-recognized stages, with the first stage consisting of the formation of metastable transition carbides. The second and third stages comprise the decomposition of retained austenite and the formation of cementite respectively. Prior to the onset of the first stage, there is an initial stage in which carbon segregates on dislocation networks. This initial stage and the beginning of the first stage occur during autotempering.

Autotempering is the process of segregation of carbon atoms in martensite to lower energy interstitial sites near dislocations and cell walls. This occurs during quenching austenite to room temperature, when the M_s temperature is above ambient. Since martensite is highly supersaturated with carbon, precipitation can take place in very short times at temperatures a little above room temperature and it cannot normally be prevented even with fast quenching rates to room temperature.

In medium plain carbon or low alloy steels, Parker [63] showed that the rates of tempering are extremely high at 240°C with approximately 50 percent of the reaction being completed in the first 3 seconds. The M_s temperatures for these steels are 50° to 100°C above this temperature and "cooling curves" for the midplane of 12 mm thick oil quenched specimens show that it takes about 10 seconds for the temperature to decrease from 300°C to 200°C. About 90 percent of austenite transforms to martensite in this range providing ample time for extensive autotempering to occur.

For Fe-C alloys, containing less than 0.2 pct C, Speich showed that about 90 percent of the carbon segregated to lattice defects on quenching [64]. This segregation was suggested as an explanation for the lack of tetragonality at carbon contents below 0.2 pct [65]. The dislocations in freshly quenched martensite are saturated at 0.2 pct C; however, in annealed Fe-C alloys the saturation of dislocations occurs at much lower carbon levels because of the lower dislocation density. In steels containing plate martensite, with an internally twinned substructure, fewer of these low energy dislocation sites are available and carbon segregation to dislocations is not the only segregation reaction. Precipitation clustering of carbon can occur at low temperatures in high carbon or high alloy-low carbon steels [65]. The presence of precipitation clusters in commercial low- or medium-carbon steels, with essentially lath martensitic structures and a high dislocation density, has not yet been clearly confirmed.

2.2.4.2 Stages of Tempering

Epsilon carbide ($Fe_{2.3}C$, hcp) is the first carbide precipitated if medium or high carbon steels are tempered at temperatures between 100° and 200°C [65]. This carbide does not form in the low alloy steels containing less than 0.2 pct C because most of the carbon in these steels remains at the lower energy dislocation sites for this range of temperatures. However, in steels containing higher amounts of carbon, these dislocation sites become saturated and carbide precipitation can occur at temperatures as low as 150°C [65]. At temperatures between 200° and 300°C, a metastable carbide intermediate between epsilon and cementite is formed in some high carbon steels [66]. The precipitation of this Hagg carbide (Fe_5C_2 , monoclinic) in lower carbon steels is however doubtful due to the similarity of its diffraction pattern to that of cementite. Needle-like cementite may form during quenching or during initial stages of deliberate tempering of most steels when they are tempered at temperatures between 250° to 700°C. The most common nucleation sites observed are martensite lath boundaries at low temperatures and ferrite grain boundaries at higher temperatures. With an increase in the time or temperature of tempering, a recovery in the dislocated structure and spheroidization of acicular cementite usually occurs.

Speich and Leslie [65] showed that there is an increase in the amount of retained austenite with the alloy carbon content (Fig. 2.3). The decomposition of retained austenite and formation of bainite occurs at 200° to 300°C in medium or high carbon steels and is sometimes referred to as the second stage of tempering, the first stage being the precipitation of epsilon carbide [34].

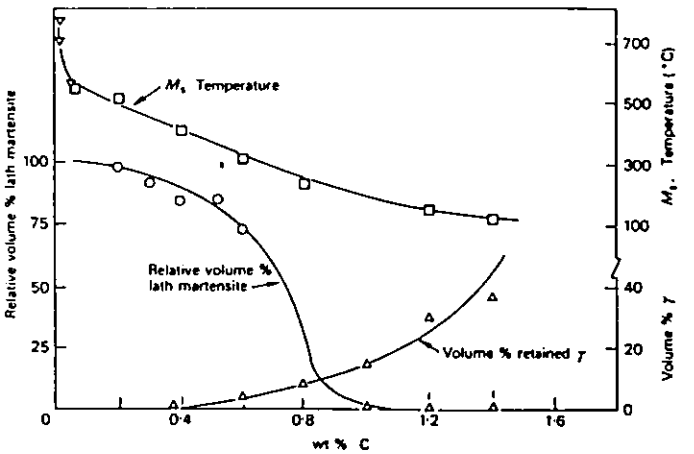

Fig. 2.3 Effect of carbon content on relative volume percent of lath and plate martensites, M_s temperature, and volume percent of retained austenite in Fe-C alloys (after Speich and Leslie, Ref.65)

The recovery of a martensitic defect structure becomes an important feature of the tempering process above 400°C, when the low angle dislocation cell boundaries and the random dislocations contained between them are annihilated and a fine grained acicular structure is developed by recovery. Recrystallization of high angle lath structure of martensite can occur at 600° to 700°C. This process can be inhibited by the pinning action of lath boundary carbides if the carbon content of the steel is high. After recrystallization is complete, growth of carbide particles and of ferrite grains are the only kinetic processes that continue.

2.2.4.3 Structure Property Relationships on Tempering

The main effect on the mechanical properties caused by the progressive precipitation and subsequent spheroidization of cementite and the recovery and recrystallization of the defect matrix is a decrease in strength accompanied by an increase in ductility. This is observed when plain carbon martensite is tempered in the range between 100° to 700°C. A slight increase in the hardness of higher carbon steels tempered to 100°C has been attributed to the increased carbon segregation to dislocations [67]. At 150° to 250°C higher carbon steels exhibit a softening due to the precipitation of epsilon carbide. This effect becomes less pronounced in the lower carbon steels as mentioned previously. Widmanstatten rod shaped cementite precipitates at around 300° to 400°C in most steels and causes substantial softening. Tempering to higher temperatures produces a further decrease in strength and improves ductility which is accompanied by spheroidization of cementite and recovery and recrystallization of the matrix.

At temperatures between 500° and 600°C, if carbide forming elements such as Mo, Ti, V and W are present in the alloy, a fine dispersion of alloy carbides can replace coarse particles of cementite, resulting in a secondary hardening with hardness values approaching that of the as-quenched

material. Chromium carbide, Cr_7C_3, cannot contribute to this effect significantly because of its high rate of coarsening at higher tempering temperatures; however a retardation in softening is expected when Cr is present in the alloy composition [68]. The finer size and more dispersed morphology of the alloy carbides compared to those of the replaced cementite, has been attributed to the lower diffusivity of substitutional elements compared to that of carbon at their formation temperature [69]. These alloy carbides have been reported to reveal dimensions of about 10 to 100 A° in diameter, thickness or length respectively [70]. They usually nucleate on the dislocations inherited from the martensitic structure. Cobalt, through preventing recovery of dislocations, provides more nucleation sites and a finer dispersion of precipitates, and hence indirectly produces a higher secondary hardening peak and retards softening [71]. This fine dispersion of alloy carbides is of considerable interest because it not only retards the decrease in strength but also promotes toughness. Void nucleation requires a higher stress level when the particles are finer and hence there is a higher resistance to fracture. The fine alloy carbides, however, may coarsen during longer tempering treatments at higher temperatures which can cause a lowering in the strength level. This overageing process is to be avoided in order to attain the desirable mechanical property combinations in the quenched and tempered alloy steels.

In plain carbon and most of the low alloy steels, martensite has poor toughness in tensile and notch impact tests. Tempering of quenched steels to a softer condition, however, usually improves the fracture toughness. The existence of easy fracture paths, such as prior austenite grain boundaries, is considered to be one of the reasons for the relatively low ductility of autotempered or lightly tempered structures. The precipitation of a coarse, non-uniform distribution of carbides along prior austenite grain boundaries provides an easy path for crack propagation. Olefjord reviewed the works on the principles of temper embrittlement [72] and a brief account of his evaluations, and that of other workers is presented in the next section.

2.2.5 Temper Embrittlement

When most commercial steels are tempered from the quench-hardened condition to improve tougness, they can become susceptible to embrittlement if they are heated in the temperature range 350°-550°C. Most earlier works tend to divide the phenomenon into either *temper embrittlement* or *350°C embrittlement* according to the heat treatment cycle. Temper embrittlement is usually characterized by an increase in the brittle to ductile transition temperature and is a consequence of heating or slow cooling in the temperature range 350°-550°C [72]. Tempered martensite embrittlement or *350°C embrittlement* is associated with a decrease in the fracture energy at room temperature and is caused by heating in the temperature region 250°-400°C [72]. In spite of the tendency in earlier work to differentiate between the two phenomena, attributing the former to the segregation of impurities (like Sb, P, Sn and As) to the prior austenite grain boundaries [73] and

associating the latter with the precipitation of film-like carbides on grain boundaries [74,87], the results of research during the past decade suggest that the underlying mechanisms are similar and the distinction is not very sharp [82].

One of the main factors determining the extent of susceptibility to embrittlement is the chemical composition of the steel. Steven *et al* [75] showed in 1959 for the first time that the propensity to embrittlement is determined by the interaction between the impurities and the alloy elements. This was supported by other works and more recently Mulford *et al* [76] noted an enhanced embrittlement when more than one alloy element was present. Low *et al* [77] supported the idea by demonstrating that it is not necessarily the levels of impurities which are responsible for the degeneration of an alloy, by showing that a plain carbon steel with a high impurity level (800ppm Sb) was not suceptible to embrittlement. However, the transition temperature was raised by about 700°C when both Ni and Cr were present, but only by 50°C with either Ni or Cr. In the case of a Ni-Cr steel doped with Sb, without carbon (<10 ppm) the increase in transition temperature was still about 200°C when the alloy was embrittled. The authors showed that P and Sn had a smaller effect than Sb and that the combinations Ni-Sn and Cr-P gave a larger shift than Ni-P and Cr-Sn. Surface-sensitive analytical methods have revealed that not only the impurities but also the alloy elements segregate [78]. The zone of enrichment is very narrow (only a few atomic layers) and the enrichment factor (i.e. the grain boundary content/bulk concentration) is of the order of magnitude 10^4 and 10 for the impurity and alloy elements respectively. McLean *et al* [79] assumed that the driving force for segregation was the misfit between the solute and the solvent atoms. This was supported by Seah *et al* [80] who showed that the grain-boundary enrichment increased with the inverse of the solid solubility of the impurities in the matrix. Attempts to determine any threshold levels for the embrittling action of impurities have not been conclusive. Several reports indicate the occurrence of embrittlement with amounts of impurities as small as 25 ppm Sb [81], or 100 ppm Sn [82], or 40 ppm P [83]. The effect of about 200 ppm P on embrittlement of rotor steels (Ni-Cr-Mo-V) tempered for long periods at 400°C, was shown to be considerably greater than that of a similar amount of Sn.

Several workers supported McLean *et al's* [79] diffusion-controlled equilibrium segregation model, in which they assumed that the driving force for the segregation of dilute elements was the difference in distortion energy caused by a solute atom in the grain interior and in the grain boundaries. The solubility, in both the interior and the grain boundaries is temperature dependent and the solute and impurity atoms migrate to the grain boundaries until an equilibrium state is reached. This causes a loss of cohesion along the grain boundaries which leads to a low energy intergranular fracture. Based upon this model, Capus [84] estimated segregation times for P and Sn at 450°C to be between 100 and 1800 hours.

Guttmann [85] discussed the simultaneous segregation of impurities and alloying elements and the interaction between the two. He showed that for most of the alloys which are susceptible to temper embrittlement, the standard enthalpy of formation of the intermetallic compounds (NiSb, Mn_2Sb, Cr_3P), $\Delta H°$ was within a range of moderate values. If the interaction became too strong, stable compounds were precipitated in the interior of the grains; if it was too weak, there was insufficient driving force for segregation.

A two-step segregation model proposed by Capus [84] suggests that the alloy elements (Mo, Cr, Mn, and Ni) are distributed at the austenitizing temperature along the γ grain boundaries which attract the impurities at the embrittlement temperature. He suggests that Mo decreases the rate of embrittlement by retarding the diffusion rate of some of the impurities in Fe, and by retaining extra trapping sites for these elements, as it tends to reduce the rate of dislocation recovery during tempering. This model has met some opposition in subsequent work since attempts to identify segregation of alloys at the austenitizing temperature have in most cases proved fruitless e.g. (ref.86).

After earlier proposals of Lement *et al* [87] and Hill *et al* [88], according to which precipitation of lath-like cementite was believed to be responsible for the embrittlement, a considerable amount of research was carried out to discover the kinetics and mechanisms of the phenomenon. In brief, according to Rellick and McMahon [89] since the solubility of the impurities in cementite is low, they are expelled from the growing carbide into the surrounding matrix. The enrichment weakens the boundary and causes intergranular fracture. However, if the alloy is heated to higher temperatures, the concentration gradient of impurities built up around the particle may diffuse away from the boundary and the material becomes de-embrittled, so that the effect appears reversible. Comparing temper embrittlement in low alloy steels with and without impurities, the authors showed that when the *impure* steel was embrittled, cracks opened at the carbide/ferrite interface, while in *pure* steel the fracture path was within cementite. Ohtani *et al* [90] showed that carbide stabilizers such as Mo and Ti can reduce temper embrittlement through preventing grain boundary nucleation of carbides. It must be indicated however, that the carbon impurity rejection model cannot be the sole mechanism of temper embrittlement since as mentioned above, Ni-Cr steels with very low amounts of carbon (<100 ppm) were shown to be susceptible to temper embrittlement [77].

A dual mechanism involving coarse carbide precipitates and high dislocation density was proposed by Irani *et al* [91] in which they indicated that the embrittlement temperature was high enough for coarse carbide formation but too low for dislocation recovery. The shift in transition temperature was calculated in 1977 by Seah [92] who produced a computer program assuming the kinetics and temperature dependence of segregation, based on

Guttmann's double segregation model [85]. The agreement of the results with those empirically determined earlier (1953) by Carr *et al* [93], indicates that the embrittled boundaries are in a near-to-equilibrium state at the embrittlement temperature. It was suggested that rejection from carbide particles only accelerated the initiation of segregation. As the expelled nickel diffused along the grain boundaries, it provoked segregation of Sb by Guttmann's mechanism. The final alloy and impurity concentrations were determined by their equilibrium values at the temperature [94].

2.3 Structure and Properties of Bainites in Steels

There are four main decomposition reactions of austenite in medium carbon steels with the transformation products and approximate temperature ranges of formation being: ferrite and pearlite (about 750° to 600°C), upper bainite (about 600° to 400°C), lower bainite (about 550°C to below the M_s), and martensite (M_s about 300°C for 0.4 pct C).

The two types of baintite can be distinguished through the differences in their microstructure. In upper bainite the carbides are often observed to form elongated particles between the bainitic ferrite grains. In lower bainite, the carbides tend to precipitate within the ferrite grains at an inclined angle to the major growth direction of the ferrite. Although both upper and lower bainites form by a shear mechanism, the two reactions also exhibit differences in the kinetics of formation. According to Pickering [95] the temperature below which lower bainite, rather than upper bainite, formed was dependent upon the carbon content, increasing from 450° to 550°C with increasing carbon for hypoeutectoid steels. The temperature of transformation for either upper or lower bainite has a major influence on the fine scale microstructural features, and hence can have a major effect on mechanical properties. The above author also showed that a linear relationship existed between the tensile strength and the transformation temperature.

The metallic elements commonly used in heat-treatable, low-alloy steels (Mn, Si, Cr, Ni, Mo, V) alter both the eutectoid composition and the eutectoid temperature.The saturation concentration of carbon in austenite at various temperatures plays an important role in determining the temperature for hypoeutectoid steels above which lower bainite does not form. It is possible therefore to shift the temperature-carbon content line by varying the amount of alloying elements in steel. In this way, the range of properties of bainitic structures is strongly dependent on the chemical composition of the alloy. In general the fracture toughness of steels having upper bainitic structures is inferior to steels of the same strength having lower bainitic structures.

The interactive effects of alloying elements are different for the two bainitic reactions and they are so complicated that it is not reasonable to expect that such effects can be expressed in simple arithmetic terms [63]. The

results of hot stage microscopy have shown that both types of bainite plates grow at slow temperature-dependent rates [96]. The activation energies for the growth were estimated to be approximately 83.7 KJ per mole for lower bainite and 4.2 to 37.7 KJ per mole for upper bainite depending on carbon content [97]. The low values of activation energies for the growth of upper bainite do not reflect the kinetics of a diffusional process. It is suggested that nucleation should be the rate controlling step of the growth process [98]. The size, distribution, and nature of the carbide particles, in both upper and lower bainite, control to a large extent the mechanical properties of steels with bainitic microstructures. In upper bainite, most of the carbides in hypoeutectoid steels precipitate as Fe_3C from the residual carbon-enriched austenite films that form between the ferrite laths. The characteristic stringers of Fe_3C between the ferrite laths can result in poor fracture properties. In lower bainite, the carbon enriched austenite is absent and the structure is free from interlath carbides. Epsilon carbide, however, precipitates at lower temperatures almost exclusively from supersaturated ferrite [99]. The uniform distribution of this semicoherent precipitate can impart a desirable combination of strength and fracture toughness to bainitic structures. The dissolution of epsilon carbide and formation of cementite on any subsequent tempering to higher temperatures can be retarded by adding a few percent of silicon to the composition of the alloy [100].

At equivalent strength levels, it was found that the toughness of lower bainite was higher than that of heavily twinned tempered martensite; however, untwinned martensite posseses better toughness than that of bainite [41].

Chapter 3

Experimental procedure

3.1 Material

Two commercial medium carbon steels were chosen to study the microstructures and mechanical properties of the ferrite+martensite mixtures produced by quenching from the (α + γ) intercritical region. Both of the alloys contained about 0.4 weight percent carbon. The first alloy, En24, is a low alloy steel containing nickel, chromium and molybdenum as alloying elements, whereas the second alloy, En8, is a plain carbon steel. The exact chemical compositions of both alloys are given in Table 3.1.

Neither of the alloys used in the present work were laboratory melts and both were observed to contain inclusions usually found in the commercial steels. En24 steel was supplied, in the form of 60x25mm forged bars, by the engineering metallurgy department of the British Steel Corporation. The second alloy was ordered in the form of 10 mm square cross section, cold rolled bars from a commercial distributing firm.

3.2 Initial Heat Treatments

Specimens of dimensions 12x12x60 mm were cut from the En24 bar, in its longitudinal direction for initial quench-hardening. The En8 bar however, simply needed to be cut into 60 mm long pieces since it was received in an appropriate cross section size for Charpy fracture toughness specimens.

Austenitizing was carried out by suspending the specimens in the hot zone of a vertical crusilite rod furnace for one hour with a continuous flow of argon to prevent oxidation and decarburization. The austenitizing temperatures were 835°C and 850°C for En24 and En8 steels respectively. The specimens were then directly oil-quenched. Some of the specimens were tempered at 700°C for five hours and oil-quenched to investigate the behaviour of the initially tempered material treated in the intercritical region.

In the earlier part of the work, the quenched or quenched-and-tempered bars were all cut into 1mm thick slices and were individually annealed at different temperatures within the (α + γ) range for different times, for structural studies and hardness measurements. However, identical Charpy size specimens were also utilized at a later stage to examine the microstructure and hardness as well as the fracture behaviour of the intercritically treated material. The exercise was intended to avoid any

Table 3.1 Composition of alloys in weight percent

Alloy	C	Si	Mn	P	S	Cr	Mo	Ni	Cu	Sn	V
En24 (analysed)	0.38	0.26	0.66	0.025	0.028	1.21	0.27	1.43	0.19	0.006	0.013
En8 (nominal)	0.40	0.20	0.70	0.020	0.020						

incorrect association of characteristics which might have resulted from the differences in the heating and/or cooling rates due to the size changes of the specimens. The terms *thin* and *thick* hereafter specify the size of the specimens during the course of intercritical treatment. Further explanations are given in the relevant sections.

3.3 Intercritical Annealing of the Specimens

The treatment to produce duplex ferrite/martensite structures consisted of annealing either 100 percent martensitic structures or fully tempered material in the intercritical ($\alpha + \gamma$) range. The processing involved only thermal treatment without recourse to the thermo-mechanical treatments.

Thin specimens were annealed at different pre-set temperatures within the ($\alpha + \gamma$) range, in a molten barium chloride bath into which a reagent [123] was added to prevent decarburization. This heating medium was utilized for times ranging from 5s to 10^4s, and the temperature was controlled with an accuracy of ±3°C. However, due to lack of sufficient control on the temperature for longer periods, the salt bath did not prove to be the most suitable equipment. Thin specimens were sealed in evacuated silica capsules with a partial argon pressure and annealing was carried out in a crusilite furnace. Individual thin specimens were then water quenched, either directly from the salt bath or from the furnace; in which case the capsules were immediately broken in the water. Inevitable differences in the heating and/or cooling rates of the specimens, due to the different means of heat treatment, will be taken into account when the results are compared.

3.4 Final Tempering Treatments

Experiments were carried out to investigate the effect of tempering on the microstructure and mechanical properties of the alloys after the intercritical treatments. For this purpose, Charpy specimens identical in size and previous intercritical treatment, were tempered for one hour at temperatures from 100°C to 650°C in a furnace, followed by water quenching. In these series of experiments, furnace heating was utilized for all heat treatments, namely initial quench-hardening, intercritical annealing and final tempering. This was intended to produce lower rates of heating, similar to those normally practised in industry.

3.5 Hardness Tests

The Vickers hardness testing was relied on as an assessment of strength after all treatments. The specimens were wet ground using different grades of silicon carbide abrasive paper down to 600μ. They were then polished using 3μ and 1μ diamond paste. The hardness measurements were then carried out on these polished samples using a Vickers hardness tester with either 5 or 10 Kg loads. Mean values from 10 to 15 impressions on each specimen were obtained and standard deviations from the mean were

calculated.

3.6 Light Metallography

After appropriate heat treatments, the specimens were ground by wet grinding on progressively finer SiC papers mounted on rotating wheels. Polishing was carried out on diamond laps containing decreasing particle sizes down to 0.25μm.

In different stages of the heat treatment, several solutions were used for etching the specimens, three of which appeared to be most appropriate:

1. Nitric Acid (density 1.42)	1.5cc	
+ Ethyl alcohol	100cc	
2. Hydrochloric acid	5cc	(Ref.125)
+ Picric acid	1g	
+ Ethyl alcohol	100cc	
3. Saturated aqueous solution of picric acid		(Ref.126)
+ Hydrochloric acid	15 Vol.pct.	
+ Teepol	15 Vol.pct.	

Solutions 1 and 2 were used mostly in order to reveal the martensite grains, whereas solution 3 appeared to be more effective on the prior austenite grain boundaries especially when the oil quenched Charpy specimens were embrittled by tempering at around 350°C. In some cases solutions 2 and 3 were used successively. A new technique [127] which resulted in distinguishing martensite more clearly was also tried. This technique consisted of etching the specimen first in a 4 percent picral solution and then immersing it in boiling alkaline chromate solution (8g CrO_3, 72ml H_2O and 40g NaOH).

3.7 Scanning Electron Microscopy

A Cambridge Stereoscan 600 electron microscope was utilized to observe very fine grained structures when the highest magnification on the optical microscope did not seem to be sufficient to resolve the structures clearly. This equipment was also used to study the fractured surfaces of broken Charpy specimens. The composition of the inclusions observed in these surfaces were then studied in a JEOL Stereoscan M35 electron microscope.

3.8 Transmission Electron Microscopy

Specimen preparation was commenced with 1mm thick specimens, either heat treated in the same thickness or sliced from a treated fractured Charpy specimen; the samples were ground down to a thickness of about 0.1mm using silicon carbide abrasive papers. A rotating wheel with different grades of grinding paper was utilized and an oil/water emulsion continuously lubricated and cooled the specimens. The specimens were held by double-

sided adhesive tape on a steel block. The window technique [124] was used for electro-thinning the specimens to a thickness transparent to electrons.

Several solutions were tried as electrolytes at subzero temperatures with current densities between (50-20)x10^3 amp/m^2 and finally two different solutions of nitric acid in ethyl alcohol appeared to produce reasonably thin foils with relatively large ($\sim 10\mu m$) dimensions with evenly polished and smooth areas. The first solution consisted of 1 volume of nitric acid in 2 volumes of ethyl alcohol and it was used in the initial stage to obtain rapid thinning. However, in the final stages, a stricter control on the rate of thinning was provided, using a more dilute solution containing 10 vol. pct. nitric acid in ethyl alcohol . At temperatures between -20 and -30°C with a current density of (8-12)x10^3 amp/m^2 the conditions were set most favourably.

In making the above solutions, since the action is extremely exothermic alcohol was stirred continuously and kept cooled below -20°C when acid was added in drops to maintain the solution cool.

A recent development in high resolution metallography is the facility for carrying out chemical analysis in-situ in the electron microscope using modern STEM instruments. In the present study a JEOL 120CX TEMSCAN was utilized for a qualitative analysis of the carbides collected on carbon replicas, after different heat treatments. A Philips EM 301 transmission electron microscope was used throughout the work at 100 Kv.

3.9 Replica Electron Microscopy

Carbon extraction replicas showing carbide particle size and morphology were prepared by standard techniques. The specimens were polished and etched as previously described. A fine ($\sim 400\mu$) layer of carbon was then deposited on each sample using a "Balzers" vacuum evaporation apparatus. Surfaces of specimens were then scored into 1mm squares and etching was carried out for a few seconds in a solution of 2% bromine in ethyl alcohol. The specimens were then washed in ethyl alcohol. Finally the carbon films were floated off by carefully immersing the specimens in distilled water and were collected on 400 mesh copper electron microscope grids of the appropriate diameter to fit into the electron microscope specimen holder.

3.10 Identification of Precipitating Phases

The composition and structure of precipitated particles in a number of specimens were investigated by two different techniques. Initially the precipitates were extracted electrolytically using 10% HCl in alcohol and maintaining a current density of 10^3 amp/m^2 for 20 hours. The extract was washed successively in distilled water, alcohol and ether, and was allowed to dry completely prior to placing in a 0.3 mm capilliary glass tube. X-ray diffraction patterns were obtained using Cu K_α radiation and a Straumanis type camera. The calculated lattice parameter values were compared with

the lattice parameters in the ASTM card index.

3.11 Alloy Partitioning Experiments

Electron microprobe analysis was carried out on some of the specimens after intercritical treatments, to detect the concentration of some of the alloying elements in different phases. Specimens of both sizes were examined in the intercritically treated condition before and after tempering.

3.12 Charpy V-Notch Tests

Standard Charpy specimens (10x10x55 mm) were prepared and a 45°, 2mm deep notch with a root radius of 0.25mm was machined after the final heat-treatment to avoid any notch root oxidation or cracking during the course of treatment. Room temperature Charpy impact tests were in most cases carried out to determine the toughness of the materials.

Chapter 4

Results

Section A En24 Steel

4.1 Preliminary Treatments

4.1.1 The Effect of Quenching Rate

As mentioned in the previous chapter, specimens of different sizes were heat treated in either a crusilite furnace or a salt bath and were quenched in either water or oil. The differences in the specimen dimensions and in heat treatment procedures produced effects on the properties of the heat-treated material which in some cases were quite considerable. For example the hardness of an identical En24 Charpy size specimen solution treated for one hour at 835°C in the furnace decreased from 730 Hv to about 630 Hv when the quenching media was changed from water to oil. This decrease may be attributed to the extent of autotempering of martensite as a consequence of the lower cooling rate in oil. These effects will be mentioned throughout the presentation of results where applicable.

4.1.2 Water Quenched Specimens

The first series of hardness tests were carried out on the thin specimens, sliced from material that was solution treated for one hour at 835°C and water quenched. The thin specimens were annealed for 20 h at different temperatures in the furnace and water quenched. Table 4.1 and Fig.4.1 show the effect of annealing temperature on the hardness of the specimens.

4.1.3 Austenitizing Temperature

A number of experiments were carried out in order to determine the extent to which the hardness could be altered by changes in the quenching medium and in the temperature at which the specimens were solution treated, both before and after the intercritical treatment. Charpy size bars of En24 steel were austenitized at either 835°C or 950°C for one hour and oil quenched. They were then either sliced for intercritical treatment or were tempered at 700°C for 5 hours before being sliced, to produce the fully tempered properties before intercritical treatment. Table 4.2 shows the result of hardness measurements on the surface of the specimens. It can be seen from Table 4.2 that a higher austenitizing temperature had little effect

Table 4.1 The effect of annealing at different temperatures followed by water quenching on the hardness of En24 specimens; Initial condition: water-quenched from 835°C

Annealing Temperature, °C	As-quenched from 835°C	700	710	720	730	740	760	780	800
Hardness, Hv	730	210	201	275	331	600	740	750	750

Table 4.2 The effect of austenitizing temperature prior to intercritical treatment on the hardness of En24 steel

Final Annealing Temperature°C	835°C Solution Treatment		950°C Solution Treatment	
	As-Quenched Hv	OQ+Tempered Hv	As-Quenched Hv	OQ+Tempered Hv
No anneal	633	274	629	246
735°C+OQ	321	333	319	322
750°C+OQ	551	537	574	505
765°C+OQ	627	664	661	652
780°C+OQ	683	675	660	665

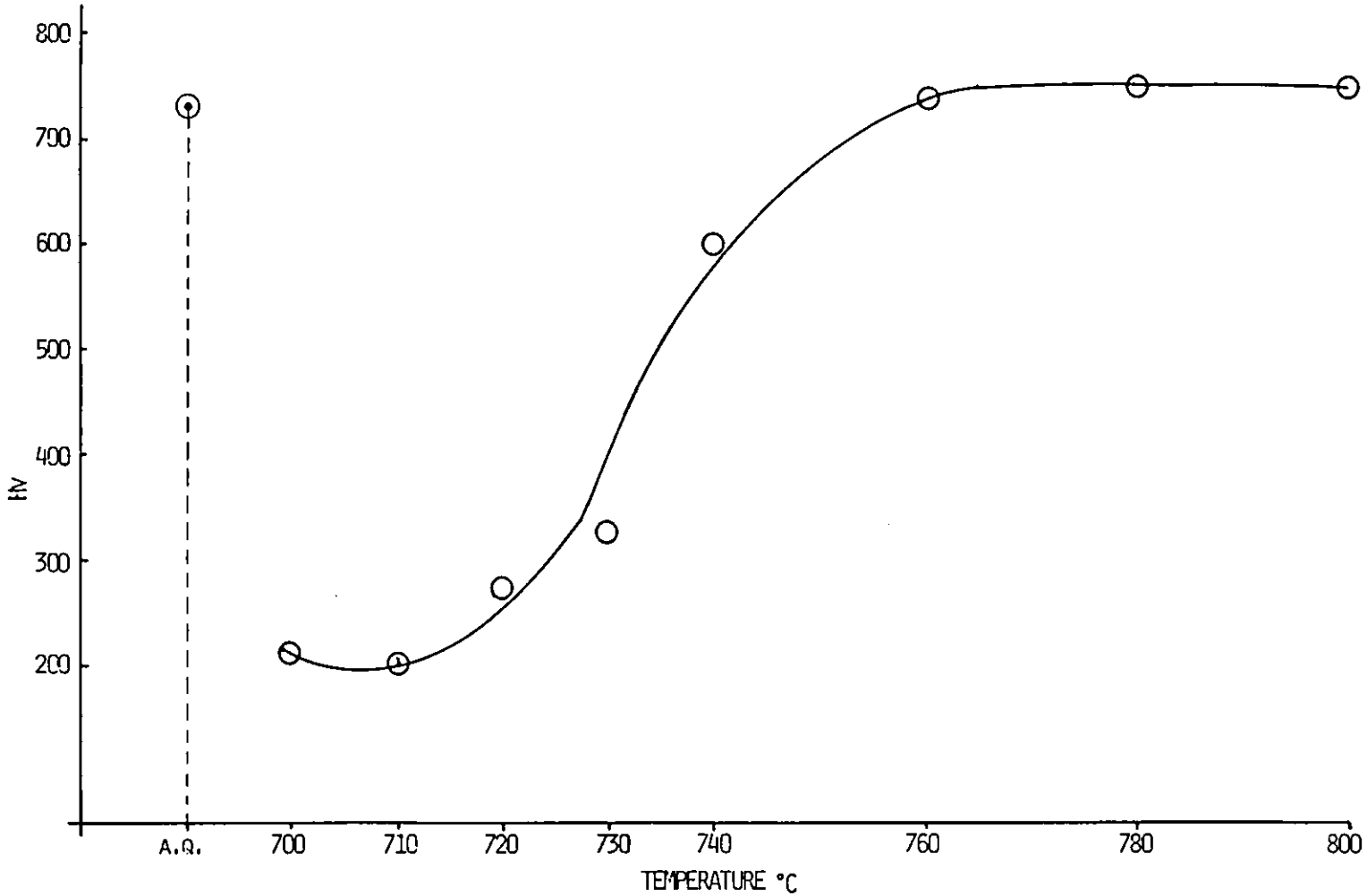

FIG. 4.1 - EFFECT OF ANNEALING TEMPERATURE ON THE HARDNESS OF AS-QUENCHED EN 24 STEEL

on the hardness of the as-quenched material and the effect on the subsequent tempering and/or intercritical treatment was thought to be within the experimental error. The lower austenitizing temperature, i.e. 835°C, was then chosen as standard for En24 in order to attain a lower rate of austenite grain growth.

Comparing Tables 4.1 and 4.2, a decrease in the hardness of the as-quenched material caused by a decrease in the cooling rate can be seen. This effect, i.e. attaining higher hardness values after a faster quench was diminished when the material was subsequently annealed at lower temperatures within the ($\alpha + \gamma$) range.

4.2 The Initial Conditions

4.2.1 As Quenched Material

En24 is a high-strength medium-carbon low alloy steel used extensively in the quenched and tempered condition. The hardenability of this alloy [128] is high enough to produce 100 pct martensite in a 10 mm diameter bar, even when air cooled from the austenitizing temperature (Fig 4.2).

In the present work the austenite grain size prior to oil-quenching alloy was measured by the automatic counting technique (Quantimet) and in about 1000 grains the mean size was found to be ~250 square microns, corresponding to the ASTM grain size number 9 (16-18μm diameter). Plate 1 is a typical micrograph from a polished and etched section of a Charpy size specimen quenched in oil.

The martensite structure, in most of the areas examined was, too fine to resolve in the optical microscope. However, when observed in the electron microscope, the main characteristics of the fine structure were revealed. The structure consisted of a mixture of both lath and plate martensites. A tangled dislocation substructure and parallel long laths of about the same size (Plate 2.a) are characteristics of the lath type; whereas nonparallel fine plates and a large range of plate sizes (Plate 2.b) are indications of the plate type martensite [27].

Fine internal twins of the $\{112\}_M$ type, first observed by Kelly and Nutting [28] were revealed (Plate 3) in plate martensite. Another feature of the structure was a rather high population of finely dispersed undissolved particles which were observed both in scanning (Plate 4.a) and transmission electron microscopy (Plate 4.b) and in carbon replicas obtained from a polished and etched cross section of as-quenched En24 steel. These techniques revealed that the particles were approximately spherical in shape and up to 0.25 micron in size (Plate 4.c). Although at first sight the particles seemed to be randomly precipitated, the replica revealed signs of

105 **S CONTINUOUS COOLING TRANSFORMATION DIAGRAM**

$1\frac{1}{2}$ Ni Cr Mo

AUSTENITISED AT 850 C

PREVIOUS TREATMENT ROLLED, SOFTENED 650 C 1 h

ANALYSIS Wt% (See note on page 8)

C	Si	Mn	P	S	Cr	Mo	Ni	Al	Nb	V
0.40	0.25	0.60	0.020	0.020	1.20	0.30	1.50	—	—	—

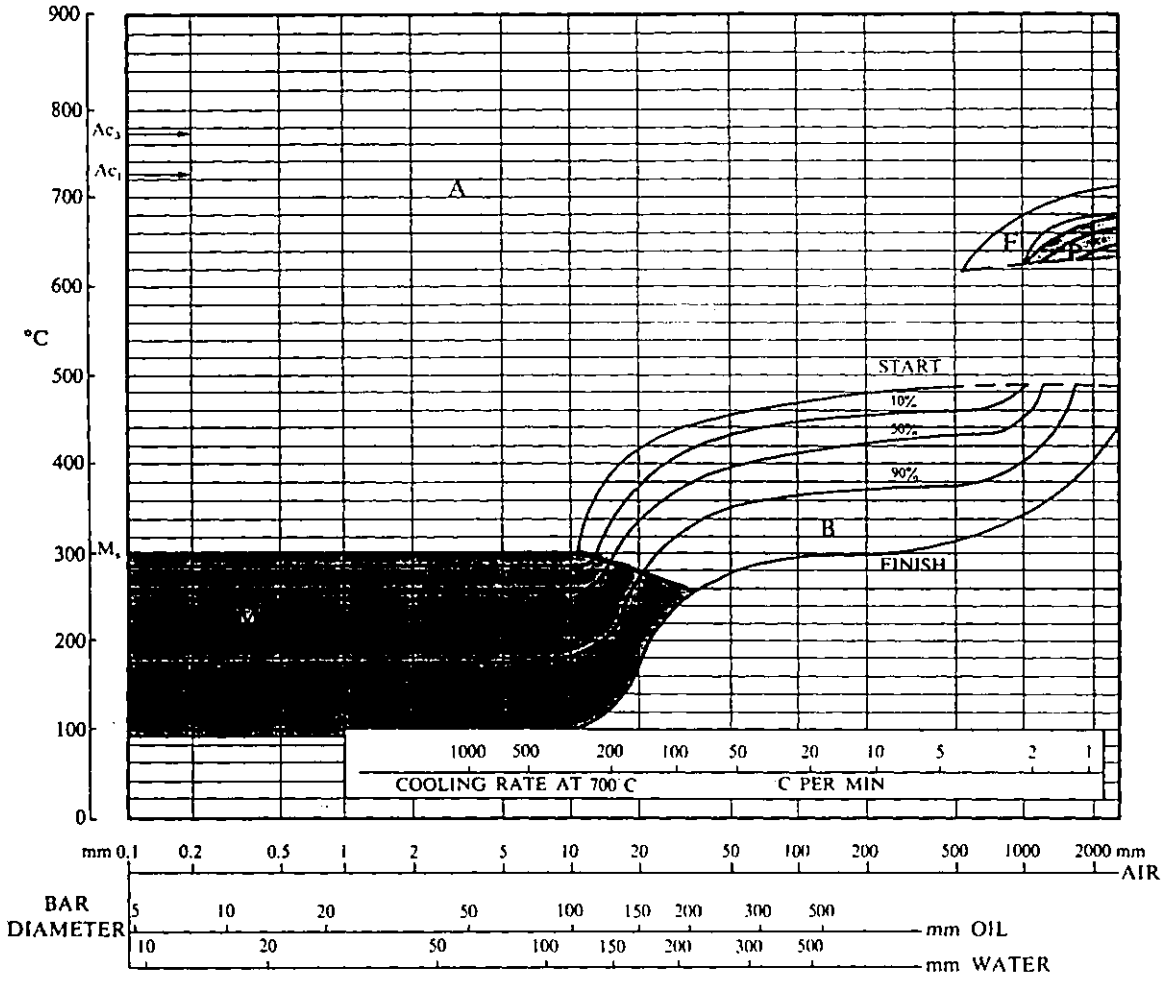

FIG. 4.2 - CONTINUOUS COOLING DIAGRAM FOR EN24 STEEL (AFTER REF.128)

Plate1-As-quenched En24 steel ⊢15μ⊣
Optical micrograph Austenite grain boundary etch+Nital

Plate 2-a-Lath ⊢0.5μ⊣
martensite in as-quenched En24 steel

Plate 2-b-Plate and lath ⊢1μ⊣
martensite in oil quenched En24

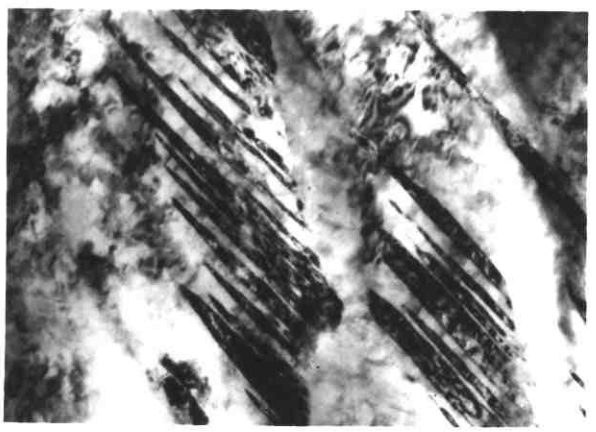

Plate3-a-Bright field⊢0.2μ⊣
showing internal twins x100K

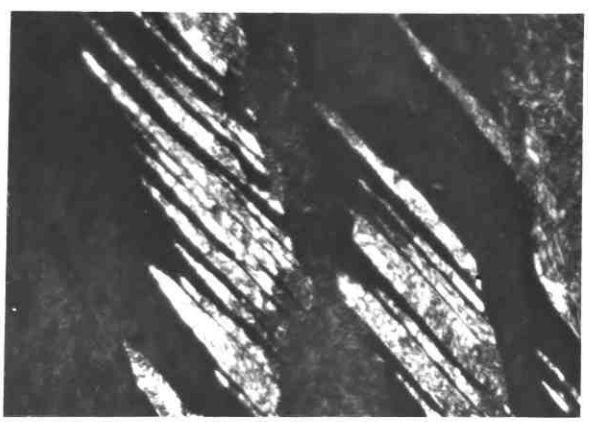

Plate 3-b-High resolution dark field of twins

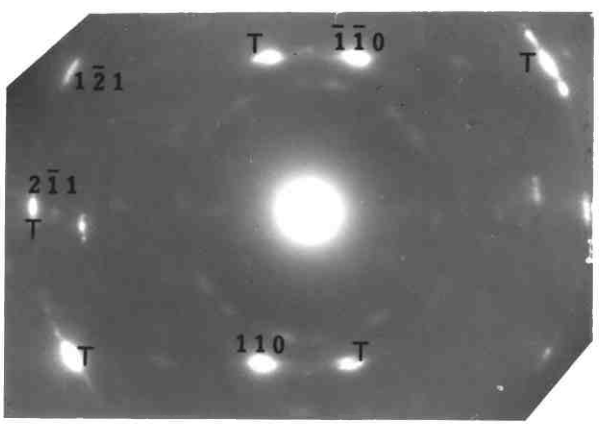

Plate 3-c-Indexed selected area diffraction pattern
[1̄13]αtwin zone

Plate 3(a-c)-Internal twins in as-quenched En24 martensite plate

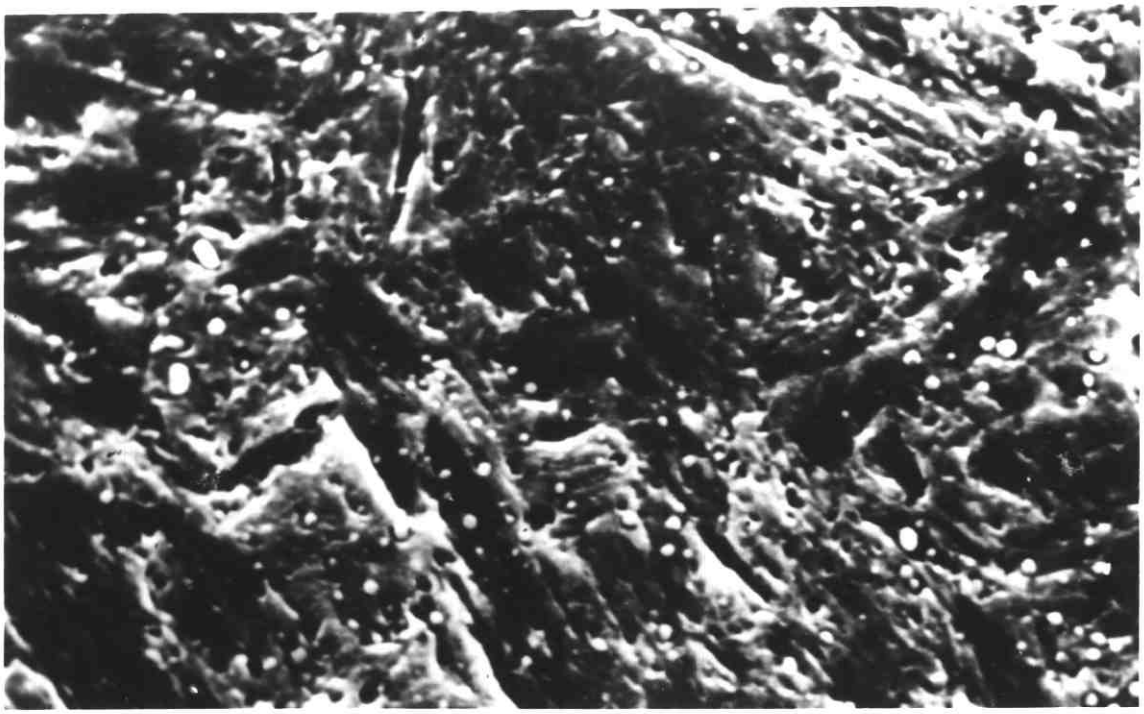

Plate 4-a-As-quenched En24 steel,polished and etched,S.E.M ⊢— 2μ —⊣

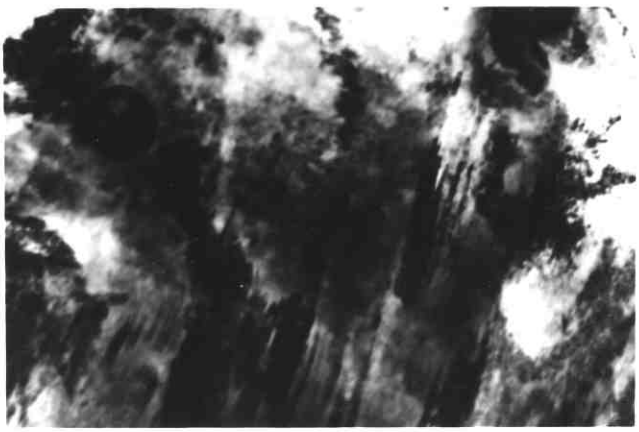

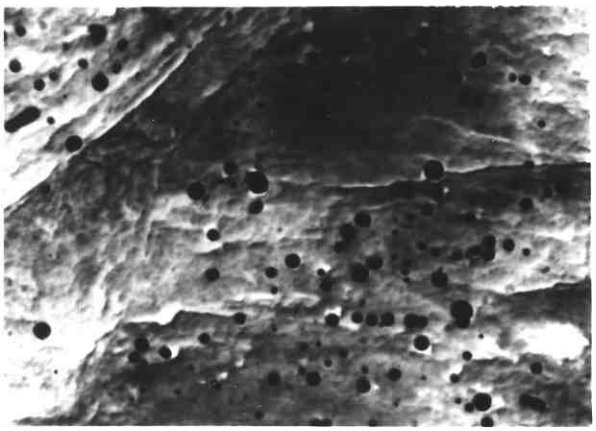

4b- Thin foil T.E.M. ⊢—0.5μ—⊣ 4c-Carbon extraction replica ⊢—2μ —⊣

Plate 4(a-c)-Undissolved carbide particles in as-quenched En24 steel

Plate 5- Autotempered martensite in as-quenched En24 steel T.E.M. ⊢0.2μ—⊣

an irregular network on which the particles were formed. Microanalysis carried out on the particles collected on carbon replicas, utilizing the TEMSCAN showed that the particles contained Fe and Cr, while smaller peaks for Si and Mo were also detected (Fig.4.3). The crystal structure of the carbides was examined by both electron diffraction and X-ray techniques. In both methods M_3C (orthorhombic) was the only structure positively identified. Table 4.3 compares the standard values for Fe_3C with those calculated from the X-ray diffraction results. A careful search for retained austenite in the areas examined resulted in virtually no sign of this phase.

4.2.2 Quenched and Tempered Material

The main characteristics of the material after a heavy tempering treatment (5h at 700°C), which produced a different starting structure in which the effect of intercritical treatments were studied. The tempered structure mainly consisted of fine-grained recovered ferrite and intra-lath carbides (Plate 6.a); however, in some areas, evidence of partial recrystallization was observed (Plate 6.b). Ferrite grains observed were mostly acicular-shaped with an average width of about 0.5 micron and a few microns long (Plate 6.c). As a result of high temperature tempering the precipitates are expected to be spheroidized; however, rod-shaped carbides were frequently observed both within the grains and on the grain boundaries (Plate 6.d).

The only carbide identified through X-ray diffraction was M_3C (orthorhombic Fe_3C containing substitutional alloying elements); the search for other carbides was not conclusive. The size of the carbides fell within a very wide range, starting from a very fine particle size up to about 0.5 micron in diameter and of the same order of length (Plate 6-d).

Prolonged tempering of the quenched material at this temperature resulted in a further spheroidization of the carbides and progressive recrystallization of the ferrite grains. Plate 7 is a scanning electron micrograph from a specimen held at 700°C for 20 hours. It can be seen that both carbide and ferrite grains are approximately equiaxed and some carbide particles were $\sim$ 1μm in diameter.

4.3 Rapid Intercritical Heat Treatments

The A_1 and A_3 phase boundaries for En24 are suggested to be about 727°C and 780°C respectively. Charpy size specimens were either oil-quenched from 835°C or quenched-and-tempered at 700°C for 5 hours, before being cut into 1 mm thick slices. They were then heated at pre-set intercritical temperatures, namely 735°,750°,765°C and for times from as short as 5 seconds to several hours. Treatments were also given at 780°C

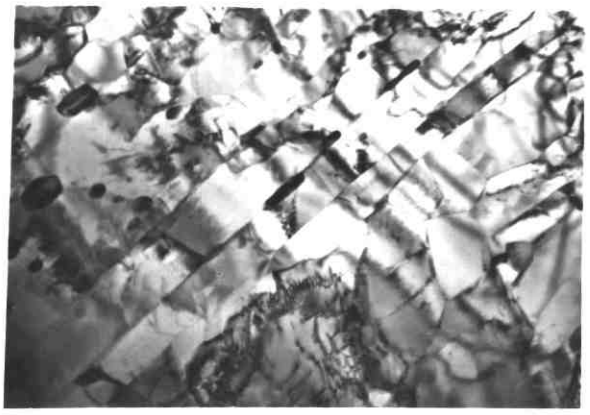

6-a-Recovery of the laths ⊢0.5μ⊣

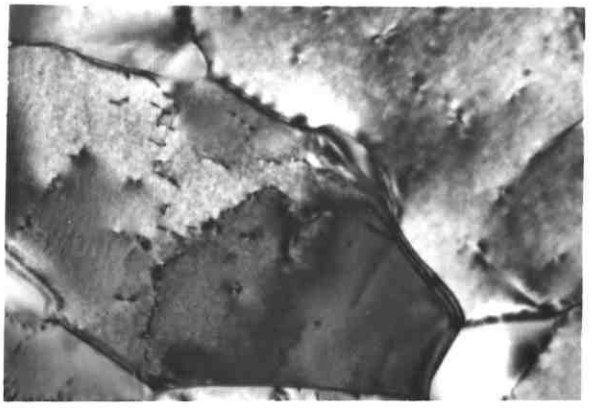

6-b-Recrystallized α grains ⊢0.2μ⊣

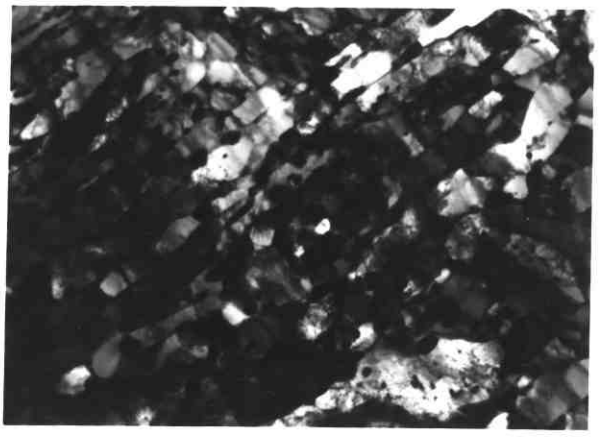

6-c-Partially recovered laths and carbides ⊢— 2μ —⊣

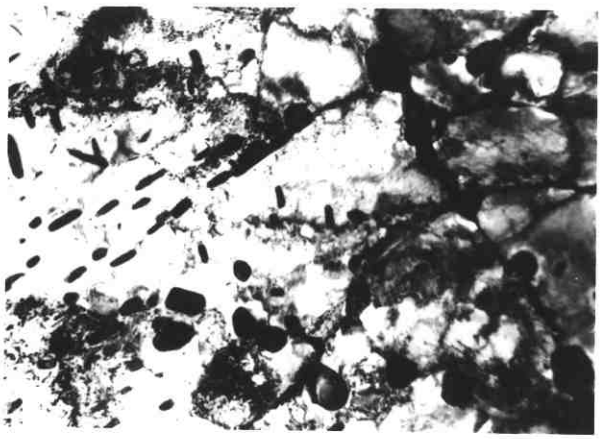

6-d-Rod-shaped and equiaxed carbides within the grains and on the grain boundaries,thin foil TEM ⊢—1μ —⊣

Plate 6(a-d)-Quenched-and-tempered(5h700°C)structure,En24 steel,T.E.M.

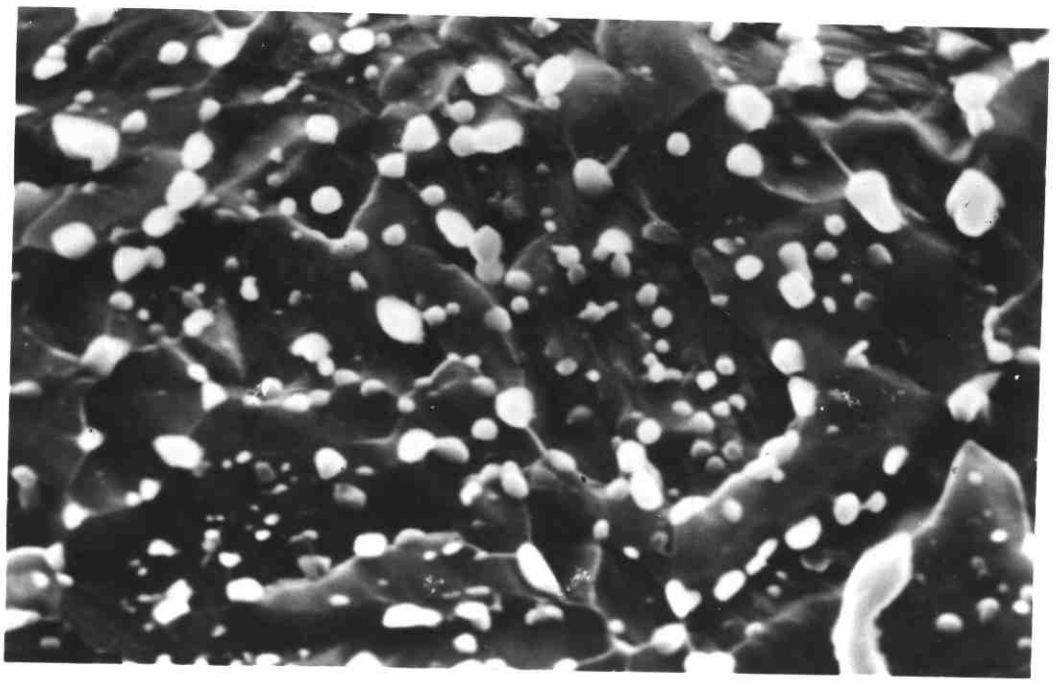

⊢— 2μ —⊣

Plate 7- En24 steel tempered for 20 hours at 700°C

Coarse equiaxed carbide particles on α grain boundaries
Polished and etched specimen,scanning electron micrograph

Table 4.3 Calculated d-values from X-ray analysis of carbides extracted from En24 steel and the equivalent Fe_3C planes with the relevent standard d-values Cu K_α radaiation λ=1.54178

Fe_3C :Orthorhombic; a_o=4.524A° b_o=5.088A° c_o=6.741A°

order of reflection	observed d-value A°	standard d-value A°	h k l	order of reflection	observed d-value A°	standard d-value A°	h k l
1	3.414	3.381	1 1 0	21	1.633	1.640	2 2 1
2	3.003	3.022	1 1 1	22	1.613	1.600	0 1 4
3	2.772	2.810	0 1 2	23	1.580	1.578	1 2 3
4	2.714	2.703	1 0 2	24	1.522	1.521	2 1 3
5	2.556	2.544	0 2 0	25	1.508	1.508	3 0 0
6	2.374	2.380	0 2 1	26	1.471	1.472	3 0 1
7	2.254	2.262	2 0 0	27	1.402	1.405	0 2 4
8	2.225	2.247	0 0 3	28	1.387	1.377	3 0 2
9	2.194	2.218	1 2 0	29	1.371	1.357	2 3 0
10	2.125	2.145	2 0 1	30	1.348	1.348	0 0 5
11	2.099	2.107	1 2 1	31	1.327	1.329	3 1 2
12	2.062	2.067	2 1 0	32	1.281	1.274	3 2 1
13	2.038	2.031	0 2 2	33	1.241	1.250	0 4 1
14	2.010	2.013	1 0 3	34	1.216	1.216	3 1 3
15	1.973	1.976	2 1 1	35	1.191	1.191	0 2 5
16	1.908	1.878	2 0 2	36	1.160	1.162	2 0 5
17	1.875	1.872	1 1 3	37	1.151	1.151	1 4 2
18	1.847	1.853	1 2 2	38	1.140	1.131	4 0 0
19	1.735	1.762	2 1 2	39	1.116	1.115	4 0 1
20	1.702	1.691	2 2 0	40	1.098	1.097	0 1 6
				41	1.051	1.053	2 4 2

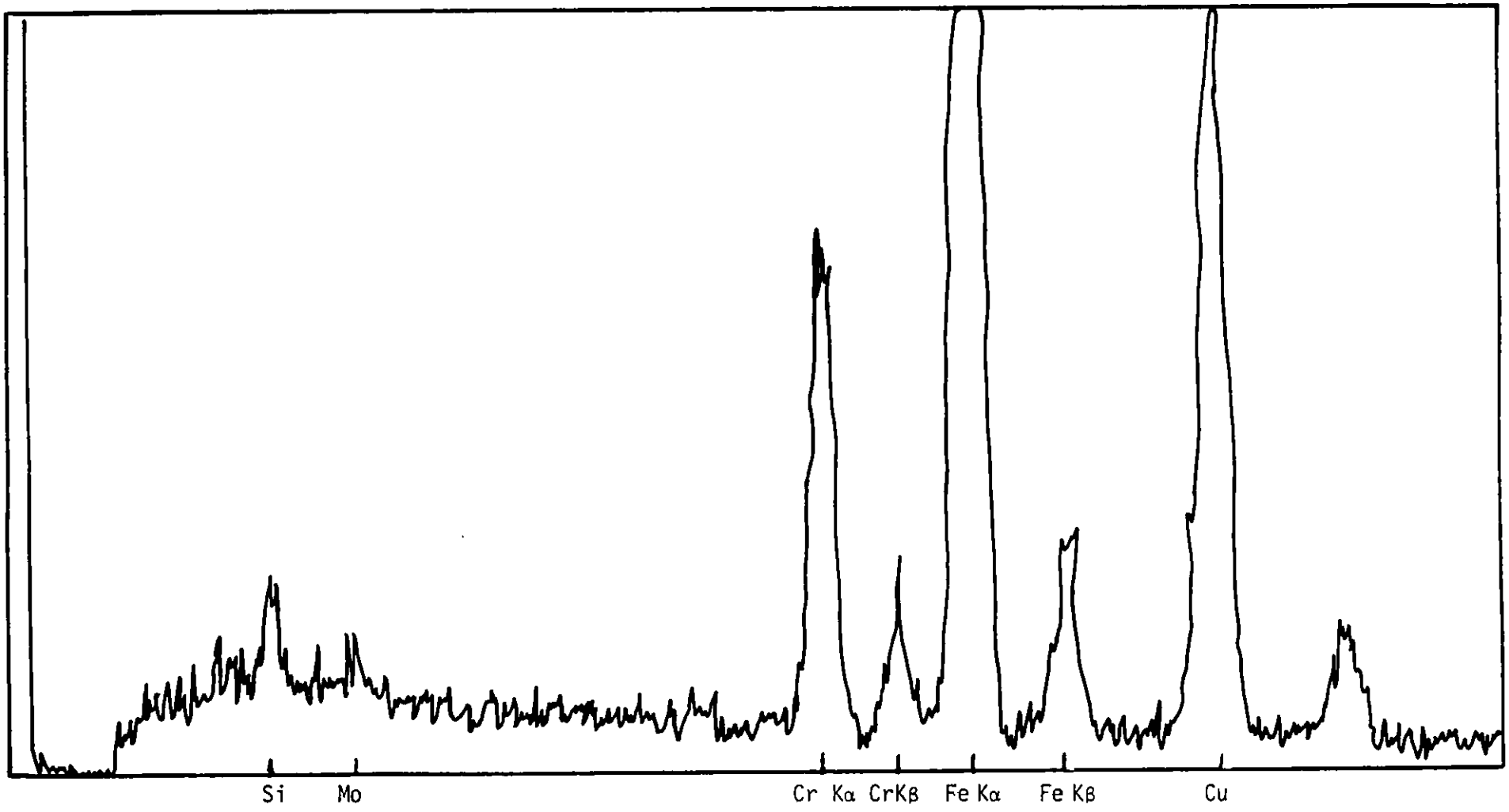

FIG. 4.3 - SPECTROGRAM SHOWING THE ELEMENTS IN AN UNDISSOLVED CARBIDE IN EN24 STEEL, TEMSCAN MICROANALYSIS

(which is estimated to be just within the austenite range) and at 720°C (which is a *sub-critical* temperature). Salt bath heating resulted in a relatively high heating rate.

Due to the restrictions in the temperature stability of the equipment, longer heat treatment times had to be carried out in a furnace. The thin specimens were protected from oxidation by sealing in evacuated silica capsules with a partial argon atmosphere. All of the thin specimens were water-quenched after annealing at the above temperatures.

4.3.1 Heating at 720°C

As expected, this temperature was found to be below the critical range. In the as-quenched specimens heat-treated at this temperature for the times studied, a progressive tempering of martensite was observed. Plate 8 shows an early stage of this process (5s at 720°C) in which the precipitation of cementite started on the lath boundaries and inside the laths. Plate 9 is the same as-quenched material after being tempered for 10^5 seconds at 720°C. The ferrite grains were observed to be partially recovered.

The carbide particles were spheroidized and had grown considerably. This resulted in a progressive softening to about 271 Hv when it was held at the temperature for 10^5 seconds. (Fig.4.4 and Table 4.4). As a result of heating the previously tempered material at this temperature, the recovery and recrystallization of ferrite and growth and coarsening of carbides developed further (Plate 10). Consequently the hardness slightly dropped from 270 Hv to 244 Hv (Fig.4.4).

4.3.2 Heating at 735°C

a. Hardness Response

Heating the as-quenched thin En24 specimens to 735°C for times shorter than 10s resulted in a substantial decrease in hardness to about 380 Hv (Table 4.5). This softening was followed by a sharp increase in hardness within the period 30-100 seconds up to a value approximately corresponding to that of the water-quenched material (Fig.4.5). Beyond ~1000 s a softening started to occur followed by a slight increase in hardness from a minimum value of ~480 Hv. As indicated earlier, for long heat treatments ($>10^4$s), furnace heating was utilized. The as-quenched specimens treated for a similar time (10^4s) in the furnace, revealed a lower hardness value (441 Hv) than those annealed in the salt bath (513 Hv).

The initially tempered material annealed at 735°C took longer before revealing an increase in hardness. For times up to ~30s the hardness was similar to the starting condition (Table 4.5). This was followed by a sharp increase in hardness within the period 30 to 300s. A peak hardness of

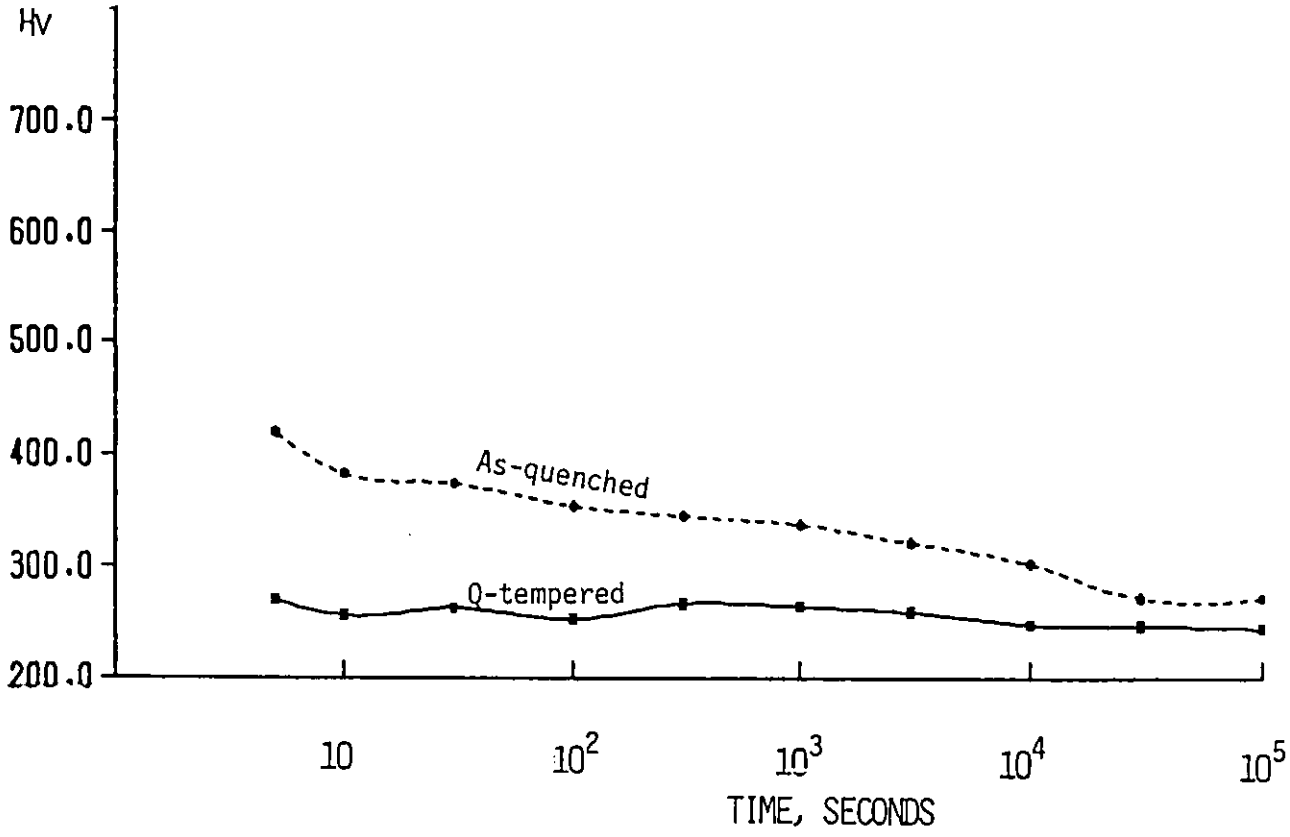

FIG. 4.4 - HARDNESS VS HEATING TIME AT 720°C FOR EN 24 STEEL IN AS-QUENCHED AND Q-TEMPERED CONDITIONS

Table 4.4 Pyramidal Vickers hardness values for oil-quenched and quenched-and-tempered En24 steel annealed at 720°C

Starting Condition	Annealing Time s										
	0	5	10	30	10^2	$3x10^2$	10^3	$3x10^3$	10^4	$3x10^4$	10^5
1h 835 °C+OQ	633	419	382	373	353	344	337	320	302	272	271
OQ +5h 700°C	270	270	256	263	252	266	264	259	248	247	244

Table 4.5 Pyramidal Vickers hardness values for oil-quenched and quenched-and-tempered En24 steel annealed at 735°C

Starting Condition	Annealing Time s										
	0	5	10	30	10^2	$3x10^2$	10^3	$3x10^3$	10^4	$3x10^4$	10^5
1h 835°C + OQ	633	405	380	648	747	752	749	580	513	478	496
OQ + 5h 700°C	270	260	269	275	436	619	649	490	410	439	467

Table 4.6 Pyramidal Vickers hardness values for oil-quenched and quenched-and-tempered En24 steel annealed at 750°C

Starting Condition	Annealing Time s										
	0	5	10	30	10^2	$3x10^2$	10^3	$3x10^3$	10^4	$3x10^4$	10^5
1h 835°C + OQ	633	390	388	696	744	754	746	747	738	715	731
OQ + 5h 700°C	270	259	251	281	473	650	675	676	659	589	607

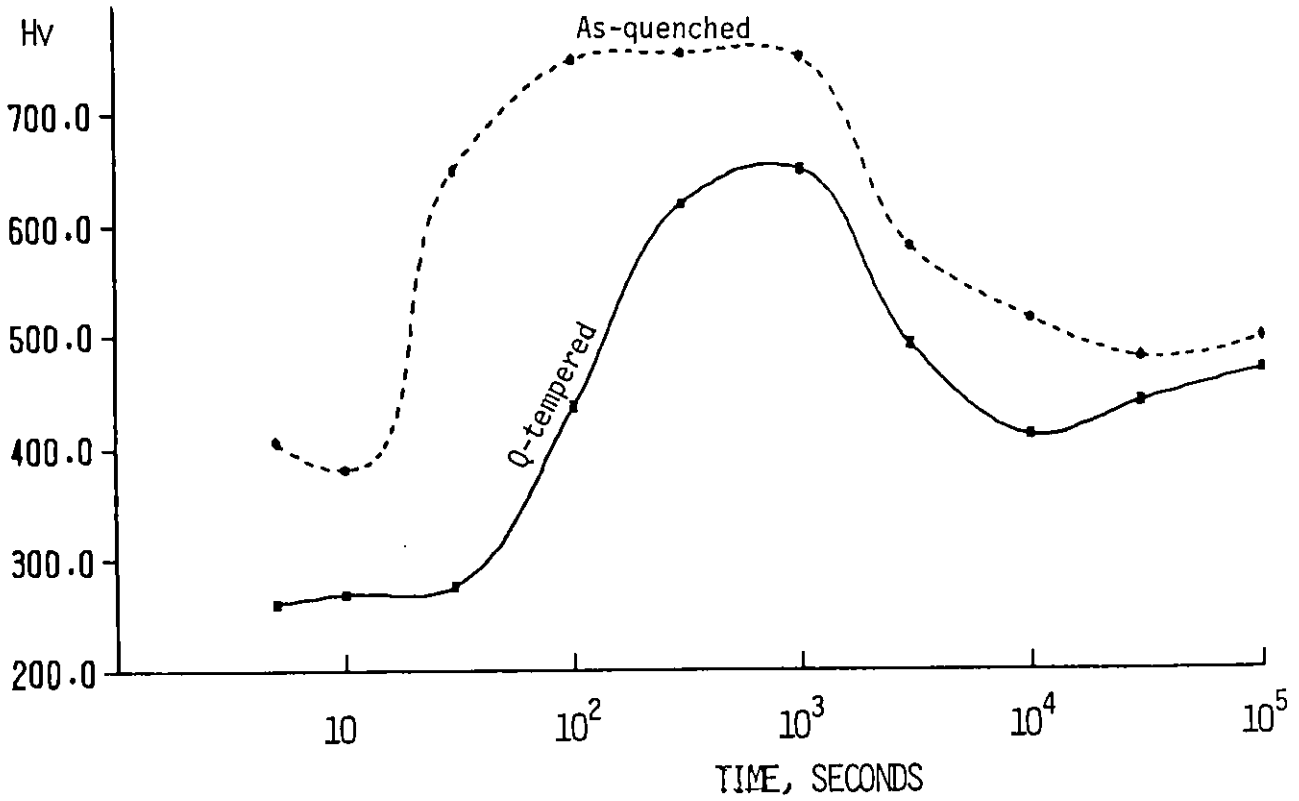

FIG. 4.5 - HARDNESS VS HEATING TIME AT 735 °C FOR EN 24 STEEL IN AS-QUENCHED AND Q-TEMPERED CONDITIONS

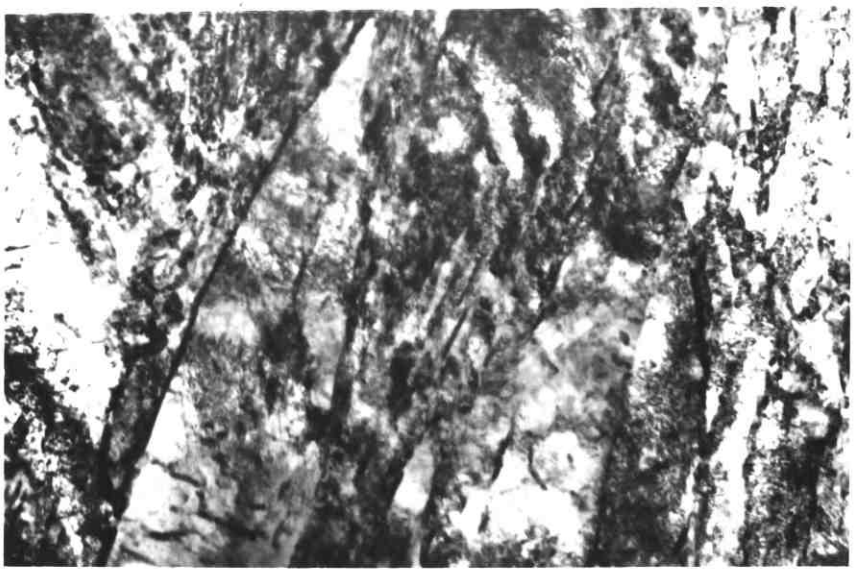

Plate8-OQ.En24 steel,5s at 720°C+WQ ⊢—0.5μ—⊣

Plate9-OQ.En24 steel,10^5s at 720°C+WQ ⊢—0.4μ—⊣

Plate10-QT.En24 steel,10^5s at 720°C+WQ ⊢—0.5μ—⊣

~650 Hv was observed after 10^3 s (Fig.4.5). The change in the heating medium for 10^4s treatment of pre-tempered material resulted in a small difference in hardness. Salt bath and furnace annealing produced values of 410 Hv and 397 Hv respectively. An increase in hardness to 467 Hv was observed (Table 4.5) after 10^5s.

b. Microstructure

The as-quenched structure heated at 735°C for times shorter than 10s was rapidly tempered on heating to this temperature (Plate 11.a). On further annealing for periods up to 300 s, optical microscopy revealed a relatively fine (~10μm) prior austenite grain structure with submicron particles (Plates 11.b and c). After 10^3s at this temperature banding was observed to occur (Plate 11.d). Some lighter etched grains resembled those treated for shorter times while a fine lamellar structure was resolved within the darker regions. Annealing the specimens for 10^4s resulted in a coarser lamellar structure (Plate 12.a). The ferrite/martensite laths were coarser after furnace treatments for similar times (cf Plates 12.a and b). The width to length ratio of the laths appeared to increase as a result of prolonged annealing at this temperature (cf Plates 13.a and b). In the structure obtained after 65 h at 735°C (Plate 13.b) the volume fraction of martensite (black) was determined by automatic counting techniques (Quantimet). This was measured in 25 frames of 100 x 100 μm and an average value of ~70 percent was obtained. The hardness of material water quenched after 65 h at 735°C was 475 Hv. Transmission electron microscopy revealed ferrite and martensite laths of submicron thickness after 10^4s treatment in the salt bath. Ferrite grains were observed to be heavily dislocated while internal twinning was frequently detected in the martensitic regions (Plate 14).

The previously tempered material maintained its initial structure after short times at 735°C (Plate 15.a). Upon longer annealing the martensite transformed on quenching contained a high twin density (Plates 15b,c and d). Submicron undissolved carbides were frequently observed after relatively long time (10^4 s) annealing (Plate 15.c). However, the particles were more difficult to trace after prolonged annealing (Plate 15.d). The ferritic areas examined revealed dislocation densities unusual for a fully recovered material.

4.3.3 Heating at 750°C

a- Hardness Response

The oil-quenched, thin sliced En24 specimens held in the salt bath at 750°C, exhibited a similar hardness response as when held at 735°C. The two main differences were:

11-a ⊢10μ⊣

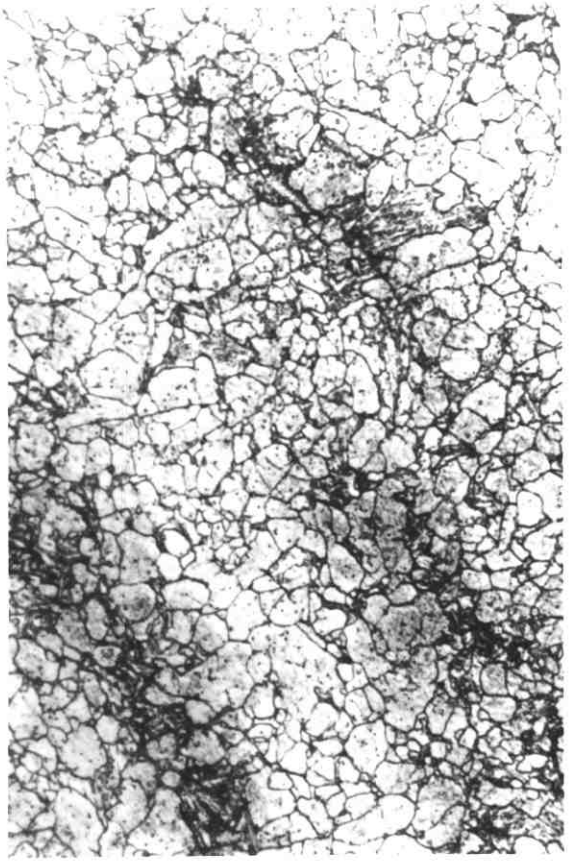

11-b ⊢20μ⊣

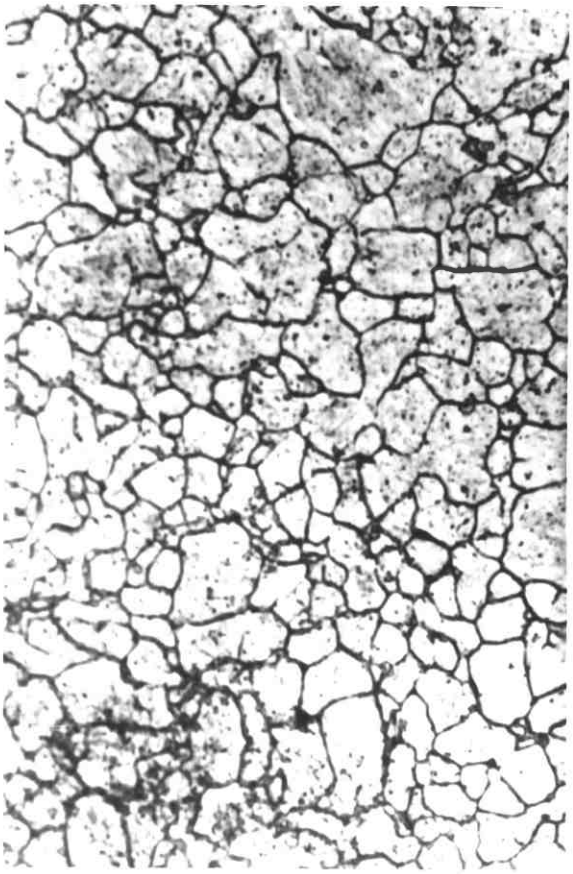

11-c ⊢10μ⊣

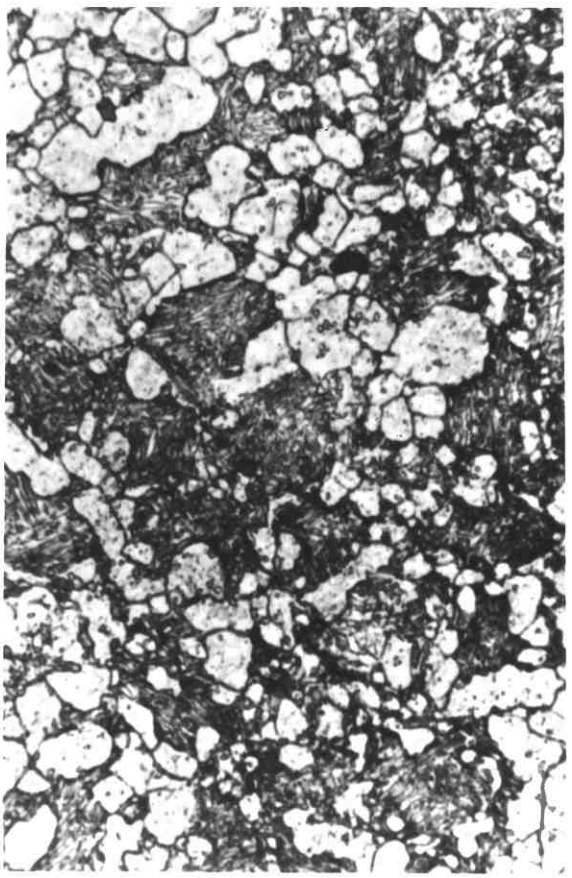

11-d ⊢10μ⊣

Plate11-As-quenched En24 steel heated at 735°C(salt bath)for:
a-10s,b-30s,c-300s,d-1000s +WQ
Optical micrographs ,austenite grain boundary etch

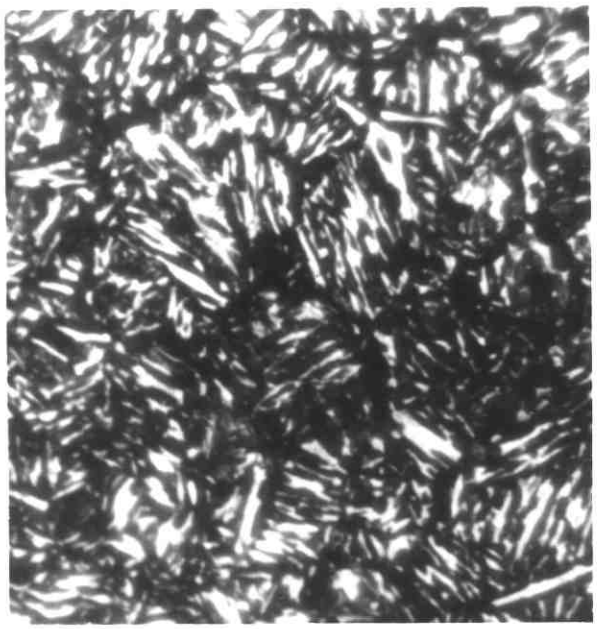

12a-OQ.En24, 10^4s735°C(S.B.)+WQ ⊢10μ⊣ 12b-OQ.En24, 10^4s735°C(Furn.)+WQ

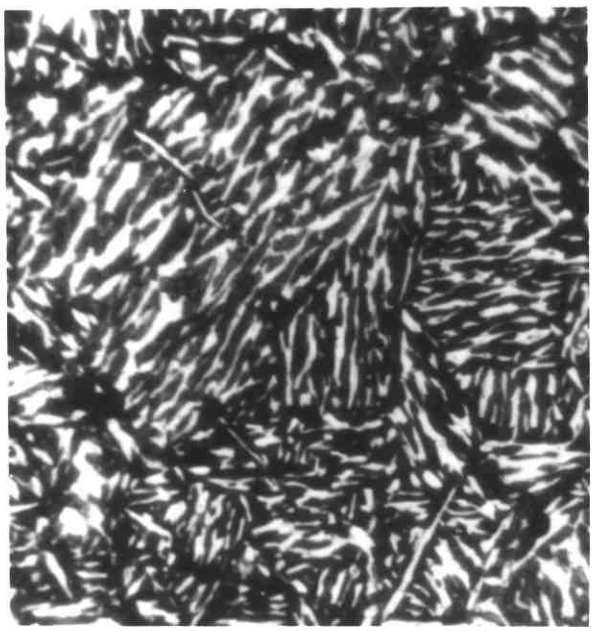

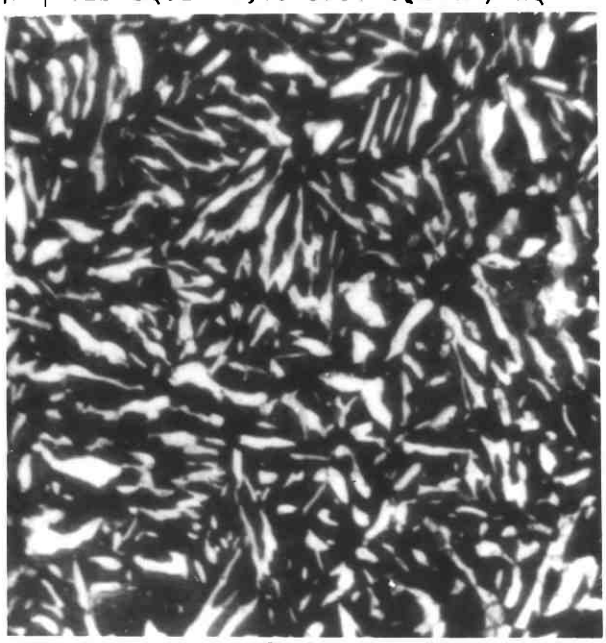

13a- $3X10^4$s(∿8h)+WQ 13b- $234X10^3$s(65h)+WQ

Plate13- OQ.En24 steel, held at 735°C(furnace)for the times indicated

Plate14-OQ.En24 steel, heated fcr 10^4s at735°C(S.B.)+WQ ⊢0.5μ⊣

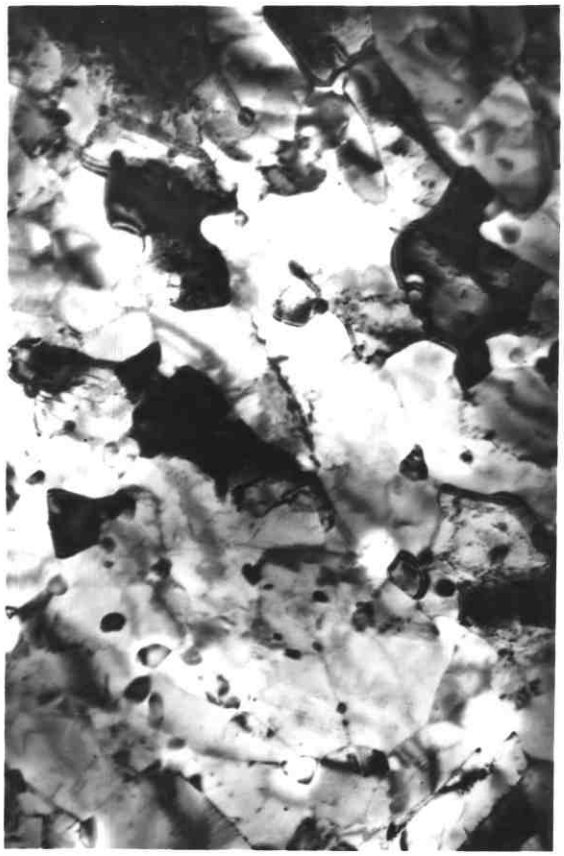

15-a ⊢—— 1μ ——⊣

15-b ⊢0.25μ⊣

15-c ⊢—0.4μ——⊣

15-d ⊢0.25μ⊣

Plate15-Quenched and tempered En24 steel,held at 735°C for:
a-30s,b-10^3s,c-10^4s,d-65h($234X10^3$s),+WQ

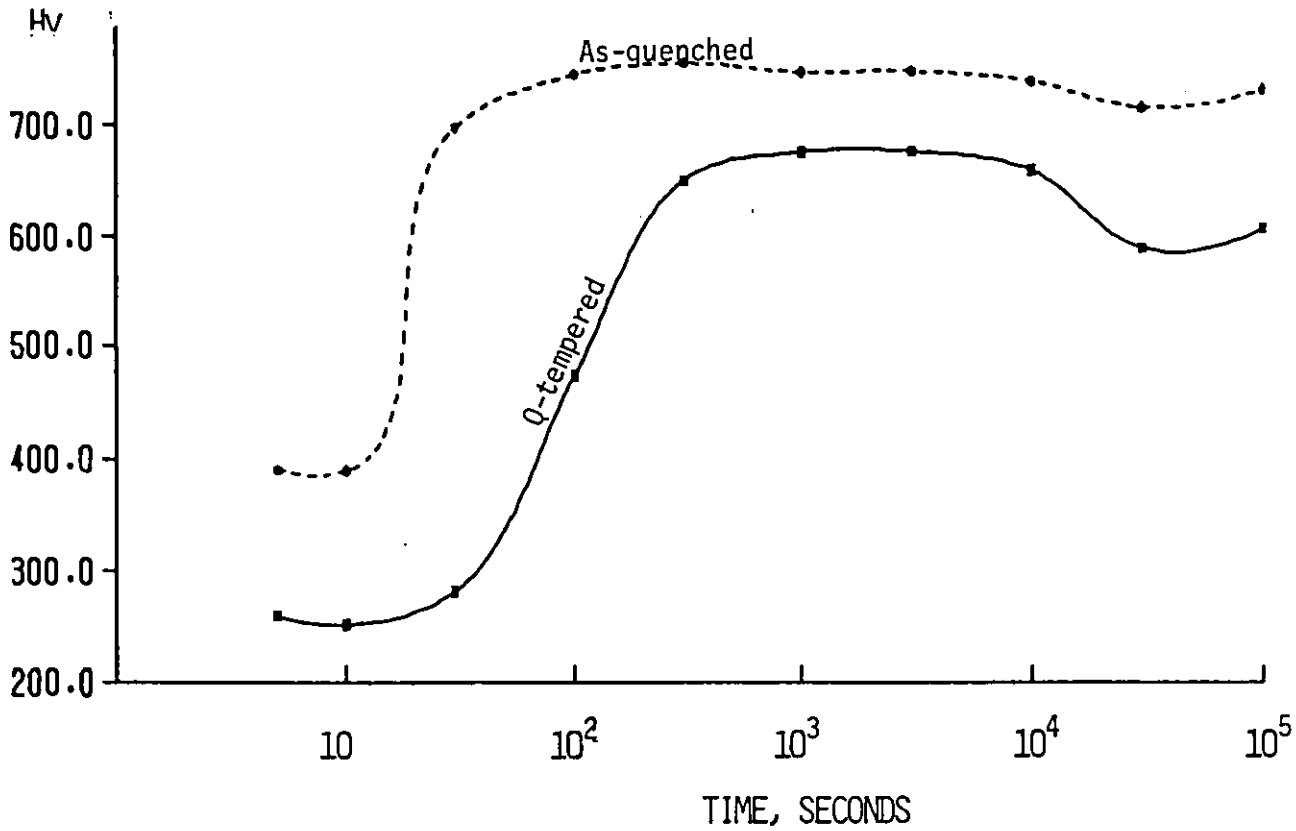

FIG. 4.6 - HARDNESS VS HEATING TIME AT 750°C FOR EN 24 STEEL IN AS-QUENCHED AND Q-TEMPERED CONDITIONS

a-Each stage of the process terminated in a shorter time at 750°C
b-The softening on long-time annealing at this temperature was less pronounced.

For the shortest period examined, i.e. 5 s, the specimens held at 750°C were ~ 15Hv softer than those held at 735°C (Fig.4.6 and Table 4.6). However, this softening was more rapidly counteracted at 750°C. After 10s the difference in hardness values is small, (388 Hv for 750°C vs 380 Hv for 735°C) but after only 30 s the higher rate of hardening in the material held at the higher intercritical temperature was more positively observed (696 Hv for 750° vs 648 for 735°C).

For the period between 100-1000 s, the as-quenched material held at 750°C, exhibited the same level of hardness as when held at 735°C (i.e.~ 750 Hv). Furthermore, this level was maintained for longer times of up to 10^4s. A small minimum of 715 Hv was observed after $3x10^4$s annealing in the furnace, but the same heating medium caused a rehardening to 731 Hv when the material was held for 10^5s.

The pre-tempered thin specimens, when subjected to 750°C intercritical annealing also exhibited some similarities with the 735°C treatment, e.g.:

a. A lower hardness value was always obtained when compared to the as-quenched material treated for the same period at the same temperature (Fig. 4.6)

b. The rate of hardness increase was lower in the case of pre-tempered material,

c. The final softening, due to long-term intercritical treatment in the furnace, was more extensive in the case of the pre-tempered material (cf Fig.4.5 and 4.6). However in either starting condition, i.e. OQ or QT, this final softening was smaller in the case of treating at 750°C. Also, if similar starting conditions were compared, it was noted that annealing the pretempered material in the salt bath at 750°C caused a higher rate of hardness increase and the hardness of material treated at this temperature remained greater at all times.

The increase in the first 30 s of treatment was not very notable, (Table 4.6 and Fig.4.6) but after 100 s the hardness reached a level halfway between the minimum value and the maximum. For the period between 300 to 3000s it was maintained at ~ 650 Hv and after $3x10^4$s treatment in the furnace it decreased to ~ 590 Hv. A slight increase to 607 Hv was finally observed as a result of 10^5s heating at 750°C and water quenching.

b- Microstructure

The as-quenched thin material subjected to short-term salt bath treatment at this temperature revealed a tempered structure. Transmission electron

16-a |—0.5μ—|

16-b |—0.25μ—|

Plate16-Precipitation of carbide(a)and partial recovery(b),OQ.En24,10s750°C

Plate17-Lamellar |—0.5μ—|
structure of ferrite+martensite
and equiaxed particles in OQ.En24
held for 10^3s at 750°C+WQ

Plate18- |—0.5μ—|
Fine internally twinned martensite
in as-quenched En24 steel after
10^5s at 750°C+WQ

micrographs taken from the specimen held for 10 s showed fine precipitation of carbides on the martensite lath boundaries and within the laths (Plate16.a). The same treatment also caused partial recovery in some areas (Plate 16.b). A longer treatment at this temperature produced a lamellar ferrite/martensite structure with equiaxed carbide particles observed in both phases. Plate 17 is a transmission electron micrograph obtained from the specimen annealed at this temperature for 1000 s. The carbide particles observed in this area appear to be of about the same size and morphology as those detected in the as-quenched material (cf. Plate 17 with Plate 4). The microtwinned substructure in the martensitic areas was commonly observed both in this specimen and in those treated for longer times in the furnace at this temperature (Plate 18). In the ferritic areas a nonhomogeneous density of dislocations was the common feature. Optical microscopical examination of the specimens held for 10^3-10^4s at this temperature, revealed a progressive coarsening in the lamellar ferrite/martensite structure with time (Plates 19-21).

The pre-tempered material showed a predominantly ferritic structure with sub-micron carbide particles when held for times shorter than 30s at 750°C. Plate 22.a is an example of the material held for 10s in the pre-set salt bath at this temperature and then water-quenched, which revealed a carbide particle on a subgrain boundary. For longer times a fine lamellar ferrite/martensite region appeared to be the dominant feature; an example taken from the specimen held for 1000s in a salt bath at this temperature can be observed in Plate 22.b. A relatively coarser mixture of ferrite plus martensite and carbide particles was observed in the material held for longer times in the furnace. The carbide particle in Plate 23 appeared to be on the ferrite/martensite interface. The selected area diffraction patterns obtained from the carbide particles were indexed and in all cases they were shown to have a crystal structure identical to that of cementite. The high resolution dark field in Plate 23.b was produced by the $[10\bar{1}]_c$ plane identified in Plate 23.c and indexed in Plate 23.d. Plate 24 shows a different area of the same specimen (i.e. held for 10^5s at 750°C in the furnace). The fine-twinned structure of martensite and inhomogeneously dislocated ferrite were observed to co-exist in an elongated morphology in this area. Furthermore, the carbide particle was engulfed in the martensite with no direct contact with the neighbouring ferrite.

4.3.4 Heating at 765°C

a- Hardness Response

The higher rate of increase in hardness, produced as a result of annealing at higher intercritical temperatures, was again observed when the hardness values of either as-quenched or pre-tempered material, annealed at this temperature, were compared with similar results obtained after heating the material to the lower temperatures. Furthermore, no sign of eventual softening was detected for the material annealed in the furnace for longer

Plate 19- As-quenched En24, 10^3s750°C+WQ ⊢—10μ—⊣

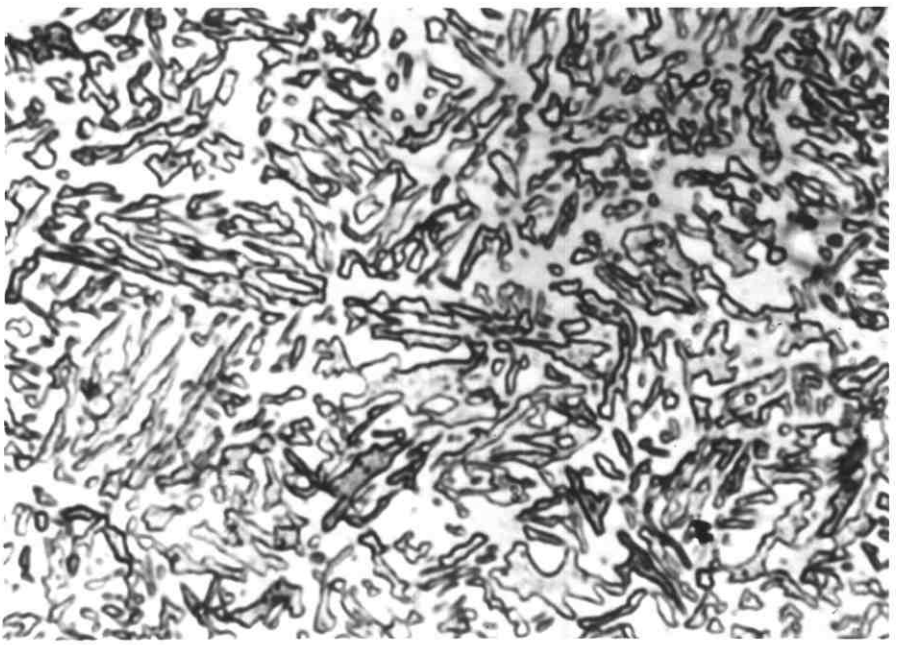

Plate 20- As-quenched En24, $3X10^3$s750°C+WQ ⊢— 10μ—⊣

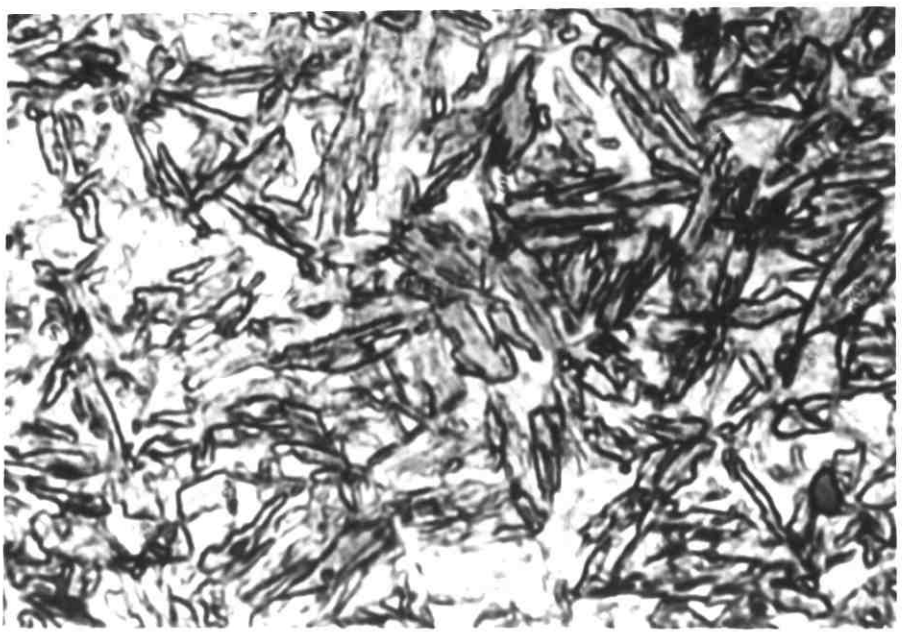

Plate 21- As-quenched En24, 10^4s750°C+WQ ⊢—10μ—⊣

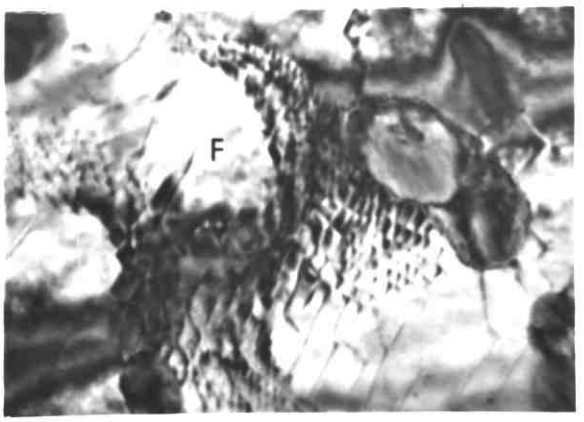

22-a ⟵0.25μ⟶

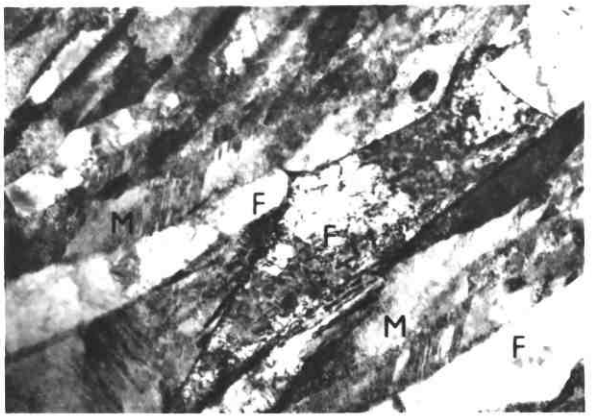

22-b ⟵1μ⟶

Plate 22- QT.En24 steel,held at 750°C for: a-10s b-10^3s+WQ

23-a-Bright field ⟵0.5μ⟶

23-b-H.R.D.F.

23-c-S.A.D.P.

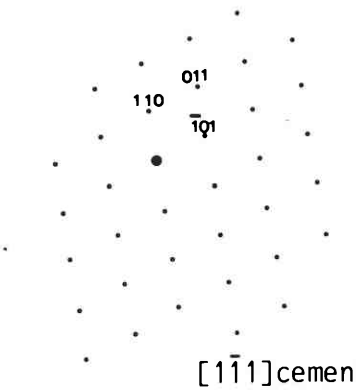

[1$\bar{1}$1]cementite

23-d-Indexing of diffraction pattern

Plate 23- QT.En24 steel,intercritically treated at 750°C for 10^5s(∿28h)+WQ

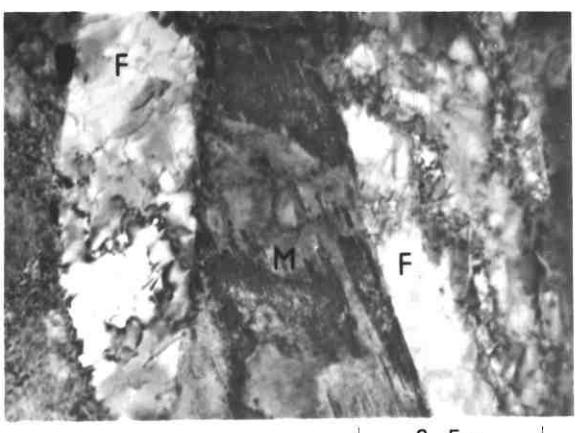

⟵0.5μ⟶

Plate 24- QT.En24+10^5s at 750°C+WQ

in all micrographs F=ferrite M=martensite

periods. An interesting observation after annealing the material at higher temperatures (765°C and 780°C) was the gradual hardening of the pre-tempered material to a level as high as those obtained for the as-quenched material after $3x10^4$s (8h, 20min) in the furnace at this temperature. The as-quenched thin specimens were softened to ~ 390Hv when water quenched after 5s at this temperature (Table 4.7). However this softening was more rapidly counteracted than the previous cases and for an immersion time of 30 s the as-quenched material achieved a hardness value up to the level of the water quench-hardened condition. The value was maintained at about the same level for all longer time treatments (Table 4.7 and Fig.4.7).

The pre-tempered material was hardened at a higher rate in the period between 10 to 300 s by which time it reached a value of ~ 700 Hv (Table 4.7). Thereafter hardening continued at a lower rate and finally after $3x10^4$ s it reached about the same value obtained for the as-quenched material. This value was maintained for the longest period examined of 10^5 s.

b- Microstructure

The initial tempering of the thin as-quenched specimens on their introduction to the pre-set salt bath at 765°C was observed. Plate 25 shows a typical area of such a specimen after 10s at 765°C followed by water quenching. Relatively large (~0.2 μm long) cementite particles were precipitated mainly within the martensite laths and on the lath boundaries. Some of the particles were partially spheroidized. The dislocation density varied in different laths and also changed within each lath. The S.A.D.P.'s obtained from carbide particles were indexed and identified as cementite. The orientation relationship between the ferritic matrix and the cementite was examined by superimposition of the diffraction patterns (Plate 25-c) and as indexed in Plate 25-d it was found to be:

$$(100)_c \;//\; (011)_\alpha$$
$$(011)_c \;//\; (011)_\alpha$$
$$(011)_c \;//\; (110)_\alpha$$

This is consistent with the Bagaryatskii relationship [129].

Upon water quenching of the specimens after a longer time at 765°C, a predominantly martensitic structure was produced. Plate 26 is an example of the as-quenched material held for 10^3s (~ 17 min) at this temperature. Fine internal twins were observed in most areas, although dislocated martensite could also be detected. Plate 26.b is a H.R.D.F. illustrating the (011) twin plane indicated in the S.A.D.P. The diffraction pattern was indexed (Plate 26.d) as the $[011]_{\alpha'}$ zone axis, with the twin spots resulting from twinning across a $\{211\}_{\alpha'}$ twin plane.

The pre-tempered material revealed no noticeable change upon short time annealing at 765°C. The structure after 10s at this temperature appeared to

Table 4.7 Pyramidal Vickers hardness values for oil-quenched and quenched-and-tempered En24 steel annealed at 765°C

Starting Condition	Annealing Time s										
	0	5	10	30	10^2	$3x10^2$	10^3	$3x10^3$	10^4	$3x10^4$	10^5
1h 835°C + OQ	633	389	402	744	755	765	755	751	744	740	751
OQ + 5h 700°C	270	253	259	390	591	695	701	717	721	735	761

Table 4.8 Pyramidal Vickers hardness values for oil-quenched and quenched-and-tempered En24 steel annealed at 780°C

Starting Condition	Annealing Time s										
	0	5	10	30	10^2	$3x10^2$	10^3	$3x10^3$	10^4	$3x10^4$	10^5
1h 835°C +OQ	633	384	668	749	763	762	755	767	762	755	758
OQ +5h 700°C	270	259	305	598	648	689	706	727	718	756	763

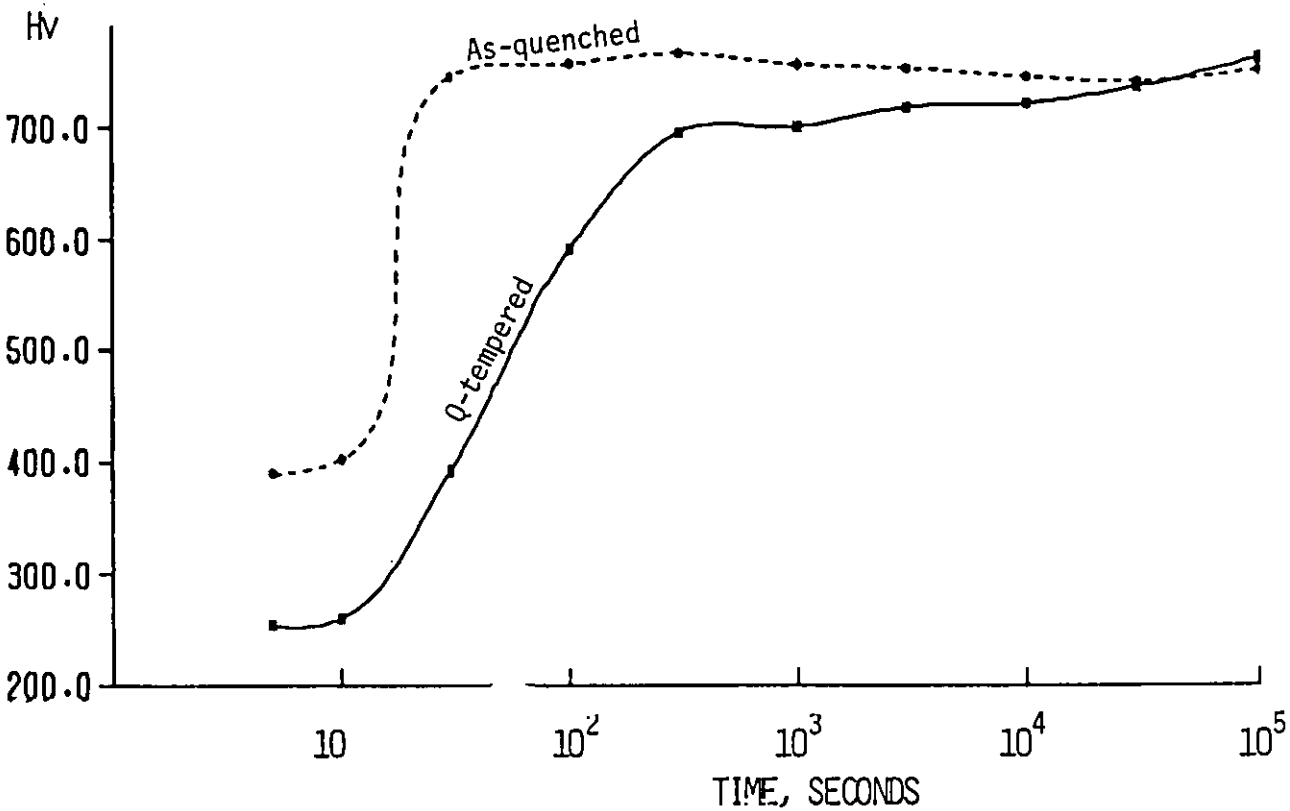

FIG. 4.7 - HARDNESS VS HEATING TIME AT 765°C FOR EN 24 STEEL IN AS-QUENCHED AND Q-TEMPERED CONDITIONS

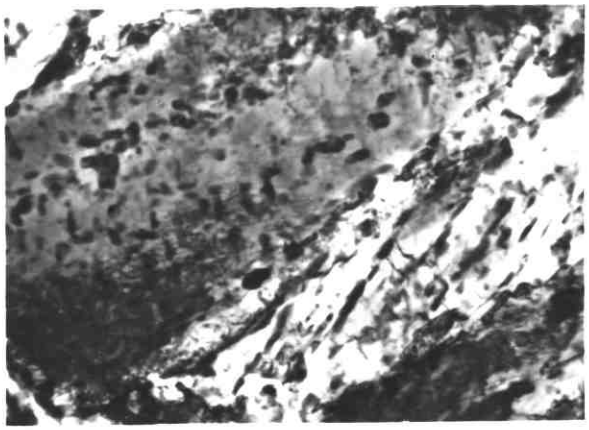

25-a ⊢ 0.5μ ⊣

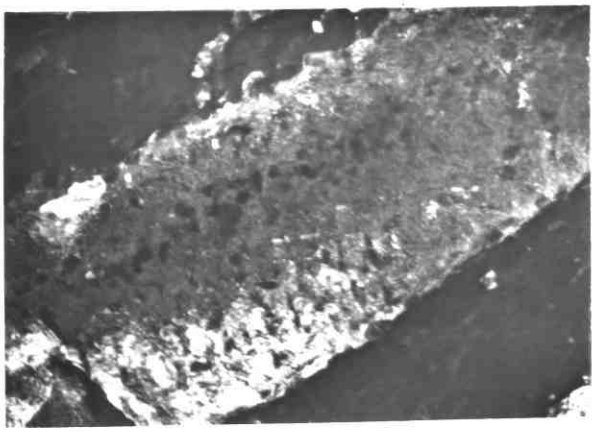

25-b

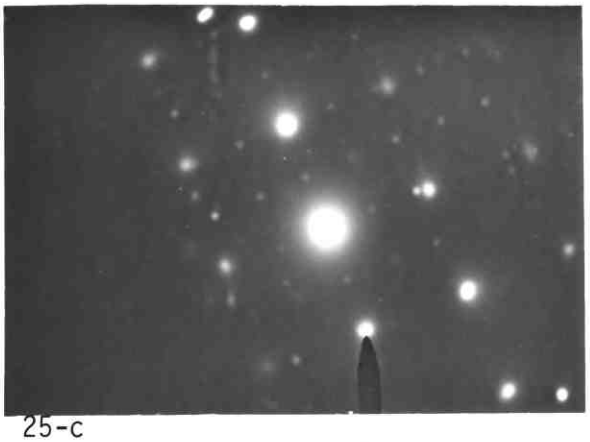

25-c

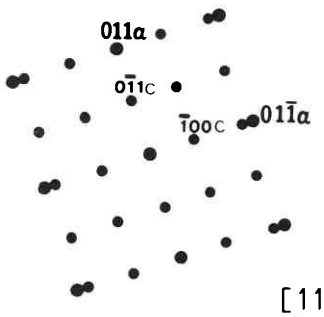

[110]α
[011]cementite

25-d

Plate 25-As-quenched En24 steel,10s at 765°c+WQ

26-a ⊢ 0.4μ ⊣

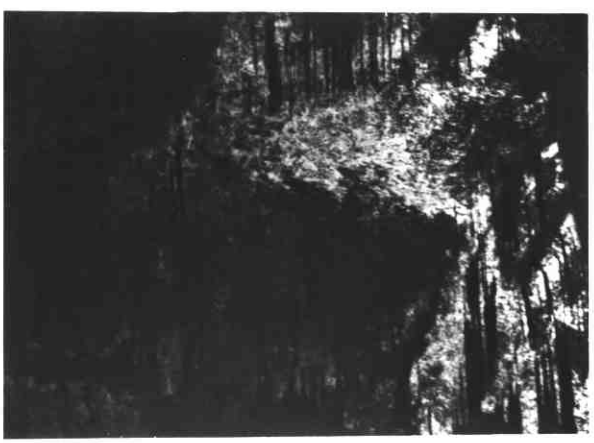

26-b

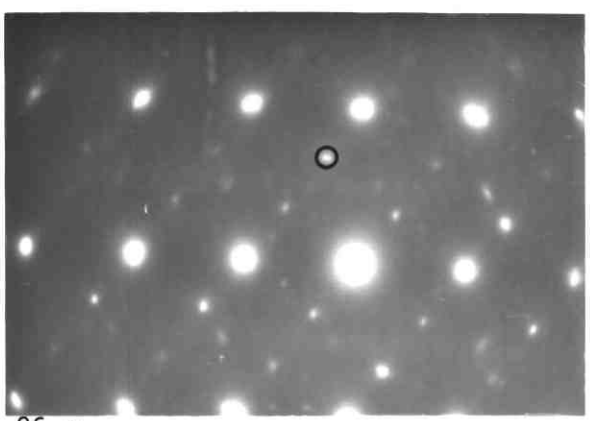

26-c

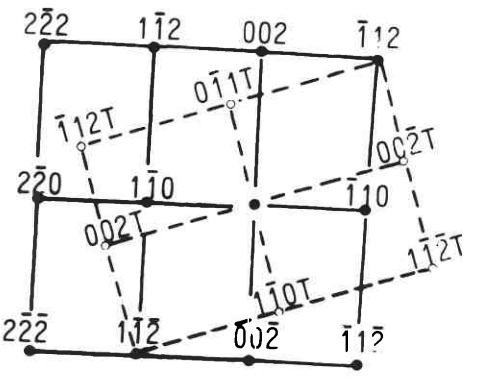

[011]α+twin

26-d

Plate 26-As-quenched En24 steel,10^3s at 765°C+WQ
a-Bright field showing internal twins in martensite,
b-H.R.D.F.using the twin spot in "c"
c-S.A.D.P.
d-Indexing of the diffraction pattern

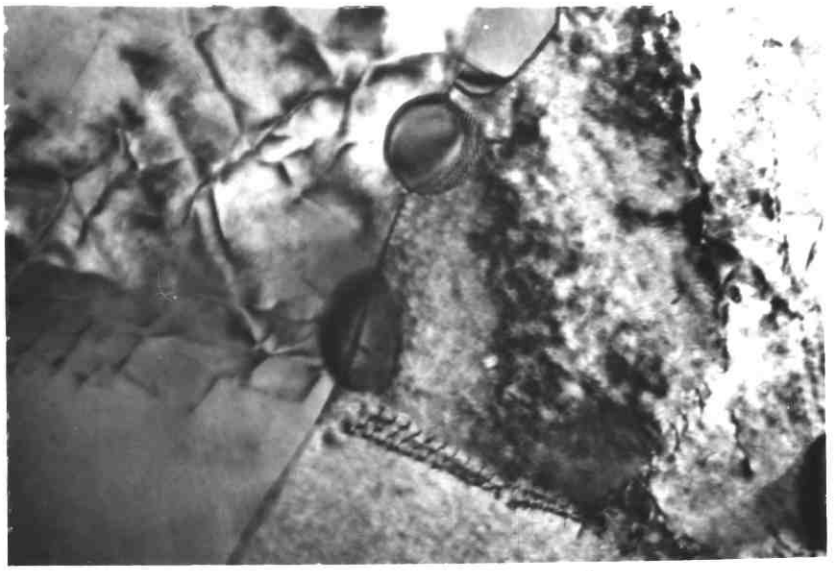

27-a ⊢— 0.2μ—⊣

27-b ⊢— 0.5μ—⊣

27-c ⊢—0.25μ—⊣

Plate 27-Previously tempered En24,held at 765°C for:
a-10s ,b-10^3s ,c-10^5s +WQ

consist mainly of partially recovered ferrite and equiaxed particles, mostly on the ferrite grain boundaries (Plate 27.a). After 10^3s at this temperature, the particles were less frequently detected and they were mostly observed to be engulfed by austenite (martensite). The structure of the matrix after this treatment was a mixture of finely twinned and dislocated martensite with the occasional appearence of small ferritic areas (Plate 27.b). Most of the areas examined after longer times (e.g. 10^5s, Plate 27.c) at this temperature, showed little evidence of undissolved carbides. The ferritic areas also became difficult to trace and the structure appeared to consist almost completely of the two kinds of martensite.

4.3.5 Heating at 780°C

This temperature was estimated to be just within the austenite range for En24 steel and the specimens quenched after longer times at this temperature revealed a fully martensitic structure.

The as-quenched thin specimens treated in the salt bath were heavily temper softened in only a few seconds to ~384 Hv (Fig.4.8 and Table 4.8) in the course of heating. In specimens held only for 5 seconds in the salt bath, extensive precipitation of carbides both between and within the laths was observed (Plate 28). However, re-dissolution of carbides and formation of austenite was postulated to occure more rapidly at this temperature; e.g. while at 765°C the main increase in hardness occurred between 10 and 30s, at 780°C this happened between 5 and 10s. After ~100s the overall hardness was maintained at a high level approximately equal to the as-quenched value, and the structure appeared to be in progress towards the equilibrium. Equiaxed particles, smaller than 0.1 micron in diameter, and a martensitic structure matrix were the predominant features in the as-quenched specimens held for 100s at this temperature (Plate 29). No evidence of carbides was detected in the specimens held for 10^5s and the structure predominantly consisted of finely twinned martensite (Plate 30).

The increase in hardness for the previously tempered specimens was also speeded up at this higher temperature. The main increase in the hardness occurred in the first 30s to ~600 Hv (Fig. 4.8 and Table 4.8) whereas it took the specimen held at 765°C about three times longer to reach the same level of hardness. From 30 seconds onwards the hardness continued to increase, although at a lower rate, and eventually after $3x10^4$seconds it reached the same level as the as-quenched material. In the previously tempered material held for only 5s at 780°C the predominantly elongated ferrite subgrains were observed (Plate 31) with large precipitates mostly on the sub-grain boundaries. After 100s, most of the areas examined, exhibited a fully martensitic structure, although the process of carbide solution was still incomplete (Plate 32). After prolonged heating at this temperature (10^5s) no evidence of undissolved carbides was detected in the areas examined.

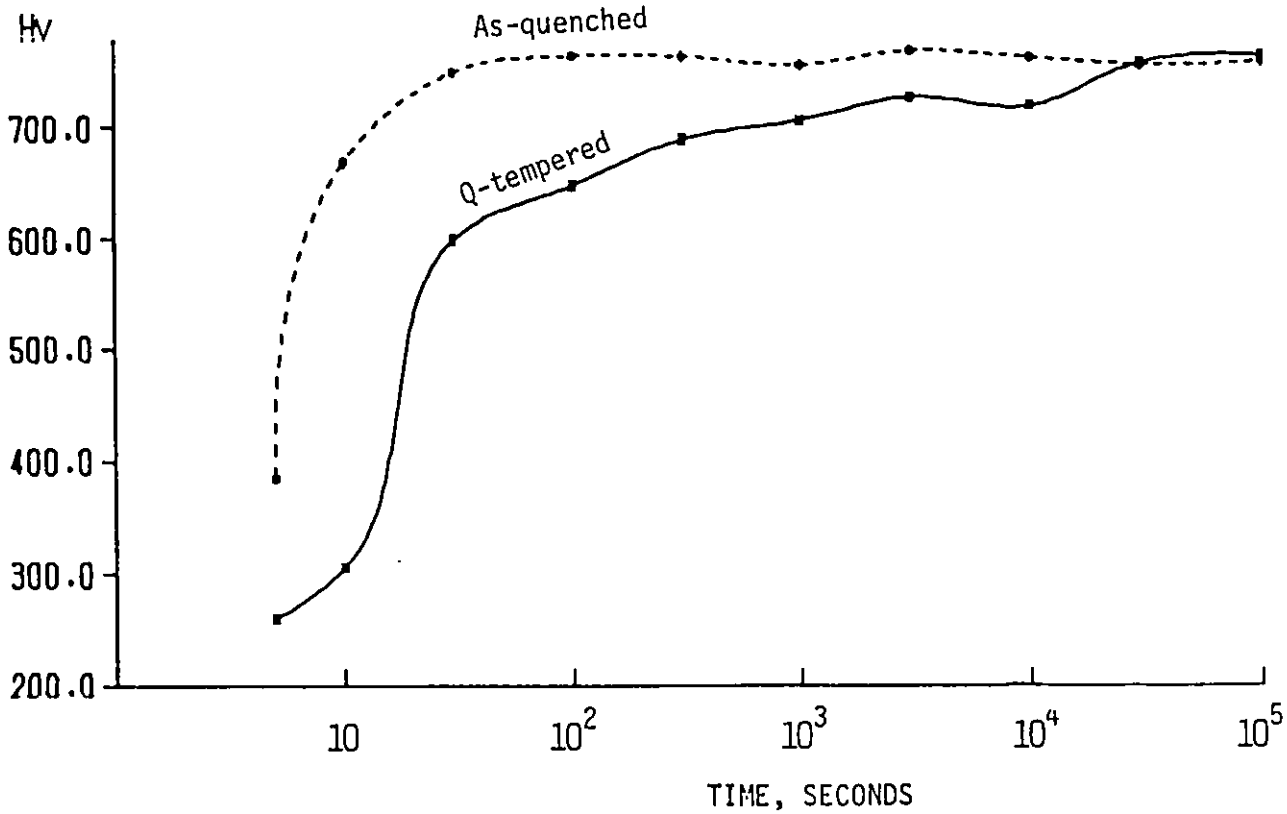

FIG. 4.8 - HARDNESS VS HEATING TIME AT 780°C FOR EN 24 STEEL IN AS QUENCHED AND Q-TEMPERED CONDITIONS

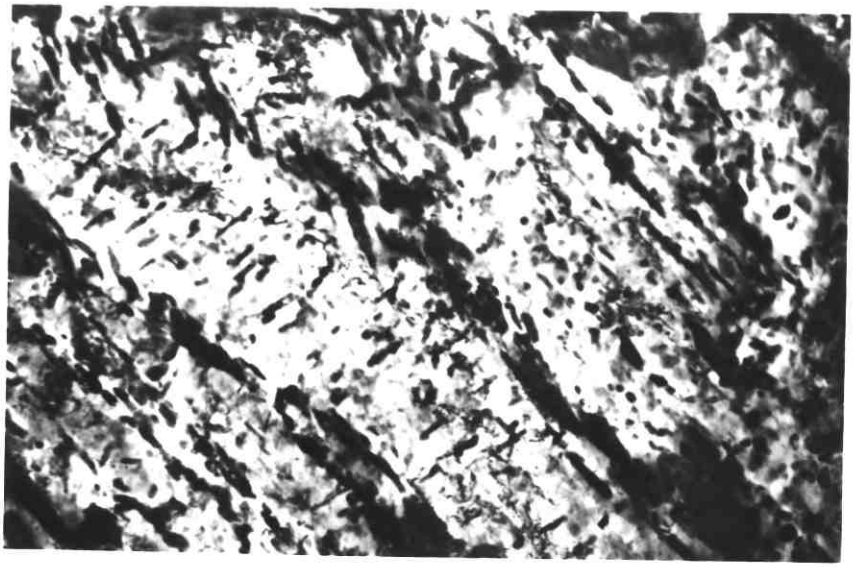

Plate 28- OQ En24, 5s 780°C+ WQ ⊢ 0.5μ ⊣

Plate 29- OQ En24, 100s 780°C+WQ ⊢ 0.25μ⊣

Plate 30- OQ En24, 10^5s 780°C+WQ ⊢0.5μ⊣

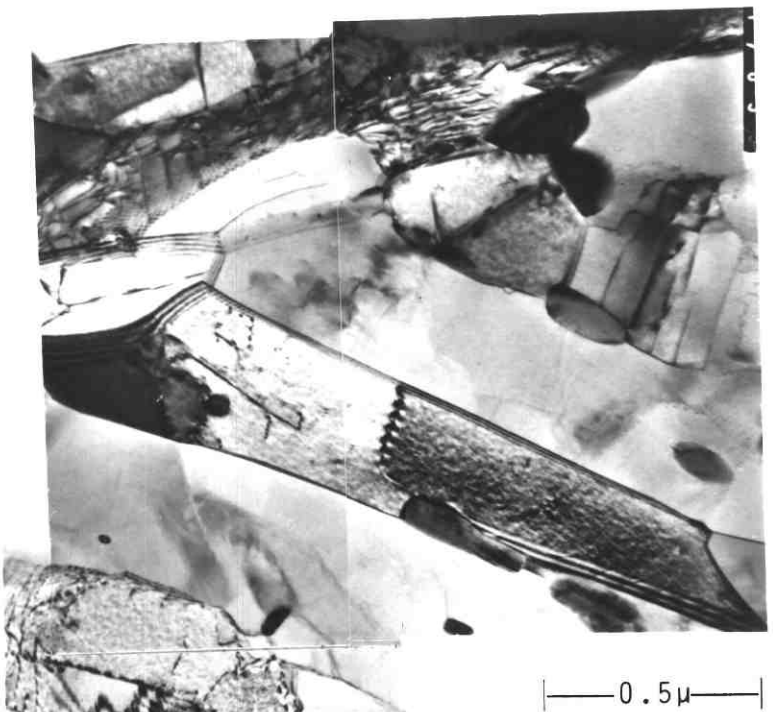

Plate 31-Quenched and tempered En24 steel, held for 5s at 780°C+WQ

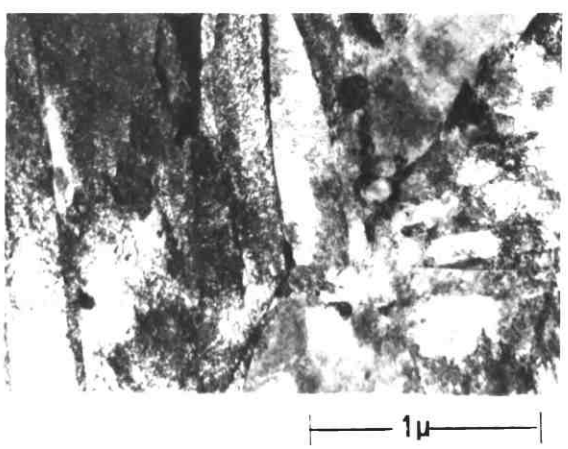

Plate 32- QT En24, 100s 780°C+WQ

4.4 The Charpy Size Specimens

As mentioned in the previous section, since the heating rate prior to the intercritical treatment appeared to play an important role in the eventual properties of the specimens, some series of experiments were planned to investigate the effect of heating rate on the material with larger dimensions. The standard Charpy specimens were cut slightly over-sized (60x11x11 mm) to allow for the final machining after the final heat-treatment, when the notch was also cut. All of the specimens were initially austenitized at 835°C for 80 min (including 20 min heating time) individually in a vertical furnace with an argon flow; they were then directly oil-quenched. This condition was chosen as standard for all the Charpy-size specimens.

Three different approaches were followed to determine the effect of intercritical treatment on these specimens of thicker section size. First a number of oil-quenched specimens were heated and held for different times at one intercritical temperature namely 735°C, either in a salt bath (for shorter times) or in a furnace, and water quenched. In the second series a number of specimens were heated for a fixed time (30 min) at different intercritical temperatures in a salt bath and water-quenched. These specimens were then tempered to different temperatures. The final series were also treated for a fixed time (30 min) at different intercritical temperatures, but this time a crusilite rod furnace was utilized to anneal the specimens and they were then oil-quenched in order to produce heating and cooling rates nearer to that of large sections relevant to the actual practice in industry. The effect of tempering was also investigated on these specimens.

4.4.1 Intercritical Treatments at 735°C

Oil-quenched Charpy-size En24 specimens were annealed at 735°C for times from 1 min to 100 min in a salt bath and from 15 min to 50h in a furnace, and water quenched. Hardness measurements were then carried out both on the surface of the specimens and on the centre of their cross sections. The results are given in Tables 4.9 and 4.10 and plotted in Fig. 4.9 where a curve from Fig. 4.5, representing the behaviour of thin specimens, is superimposed for comparison.

It can be seen from Fig.4.9 that as a result of the lower heating rate for the thicker specimens, the increase in hardness after the initial tempering on heating was considerably retarded in these specimens compared to the thin specimens, even when both were heated in the salt bath. The hardness started to increase after 3 min at this temperature and after ~10 min the rate of increase enhanced sharply. At 30 min the hardness reached a peak value of 600-634 Hv which is close to that of the thin specimens curve.

Table 4.9 The effect of intercritical annealing time at 735°C on the hardness of oil-quenched Charpy-size En24 specimens (salt bath treatments)

Initial hardness OQ.	Heating time, minutes									
	1		3		10		30		100	
	Surface	Centre	Surface	Centre	Surface	Centre	Surface	Centre	Surface	Centre
630	365	358	343	322	376	380	634	600	522	514

Table 4.10 The effect of intercritical annealing time at 735°C on the hardness of oil-quenched Charpy-size En24 specimens (furnace treatments)

Initial hardness OQ.	Heating time, minutes								
	15	30	160	300		1000		3000	
				Surface	Centre	Surface	Centre	Surface	Centre
630	298	313	377	384	388	525	524	480	472

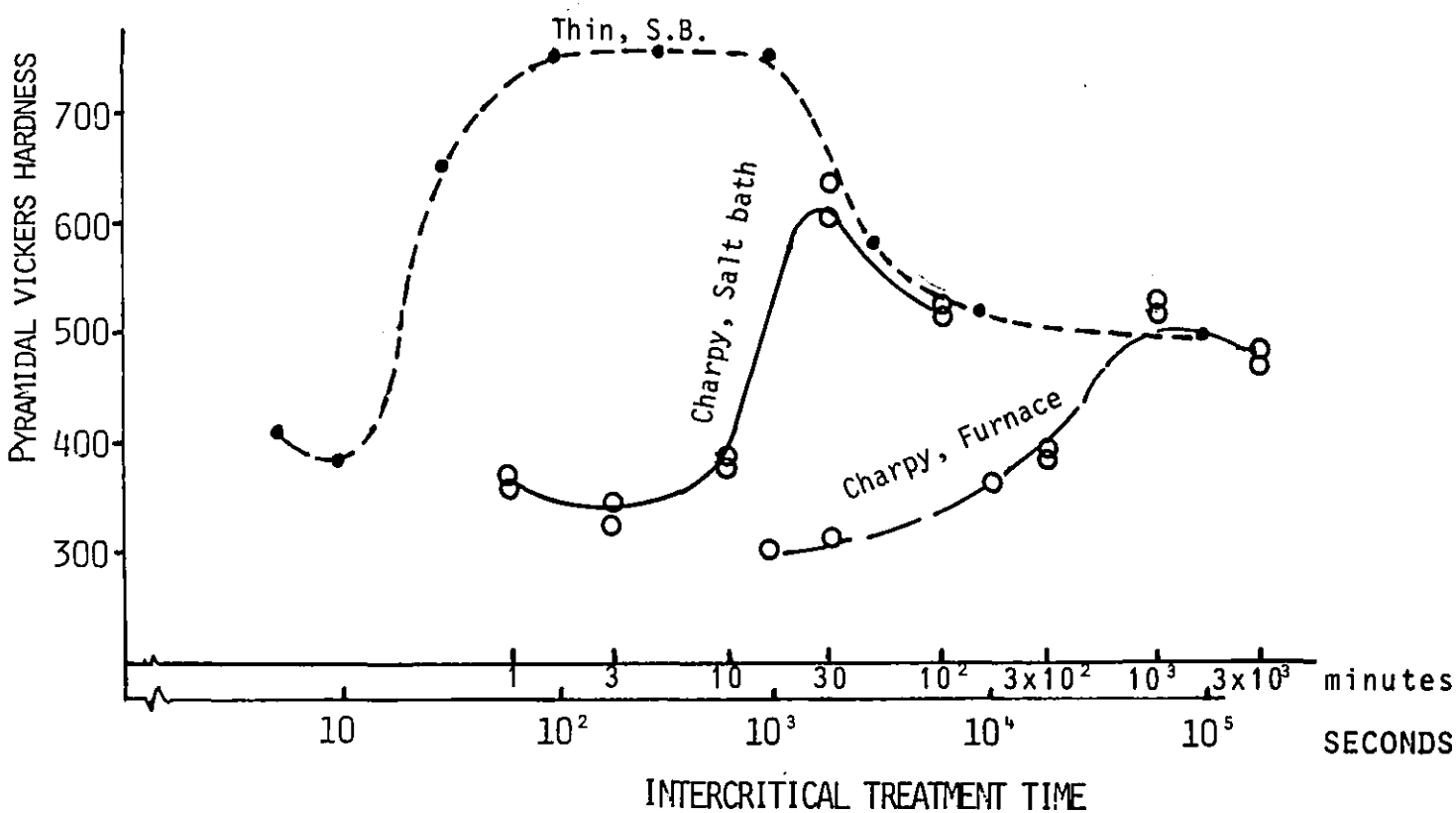

FIG. 4.9 - EFFECT OF HEATING RATE TO 735°C, EN24 STEEL

The value obtained after 100 min at this temperature is also in proximity with that of the thin specimens.

The hardness curve for the Charpy specimens held at 735°C in the furnace (Fig.4.9) shows the effect of the longer time these specimens took to reach the pre-set temperature. It took over 16 hours before they were at the same level of hardness as the thin specimens.

4.4.2 Salt Bath Intercritical Treatments

In this series a fixed intercritical annealing time of 30 min was chosen and several oil-quenched Charpy size specimens were held individually at different ($\alpha + \gamma$) temperatures and water quenched. They were then tempered to temperatures ranging from 200°C to 700°C for 1h and hardness vs tempering temperature curves were plotted for each intercritical treatment. A number of the oil-quenched specimens were also tempered conventionally, i.e. without any intermediate intercritical treatment; the tempered hardness results were compared. The specimens annealed at 750°C and 765°C followed by water-quenching initially exibited a higher hardness than the conventionally treated specimens, but the hardness values become very close when the specimens in these three condition were tempered (Fig. 4.10 and Table 4.11). However, for the specimens intercritically treated at 735°C, while the slope of softening was approximately similar to that of the other initial conditions, the actual hardness was noticeably lower both before and after tempering to similar temperatures.

4.4.3 Furnace Intercritical Treatments

In this final series of experiments on En24 the effect of slower heating to intercritical temperatures on the properties of Charpy specimens was investigated . The starting condition was oil-quenched as explained in the previous sections. The specimens were suspended individually in a vertical crusilite furnace with a prefixed temperature of either 735, 750 or 765°C for 30 min with an argon flow and then directly oil-quenched. They were then tempered to temperatures ranging from 100 to 650°C with temperature intervals of 50°C and water quenched. After the final treatment the specimens were broken in a standard Charpy machine at room temperature and the fracture energies were measured. The fracture surfaces were cover-protected in the course of cutting to a proper size for the scanning electron microscopy. Slices of ~0.5mm thick were cut from the sections nearest to the fracture surface and were thinned for transmission electron microscopy. Some slices were also cut for hardness measurements and light microscope examinations. This approach of examining the structural and mechanical properties on the same specimens was utilized, as mentioned earlier, in order to avoid any incorrect association of characteristics due to different rates of heating.

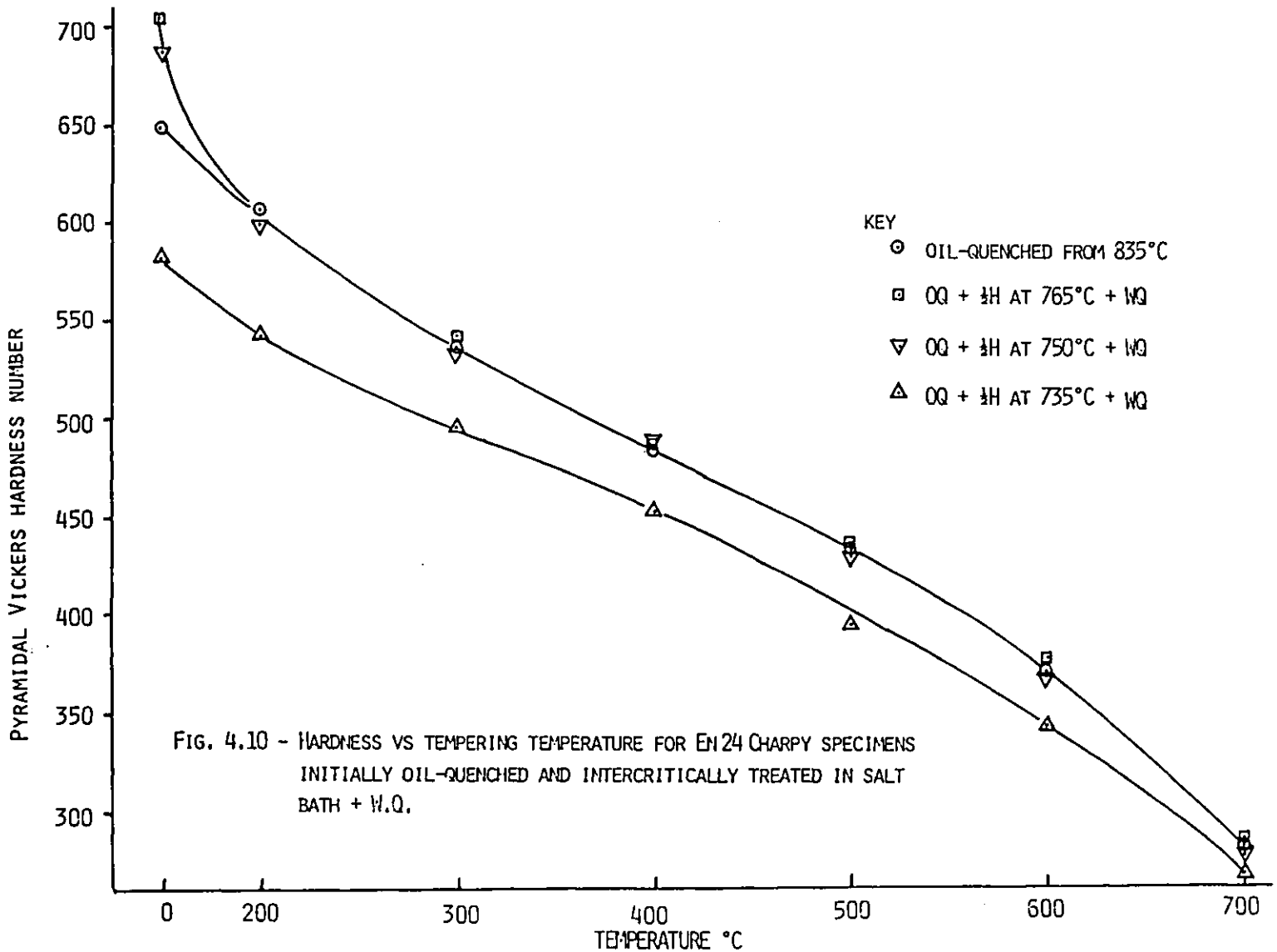

FIG. 4.10 - HARDNESS VS TEMPERING TEMPERATURE FOR EN 24 CHARPY SPECIMENS INITIALLY OIL-QUENCHED AND INTERCRITICALLY TREATED IN SALT BATH + W.Q.

Table 4.11 Effect of tempering temperature on the hardness of oil-quenched Charpy-size En24 and intercritically treated specimens in salt bath

Initial treatment	Tempering temperature°C, 1h +WQ						
	0	200	300	400	500	600	700
	Hardness Hv						
80min at 835°C+oil-quench	648	607	537	484	433	372	283
OQ+½h 735°C(S.B) + W.Q	581	542	496	454	395	344	269
OQ+½h 750°C (S.B.) + W.Q	687	599	534	487	431	368	278
OQ+½h 765°C (S.B.) +W.Q	704	609	541	487	435	377	286

Table 4.12 En24 Charpy size specimens, 1h 835°C + OQ + ½h intercritically treated in a furnace at different temperatures + 1h tempering at indicated temperatures

Charpy V Notch Energy and Hardness Vickers Result

Tempering Temperature, °C	Intercritical(α+γ) range treatment temperature											
	Conventional treatment			765°C			750°C			735°C		
	Charpy Energy, J	Hardness Hv		Charpy Energy, J	Hardness		Charpy Energy, J	Hardness		Charpy Energy, J	Hardness	
		Mean Value	Standard Dev.		Mean Value	Standard Dev.		Mean Value	Standard Dev.		Mean Value	Standard Dev.
Untempered	11	639	6	11	590	10	14	400	3	45	313	3
100	13	651	5	8	540	4	14	396	3	24	336	1
200	31	587	3	22	591	8	25	391	3	47	324	2
250	28	564	8	23	544	5	29	394	3	54	311	4
300	17	534	4	27	502	4	30	385	4	53	331	2
350	14	500	5	26	465	6	33	385	2	58	312	2
400	27	466	4	29	416	8	46	353	3	60	312	2
450	23	450	8	29	430	6	43	354	4	70	301	5
500	30	424	8	37	412	4	58	329	8	82	293	3
550	27	413	4	45	388	8	70	302	2	77	292	4
600	60	359	8	70	341	5	90	297	2	100	270	6
650	73	344	4	86	309	2	104	274	8	106	266	3

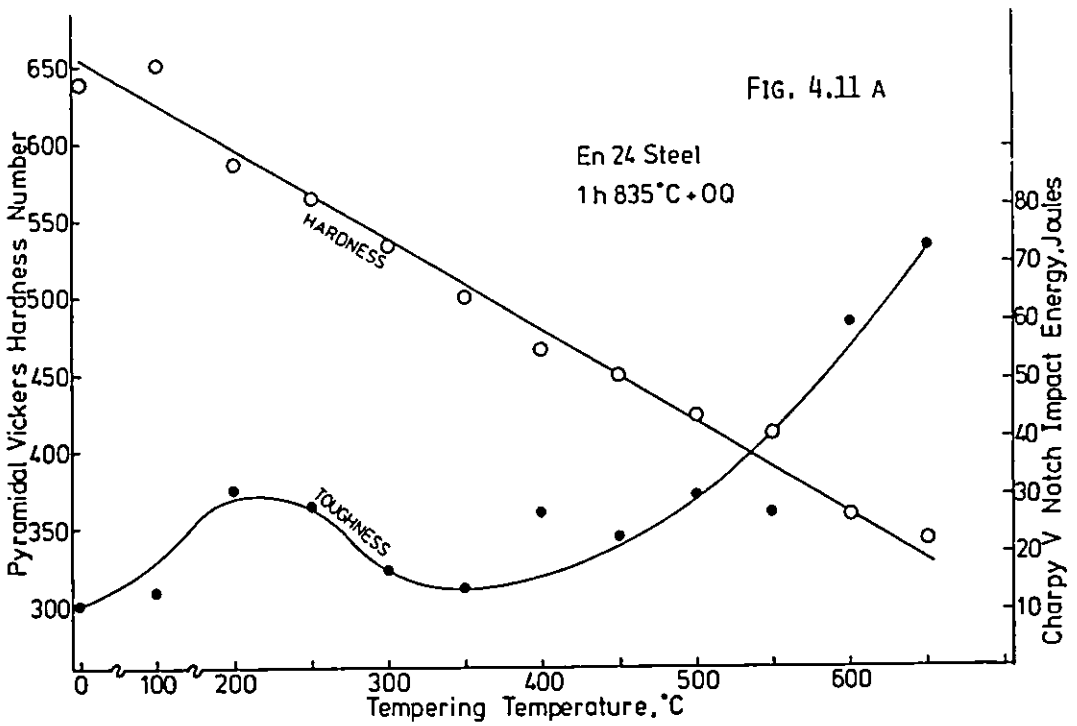

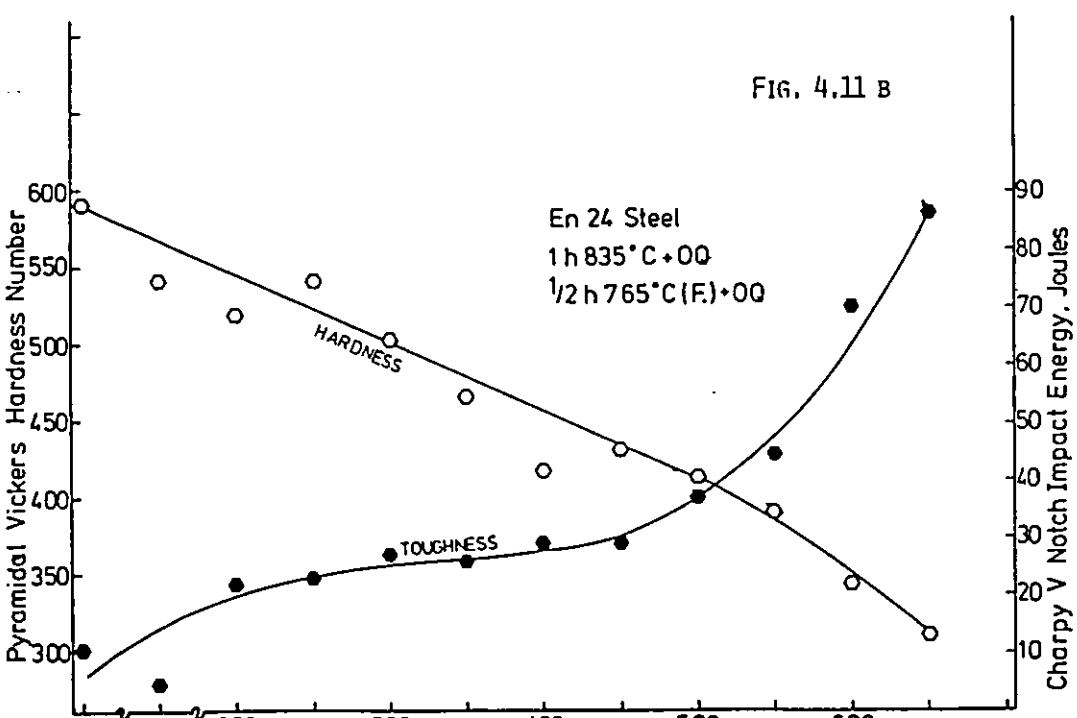

FIG. 4.11 - EFFECT OF TEMPERING ON HARDNESS AND CHARPY ENERGY FOR EN 24 STEEL; INITIAL CONDITION INDICATED INDIVIDUALLY

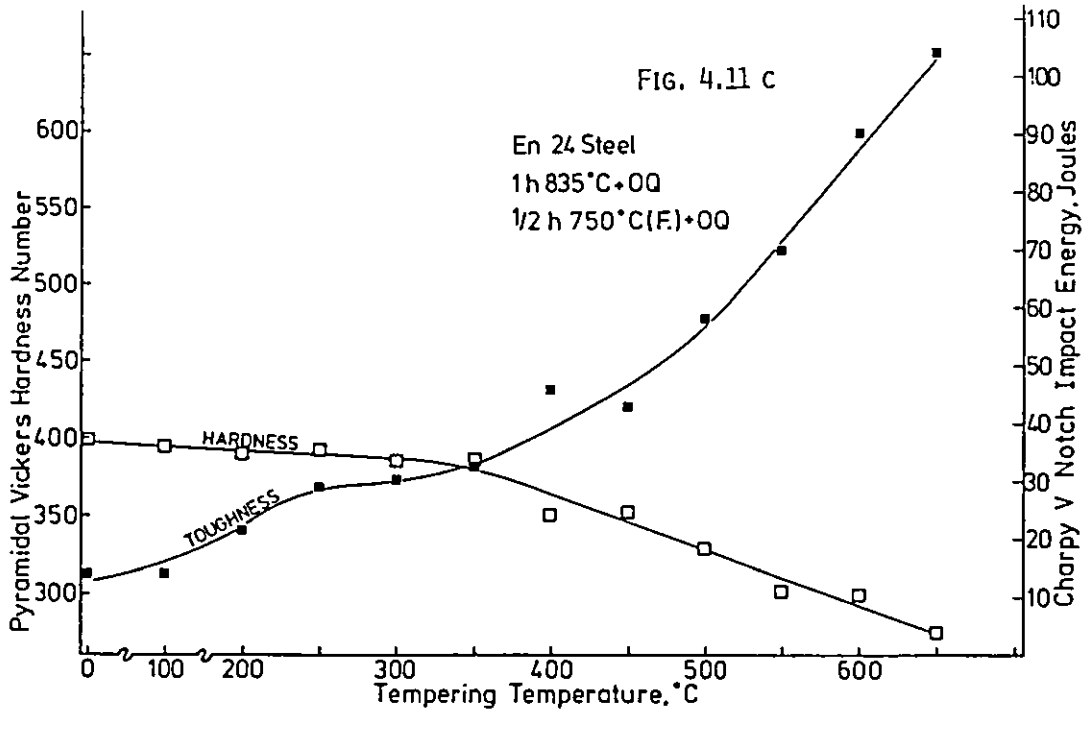

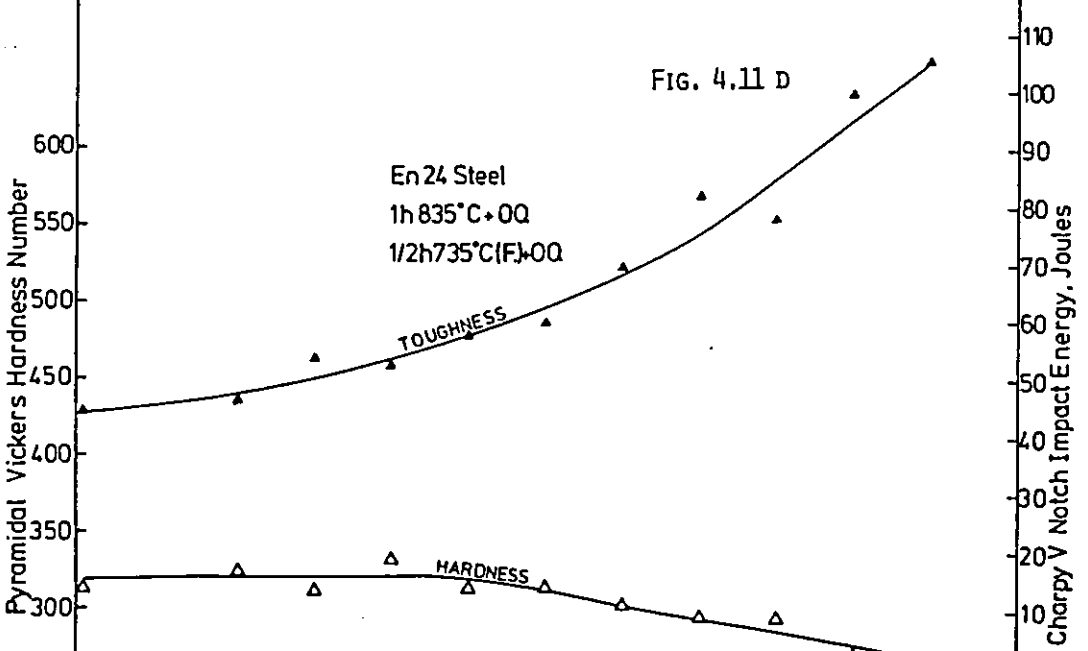

FIG. 4.11 - CONTINUED

4.4.3.1 Mechanical Properties

Throughout the mechanical testing programme, the Vickers hardness testing and room temperature Charpy impact test were relied on for the assessment of strength and toughness of material. Table 4.12 is a summary of the results obtained from the measurement of the Charpy energies and hardness measurements on the cross section of the test pieces.

The results are plotted in Fig. 4.11-b to -d for the specimens intercritically treated at 765,750 and 735°C respectively, prior to tempering. Fig.4.11.a shows the effects of tempering on the hardness and Charpy impact energy of as-quenched En24 specimens. The usual temper embrittlement trough in the range of 250-500°C with a minimum in the fracture energy absorbed at about 350°C was observed. Fig. 4.12 is a superimposition of Figs. 4.11-a to -d. The as-quenched hardness after the intercritical treatment at 765°C was lower than that of the conventionally treated specimen, and a similar tempering behaviour was observed. The embrittlement trough was almost flattened after intercritical treatment at 765°C (Figs. 4.11-b and 4.12). Treating the Charpy-size specimens at lower intercritical temperatures (Fig. 4.11-c and -d) resulted in a much lower intitial hardness and little softening was observed up to ~300°C tempering. The 350°C embrittlement trough was further reduced as a result of lower temperature intercritical treatment and specimens absorbed higher impact energies.

The comparison between the overall machanical properties will be meaningful if one property, e.g. toughness, is compared in conditions identical with the other property, e.g. hardness. One way to facilitate this comparison is plotting one property against the other for specimens of different treatment histories. The Charpy impact energy is plotted against hardness in Fig.4.13 for the conventional and intercritical heat treatments. Several interesting points can be concluded from this plot:

> When the 735°C and 750°C intercritical treatments were employed, not only were the hardness values obtained lower than 450 Hv, equivalent to a tensile stress of about 1300 MNm^{-2}, but also the toughness of the intercritical condition was inferior to that of the conventional condition. If the higher temperature (765°C) intercritical condition is compared with the conventional, the plot shows that at hardness levels lower than about 450 Hv, which corresponds to tempering temperatures in excess of about 450°C, the impact toughness of the two conditions are identical. In the hardness range from 450 to 550 Hv the impact behaviour of the intercritically heat treated samples at 765°C is noticeably superior to the conventional heat treatment condition. Finally, at hardness levels above 550 Hv, the toughness of the intercritical condition is inferior to that of the standard condition.

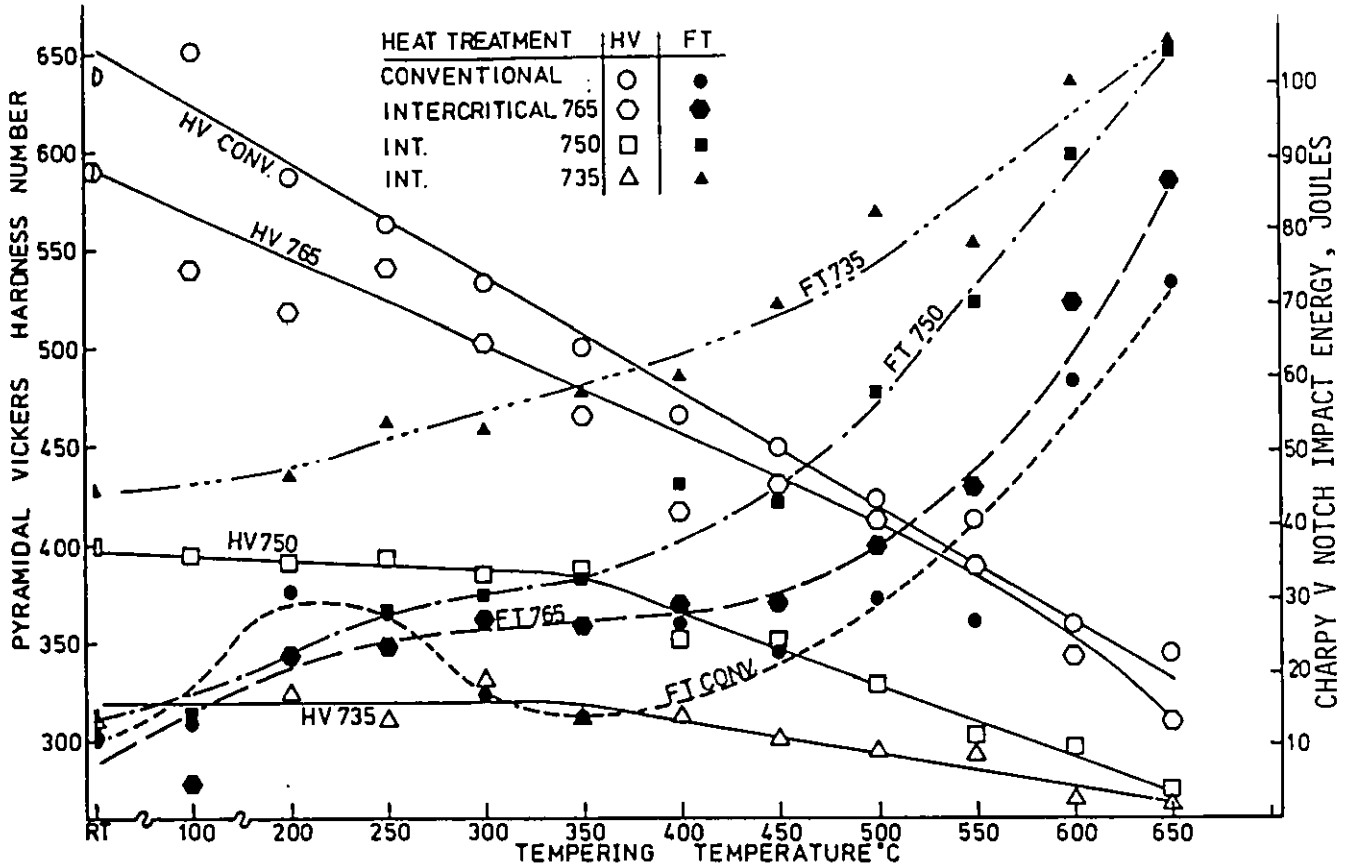

FIG. 4.12 - EFFECT OF TEMPERING ON HARDNESS AND CHARPY ENERGY FOR EN 24 STEEL WITH DIFFERENT STARTING CONDITIONS

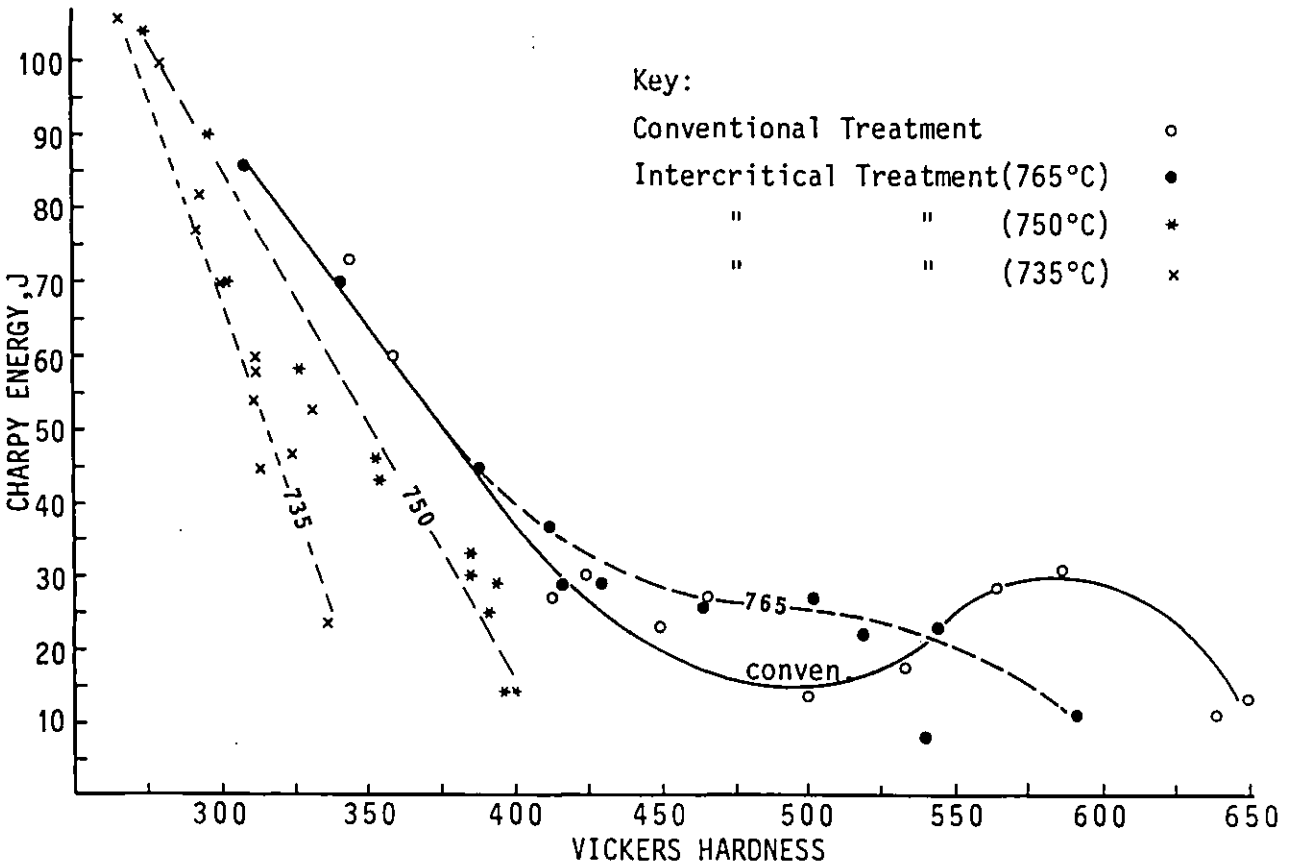

FIG. 4.13 - PLOT OF CHARPY V NOTCH ENERGY VS HARDNESS FOR EN 24 STEEL

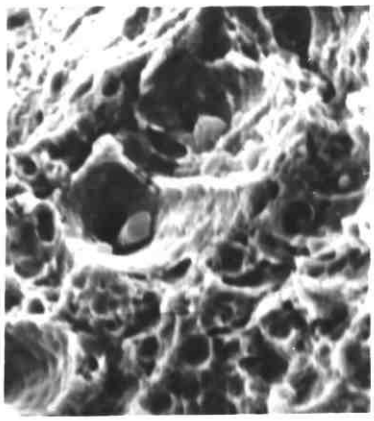

33-a ⊢10μ⊣

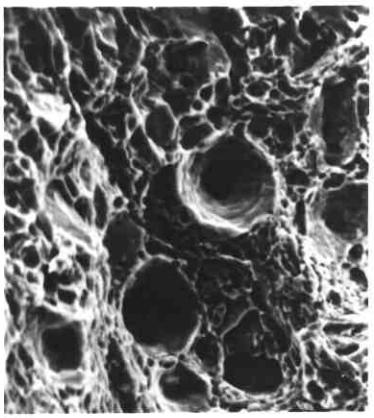

33-b ⊢15μ⊣

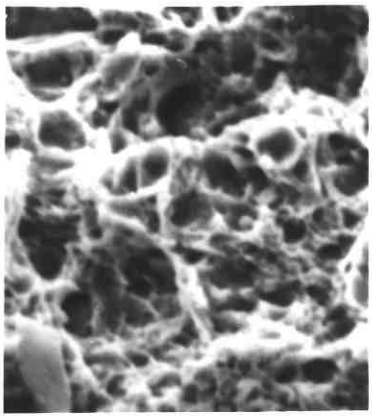

33-c ⊢5μ⊣

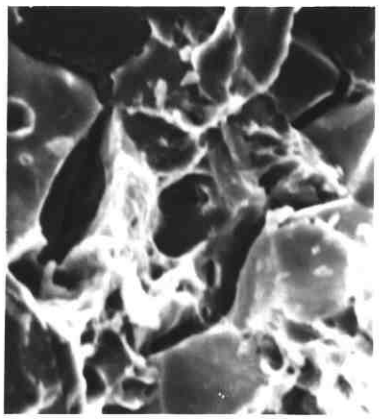

33-d ⊢10μ⊣

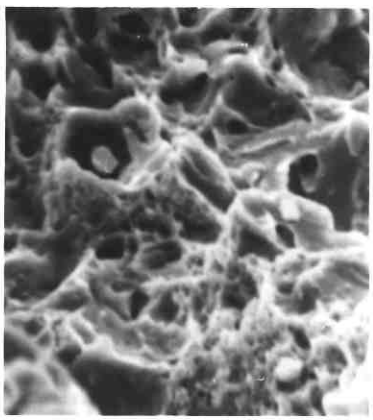

33-e ⊢5μ⊣

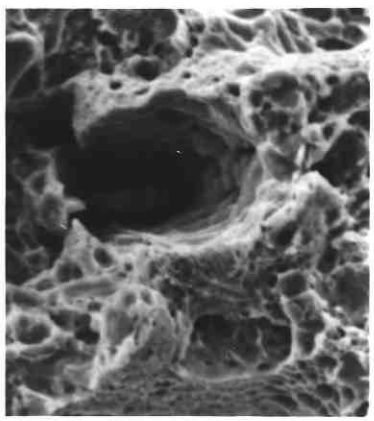

33-f ⊢10μ⊣

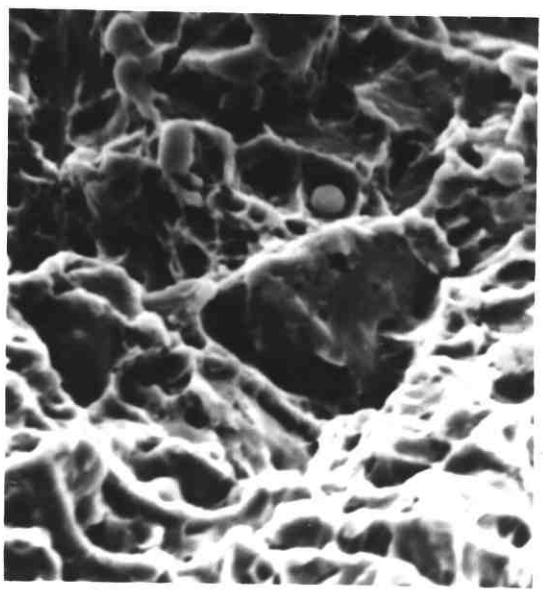

33-g ⊢10μ⊣

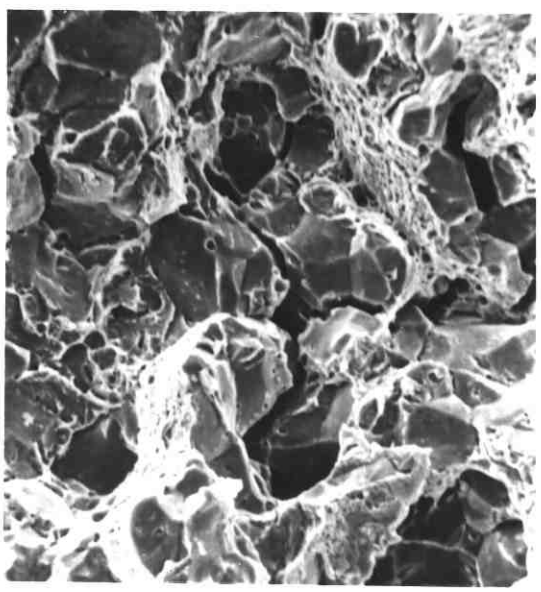

33-h ⊢20μ⊣

Plate 33-En24 steel,conventionally quenched and tempered(a,b,d&h)or quenched-intercritically treated at 765°C for ½h and tempered(c,e,f&g) at: a-600°C,b-500°C,c-450°C,d-400°C,e-350°C,f-200°C,g-300°C and h-350°C
Scanning electron fractographs

4.4.3.2 Electron Fractograph Observations

The micromechanisms of fracture for the various heat treated conditions were examined on the fractured surfaces of Charpy specimens. The conventionally treated material revealed the usual appearance for this grade of steel. Light tempering of the as-quenched En24 steel to about 200°C resulted in a high proportion of fibrous fracture. Tempering at the intermediate range of temperatures caused a substantial weakening in the prior austenite grain boundaries, and a low energy intergranular fracture was revealed upon impact testing. Plate 33-h shows a typical fractograph exhibiting a predominantly intergranular fracture in the as-quenched structure tempered for 1h at 350°C. This agrees with the toughness data which gave a Charpy energy of 14 J for the same specimen. A similar mode of fracture was also observed in the as-quenched material tempered to a slightly higher temperature, 400°C (Plate 33-d); the fracture energy, however was improved to a value of 27J (Table 4.12). Tempering to higher temperatures, associated with hardness values less than 450 Hv, revealed fracture surfaces that were largely composed of well defined dimples of various sizes (Plates 33-a and -b).

The intercritical treatment of specimens to 765°C prior to tempering resulted in an improvement in the toughness of material tempered to hardness values between 450 and 550 Hv. The hardness of material tempered to 300°C after this treatment was similar to that of the as-quenched material tempered to 350°C, i.e. ~500 Hv (Table 4.12), while the fracture energy was almost doubled. This was found to be due to a different mode of fracture; the intergranular decohesion ceased to occur as a result of this intermediate treatment and the material tempered to the embrittlement range of temperatures displayed a mainly fibrous mode of fracture (Plates 33-c,-e and -g). A comparison between Plates 33-g and 33-h shows the distinct modes of fracture in the two conditions tempered to a similar value of hardness. The intercritical treatments at lower temperatures (735°and 750°C) also resulted in a predominantly fibrous fracture.

4.4.3.3 Light Microscopy

The intercritically treated specimens, as well as the conventionally quenched ones, were lightly tempered for 1h at 200 °C for the light microscopical examination. The austenite grain boundary etchant revealed the boundaries of the original austenite grains produced by 1h austenitizing at 835°C followed by oil-quenching (Plate 34-a). The material treated in the higher intercritical range, i.e. 765°C, revealed an interesting structure (Plate 34-b). The structure consisted of a mixture of grains, of about the same order of size as the previous condition, but showing two different features. One group, etched plain grey, looked identical to the austenite (transformed to martensite) grains, observed in the as-quenched condition. The other group of original grains revealed a lamellar duplex structure. An electron microprobe analysis of this specimen detected no obvious variation in concentrations of Ni, Cr, Mn, Si and Mo; however, traces run across the section of the specimen showed peaks of Cr in places (Ni and Mn almost level) which seemed to be associated with visually dark areas. This might

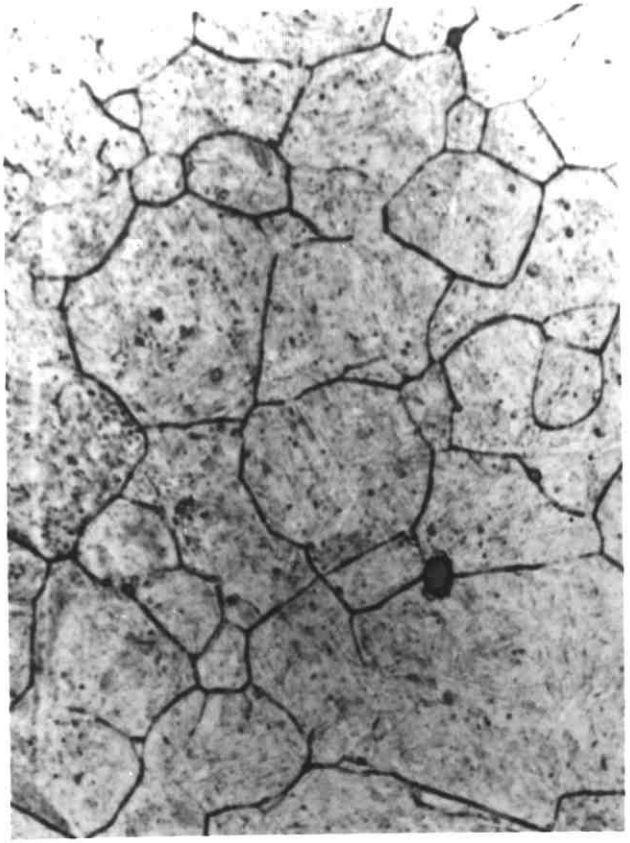

34-a

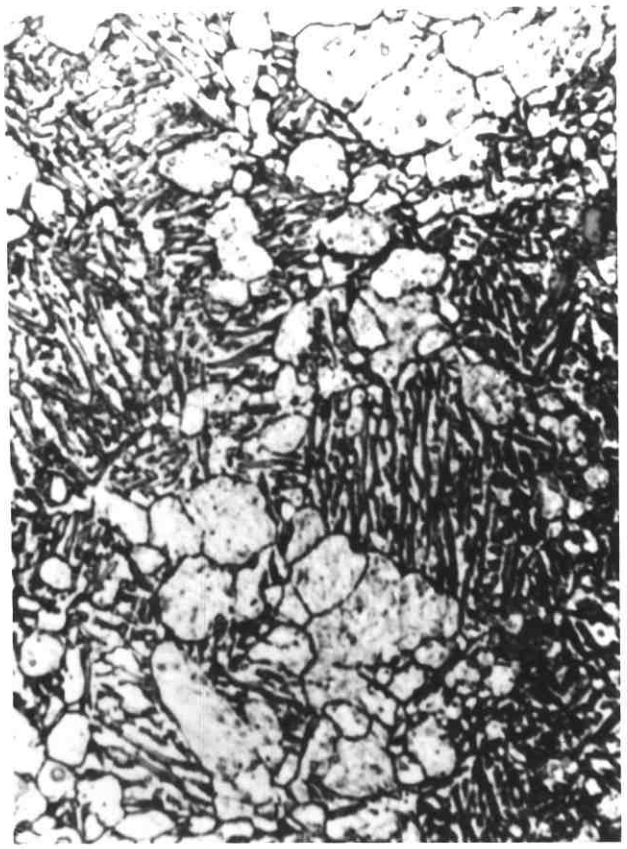

34-b

20μ

34-c

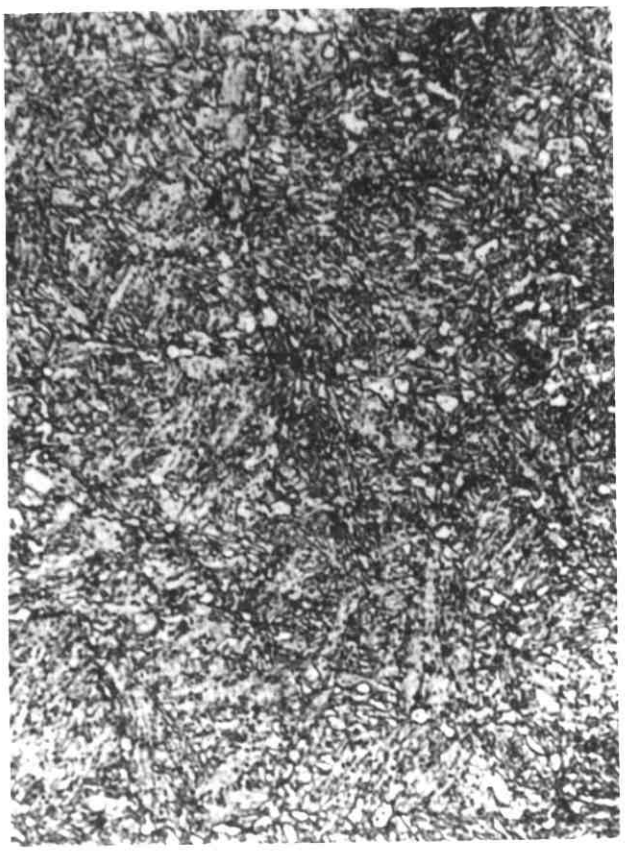

34-d

Plate 34-As-quenched En24 Charpy specimens,before(a) or after intercritical treatment for ½h at: b-765°C, c-750°C and d-735°C +Q followed by 1h tempering at 200°C
Optical micrographs, picric acid/HCl/Teepol etch, mag. all X 1400

be due to chromium carbide formation and concentration with the iron carbides, but was not proven absolutely. The X-ray resolution was about 5μm whereas the carbides in this specimen were considerably smaller. The material treated at 750°C revealed a relatively finer duplex structure with lamellar features. The prior austenite grain boundaries were not resolved (Plate 34-c). Charpy specimens furnace heated to 735°C for 30 min revealed a still finer lamellar structure (Plate 34-d).

4.4.3.4 Transmission Electron Microscopy

The fine structure of the conventionally quenched En24 Charpy specimens revealed a mixture of lath and plate martensites (Plate 35-a). Due to the limitations in the resolution of light microscopy on the one hand and restrictions in the actual area under observation in the electron microscopy on the other hand, an exact measurement of the volume fraction of lath and plate martensites was not possible. However, most of the micrographs showed a predominantly lath type structure plus some plate type. These observations are consistent with the structural studies by Krauss and Marder [27] and Speich and Leslie [65]. No evidence of retained austenite was detected in the as-quenched structure, consistent with the results from previous work on 4340 steel, i.e. austenite retention is decreased with a decrease in austenitizing temperature [39]. There was very little evidence of the undissolved particles in the areas observed; however, autotempering did occur to about the same extent as in the thin specimens.

On tempering the conventionally quenched material, interlath precipitation of cementite started at about 200°C (Plate 35-b). The formation of a Widmanstatten array of Fe_3C rods started at 250°C (Plate 35-c]. In the specimens tempered at 350°C some of the original lath boundary carbides appeared to develop branches out into the lath (Plate 35-d). At 400°C coarsening of the rod-shaped carbides was detected (Plate 35-e). Partial recovery and spheroidization of carbides was observed in the material tempered at 500°C (Plate 35-f); this process was noticed to developed to a further extent at 550°C.

Recrystallization of ferrite and further carbide spheroidization was observed when the tempering temperature was raised to 650°C (Plate 35-h). An attempt to determine the nature of these carbides through X-ray diffraction techechniques was not conclusive; however a TEMSCAN qualitative microanalysis detected peaks for iron and chromium as the major contributing elements.

The material quenched from 765°C was observed in the transmission electron microscope and the tempering behaviour of the material after this intercritical treatment was studied. The microstructure of the material before tempering or when it was lightly tempered consisted of a mixture of fine grained martensitic and ferritic islands. A quantitative assessment of the volume fraction of contributing phases was not possible due to the restrictions described earlier; however in the areas observed the structure

35-a ⊢0.5μ⊣

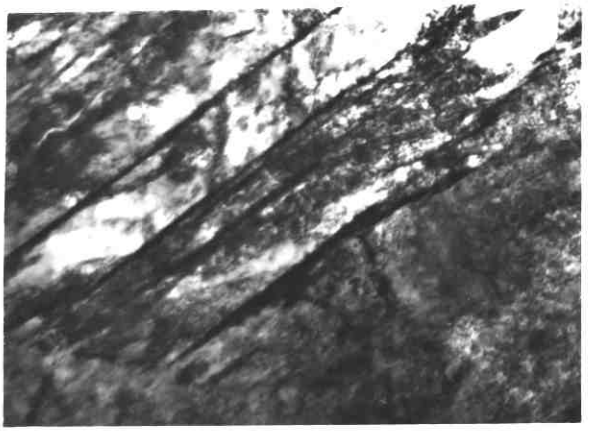

35-b ⊢0.5μ⊣

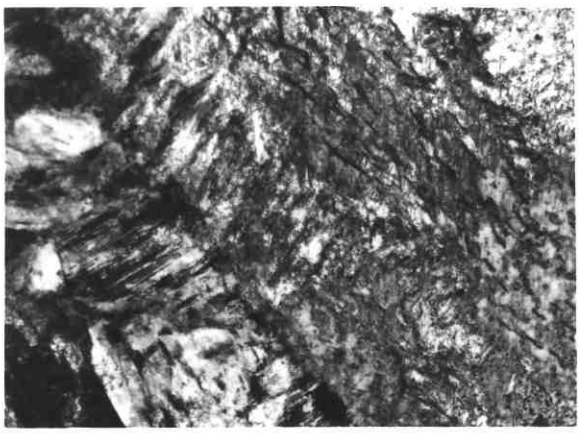

35-c ⊢1μ⊣

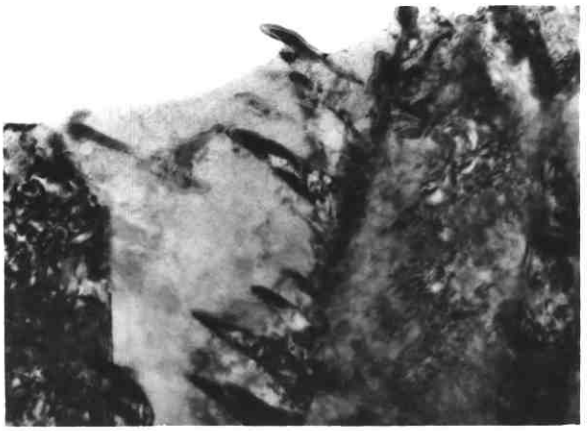

35-d ⊢0.25μ⊣

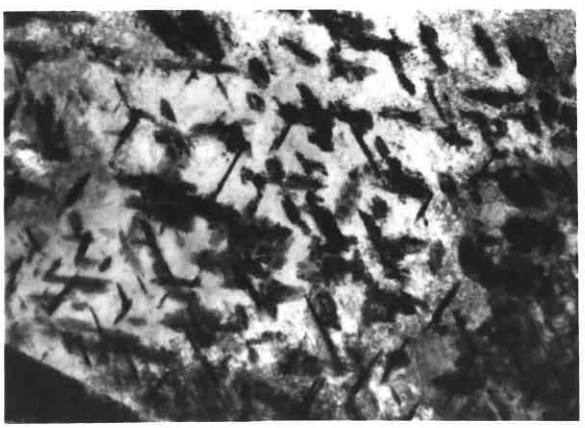

35-e ⊢1μ⊣

35-f ⊢0.2μ⊣

35-g ⊢0.4μ⊣

35-h ⊢0.5μ⊣

Plate 35-En 24 Charpy specimens,oil quenched from 835°C and tempered at: a-100°C,b-200°C,c-250°C,d-350°C,e-400°C,f-500°C,g-550°C and h-650°C
Conventional Treatment T.E.M.

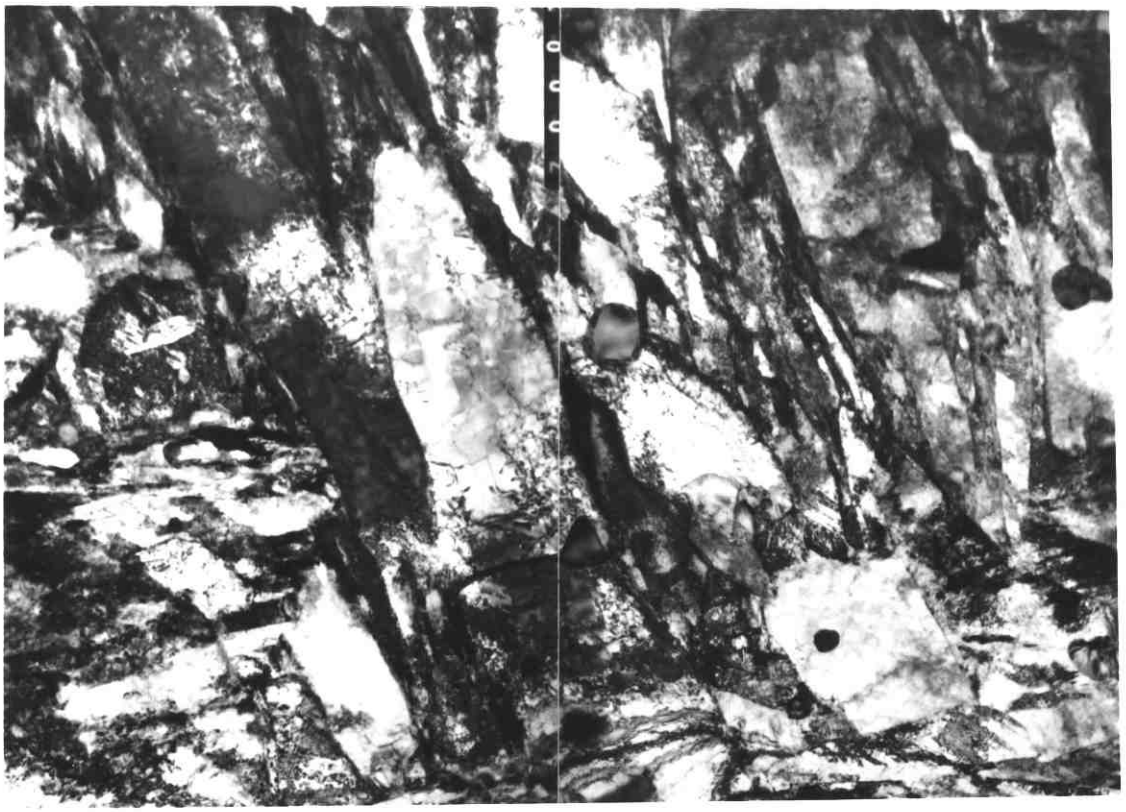

36-a

0.5μ

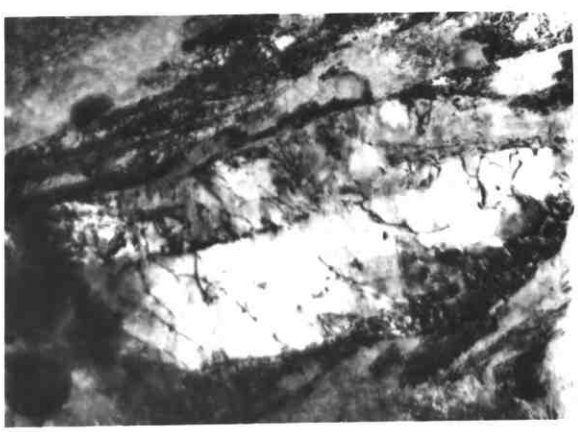

36-b

0.3μ

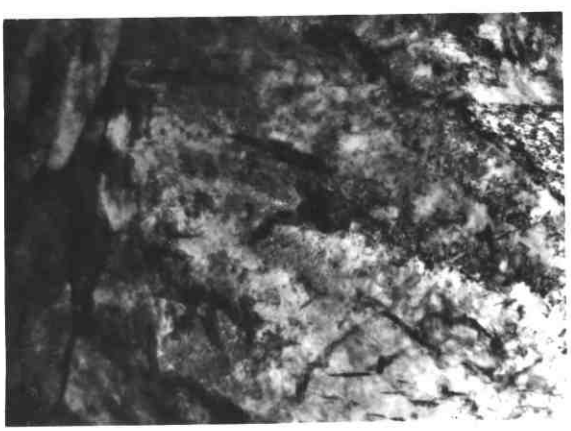

36-c

0.5μ

36-d

0.2μ

36-e

0.3μ

Plate 36-En24 as-quenched Charpy specimens, intercritically treated for ½h at 765°C +OQ, tempered at: a-200°C, b-100°C, c-250°C, d-450°C & e-400°C

appeared to be predominantly martensitic. Relatively large ($\sim 0.2\mu$) equiaxed undissolved particles were observed more frequently as compared to the conventionally treated material (Plate 36-a). The ferritic areas exhibited various morphologies and contained relatively high dislocation densities. The distribution of dislocation density in this phase appeared to be heterogeneous and higher concentrations were found in the vicinity of the martensitic laths (Plate 36-b) apparently formed as a consequence of the volume change accompanying the transformation of the austenite islands on quenching. Although the carbon content of the austenite islands is expected to be higher than the conventionally treated material, both types of martensite were observed as the result of the transformation (Plate 36-a).

The rod-shaped carbide precipitation was rarely detected after tempering of intercritically treated material (Plate 36-c). This process appeared to be retarded in the intercritically treated material. After tempering at 450°C, some coarsening in the carbide particles was detected (Plate 36-d). Partial recovery of ferrite was observed after tempering at 400°C with evidence of carbide dislocation pinning (Plate 36-e).

Section B. En8 Steel

4.5 Notes on Heat-Treatment

The En8 steel, as mentioned in the previous chapter, was supplied in the form of 10x10mm section bars. Its exact chemical composition was not specified but the nominal composition is given in Table 3.1. Variations in the heating and cooling rates of the specimens due to their size were avoided by simply maintaining a chosen size (standard Charpy) for all of the heat treatments. The initial austenitizing temperature (850°C) and heating medium to this temperature (a crusilite furnace) were both kept identical for all specimens. This material is known to have a relatively low hardenability (Fig. 4.14 from [128]) and it proved to be noticeably sensitive to the quenching rate; for example after an identical austenitizing of specimens for 1h at 850°C water-quenching produced a hardness of over 600 Hv, whereas the hardness for the oil-quenched specimens was around 550 Hv.

4.6 Initial Condition

The standard Charpy size specimens were austenitized for 1h at 850°C individually. Oil was chosen for the initial quench-hardening to avoid any risk of crack initiation as a consequence of water quenching. The as-quenched structure consisted of two constituents, difficult to interpret in the scanning electron microscope (Plate 37). However, the transmission electron microscopy observations made on the oil-quenched specimens of the En8 steel, facilitated the interpretation of the structure. Features such as fine

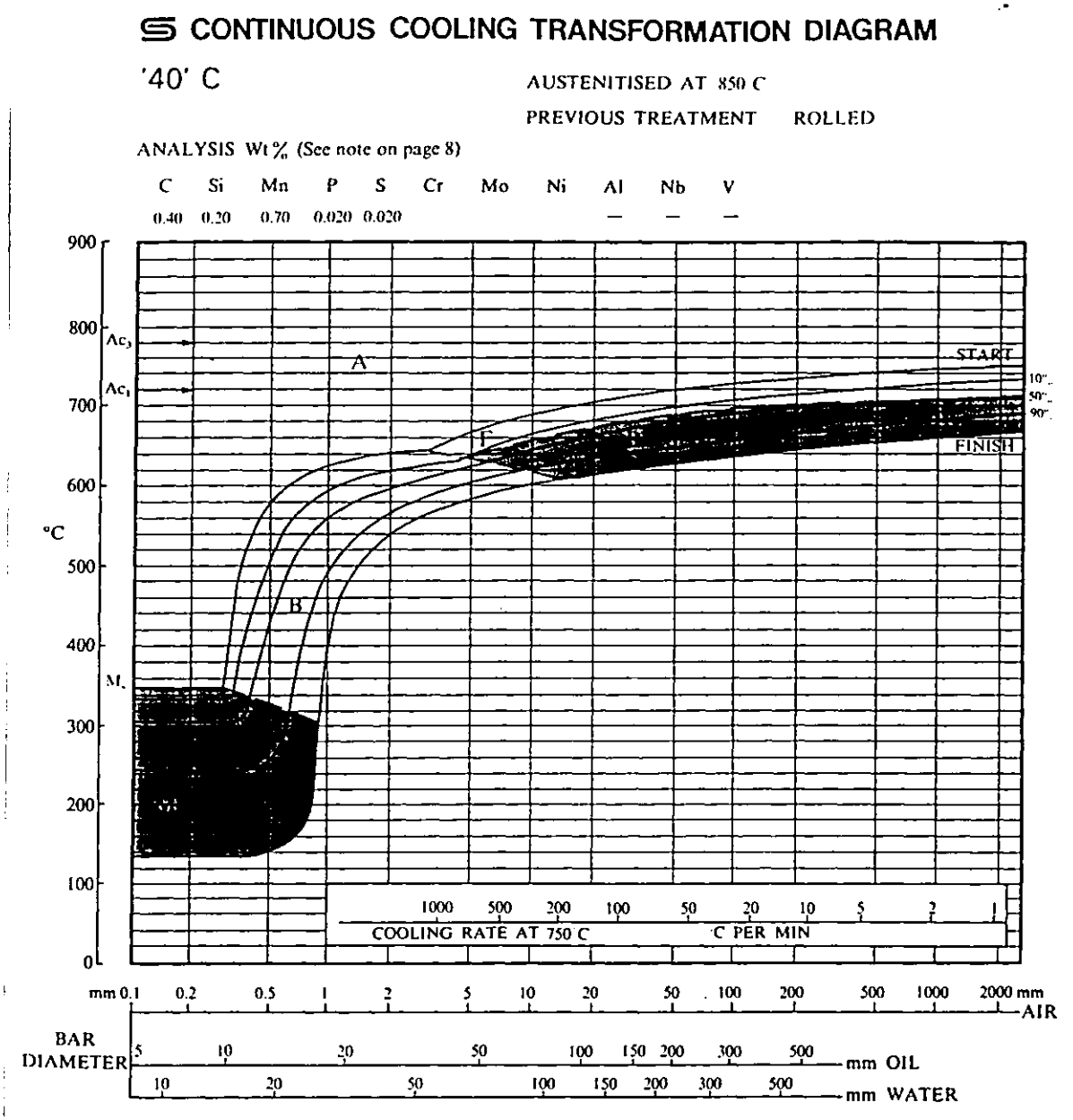

FIG. 4.14 - CONTIUOUS COOLING DIAGRAM FOR EN8 STEEL (AFTER REF.128)

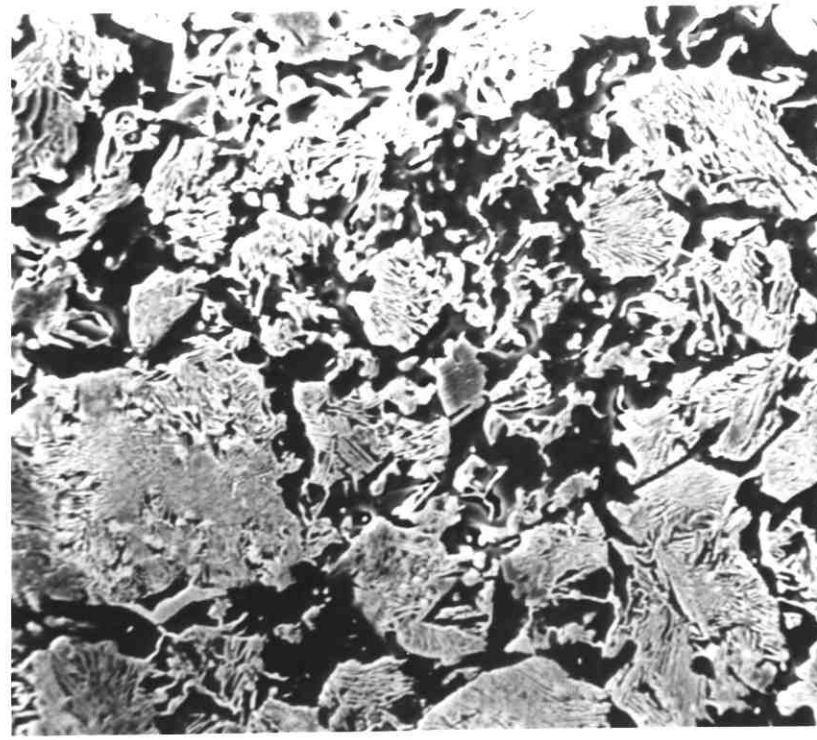

Plate 37-En8 steel,oil quenched from 850°C S.E.M.

15μ

38-a

1μ

38-b

1μ

38-c

0.5μ

38-d

0.4μ

Plate 38-Different areas of as-quenched En8 steel T.E.M.

internal twins and relatively high dislocation densities were considered to be acceptable for identifying one phase as martensite (Plates 38-a and -b) and for distinguishing it from lower bainite (Plate 38-c). The carbide particles occasionally detected in martensite were relatively fine and were precipitated during the martensitic transformation due to autotempering.

The second constituent observed in the plain carbon steel was interpreted to be lower bainitic in nature. It consisted mainly of ferrite plates with carbide particles precipitated internally at an inclined angle to the longitudinal axes of the ferrite plates (Plate 38-c). Some undissolved particles, approximately spherical shaped with a diameter of $\sim$0.25 μm were occasionally observed in the transmission electron micrographs (Plate 38-d).

4.7 Intercritical Treatments

4.7.1 Rapid Heating

A number of the oil-quenched specimens were heated to different temperatures within the intercritical range (i.e. 735°C, 750°C or 765°C) in a salt bath , held there for 30 min and water quenched. No sign of lower bainitic structure was detected in the areas of the specimens observed in the electron microscope after water-quenching from the intercritical temperatures. In the ferritic areas of the specimens held at 735°C (lower range of the intercritical temperature) elongated interlath carbides were observed and the dislocation density in the ferrite sub-grains appeared to be heterogeneously distributed (Plate 39-a). At 750°C (the intermediate range) intimate mixtures of ferrite and martensite of different morphologies seemed to be the main feature of the structure. The martensite consisted of both twinned and dislocated types (Plate 39-b). In the material water-quenched from 765°C (upper range of the intercritical temperature) the structure was observed to consist predominantly of martensitic areas (Plate 39-c). A fine lamellar ferrite/martensite mixture was frequently observed. Some undissolved particles were detected after the intercritical treatment (Plate 39-d).

The effect of tempering temperature on the hardness of the specimens intercritically treated at different temperatures for 30 min in the salt bath was examined and the results were compared to the ones obtained from tempering of conventionally oil-quenched specimens. As can be seen from Table 4.13 and Fig.4.15, the oil-quenched material exhibited a higher level of hardness, as expected, and also quenching from the upper portion of the intercritical range produced a harder material compared to those quenched from the lower ranges. Tempering gradually decreased the gap between the values in each stage and after 1 h tempering at 700°C, they all softened virtually to the same hardness.

From the preliminary hardness tests, a hardness level of 360 Hv was chosen and the tempering temperature to achieve this hardness was estimated from the curves in Fig.4.15. The pre-Charpy size specimens were oil-quenched,

39-a ⊢1μ⊣

39-b ⊢1μ⊣

39-c ⊢1μ⊣

39-d ⊢0.4μ⊣

Plate 39-Oil quenched En8 steel, intercritically treated for ½h(salt bath) at: a-735°C, b-750°C, c&d-765°C +WQ T.E.M.

Table 4.13 Effect of tempering temperature on the hardness of En8 as-quenched specimens and after intercritical treatments

Initial treatment	Tempering temperature°C, 1h						
	0	200	300	400	500	600	700
	Hardness Hv						
1h 850°C+Oil-Quench	557	555	492	405	339	275	207
OQ+½h 765°C(S.B.) + WQ	502	470	425	368	317	267	210
OQ+½h 750°C(S.B) + WQ	401	386	359	312	288	243	200
OQ+½h 735°C (S.B) + WQ	415	394	356	329	292	247	201

Table 4.14 En8 steel Hardness-Charpy energy results

Intercritical treatment in salt bath + W.Q.

No	Heat treatment	Hv	Charpy Energy Joules
1	1h 850°C + OQ, + 1h 470°C	356	69-74
2	OQ, + ½h 765°C + WQ,+1h 420°C	361	60-64
3	OQ, + ½h 750°C + WQ,+1h 300°C	382	32-33.5

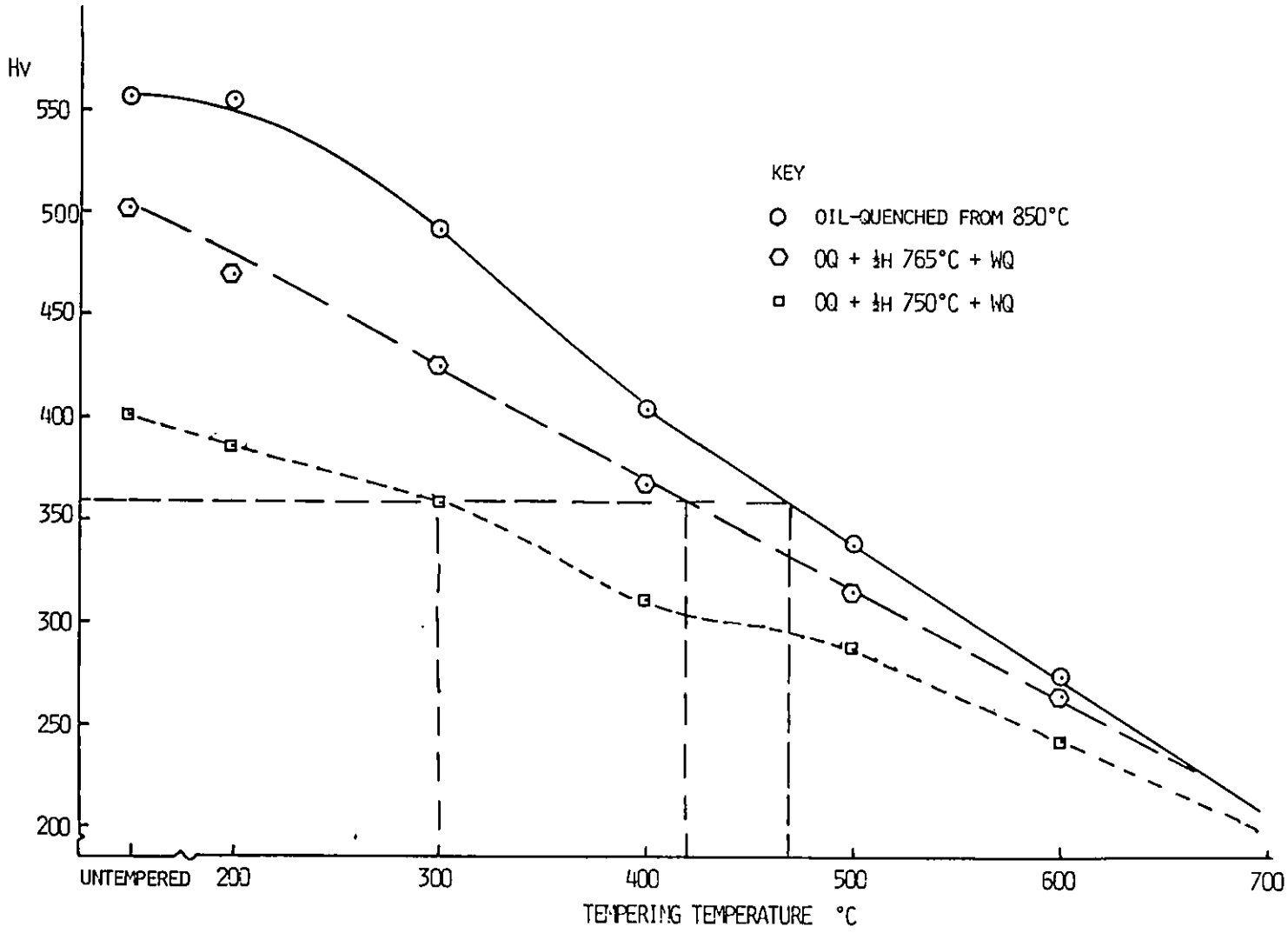

FIG. 4.15 - HARDNESS VS TEMPERING TEMPERATURE FOR EN 8 STEEL CHARPY SPECIMENS INITIALLY OIL-QUENCHED (AND INTERCRITICALLY TREATED IN SALT BATH + W.Q.)

some then intercritically treated, and finally tempered at the required temperature for 1h. They were then machine-finished and notched and fractured in a standard Charpy machine. Hardness measurements were carried out in the centre of the specimens and the values appeared to be close to the level expected. As can be seen from Table 4.14, there seems to be no improvement in the toughness of the specimens as a consequence of intercritical treatment in this steel.

4.7.2 Furnace Heating

Another series of En8 Charpy size specimens were austenitized for 1h at 850°C and oil-quenched to produce a starting point similar to those intercritically treated in the salt bath. These pieces were then individually heated in a vertical furnace to 735, 750 or 765°C for 30 min and oil quenched.

a. Structure

Electron microscopy was utilized to observe the structure of En8 specimens after the intercritical treatment. Scanning electron microscopy on the polished and etched specimens revealed features which were difficult to interpret. However the main constituents were postulated to consist of mixtures of ferrite and martensite in the material quenched from the two-phase region (Plates 40 a-c). The volume fraction of austenite increased, as expected, with increasing intercritical temperature and at the higher temperature of 765°C adjacent laths of the two constituents appeared to co-exist in the edges of the prior austenite grains (Plate 40-a). The ferrite laths were heterogeneously dislocated and some very fine particles were precipitated on the dislocation sites (Plate 41).

b. Mechanical Properties

Four series of specimens heat treated as explained earlier in this section, were tempered to temperatures ranging from 100 to 650°C with temperature intervals of 50°C. They were then notched and fractured and hardness measurements were carried out in the centre of the pieces. The strength and toughness of the material was assessed respectively on the basis of Vickers hardness and Charpy fracture energy. These characteristics are summerized in Table 4.15 and plotted in Fig. 4.16 a-d. Fig. 4.17 is a superimposition of Figs. 4.16 a-d, and Fig. 4.18 is a plot of hardness vs Charpy energy facilitating the comparison between the overall mechanical properties as explained in section A. As can be seen from Figs.4.16 a-d, the hardness vs tempering temperature curve is approximately linear for all conditions. The curves start from different as-quenched values (higher values associated with specimens quenched from higher temperatures) and soften with increasing the tempering temperature to about the same hardness at 650°C.

The 350°C embrittlement trough appears to be less pronounced compared to

En24 for the conventional treatment. The plots in Fig. 4.17 clearly indicate that decreasing the annealing temperature prior to tempering, not only produced lower values of hardness but also lowered the energy value absorbed in the fracture process; i.e. a deterioration in both strength and toughness. This effect was retained in the material after tempering. It is clearly seen from Fig. 4.18 that the more desirable combination of the overall mechanical properties at any strength or toughness level is offered by the conventionally treated material. In other words, there seems to be no sign of improvement in the mechanical properties in this alloy as a consequence of intercritical treatment.

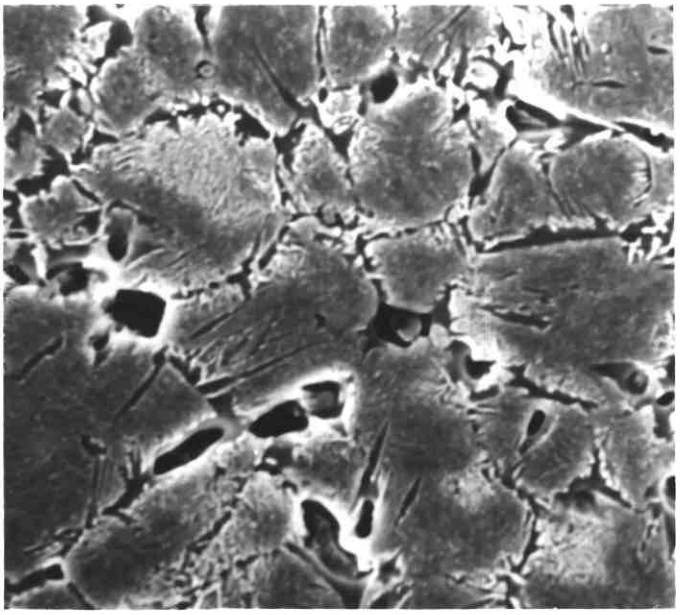

40-a ⊢—10μ—⊣

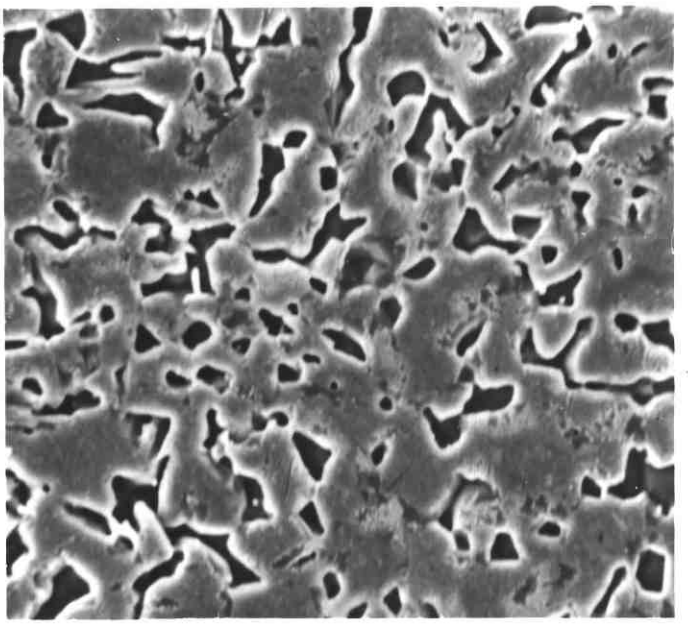

40-b ⊢—16μ—⊣

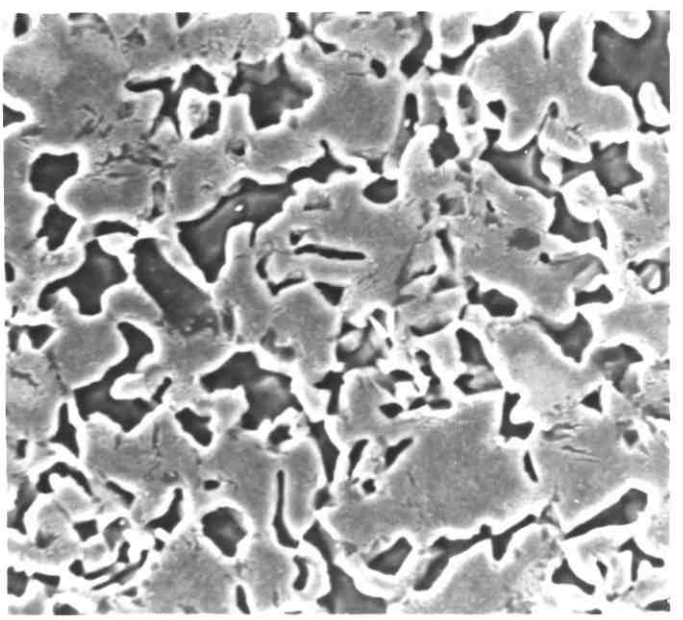

40-c ⊢—16μ—⊣

Plate40-Oil quenched En8 steel,intercritically treated for ½h at:
a-765°C, b-750°C and c-735°C +OQ S.E.M.

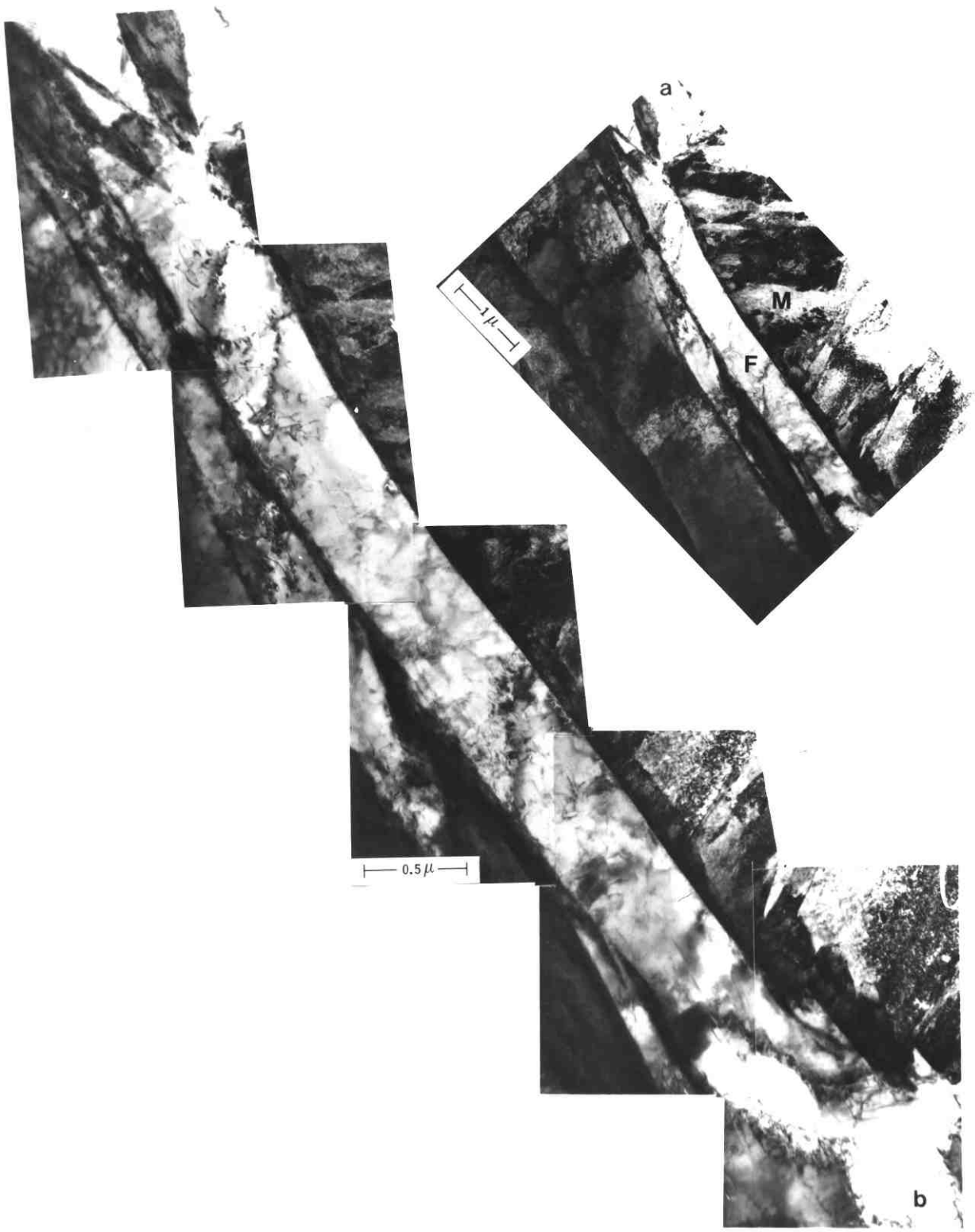

Plate 41- Oil quenched En8 steel held for ½h at 765°C (furnace)+OQ
F=ferrite M=martensite.Thin foil transmission electron mirograph

Table 4.15 En8 Charpy size specimens, 1h 850°C + OQ +½h intercritically treated in a furnace at different temperatures + 1h tempering at indicated temperatures

Charpy V Notch Energy and Hardness Vickers Result

Tempering Temperature, °C	Intercritical(α+γ) range treatment temperature											
	Conventional treatment			765°C			750°C			735°C		
	Charpy Energy, J	Hardness Hv		Charpy Energy, J	Hardness		Charpy Energy, J	Hardness		Charpy Energy, J	Hardness	
		Mean Value	Standard Dev		Mean Value	Standard Dev		Mean Value	Standard Dev		Mean Value	Standard Dev
Untempered	22	542	34	20	443	25	20	402	3	17	355	12
100°C	14	442	73	19	425	22				10	335	12
200°C	25	489	47	24	389	20	20	368	19	22	331	7
250°C	33	487	35	41	328	15				25	368	7
300°C	57	418	8	31	417	12	33	376	6	30	345	3
350°C	52	421	22	54	343	15				46	312	10
400°C	82	389	4	70	324	13	59	338	8	58	302	5
450°C	100	342	7	90	307	7				82	288	3
500°C	146	298	7	105	301	7	102	285	5	94	270	4
550°C	143	297	2	140	277	5				126	248	3
600°C	178	256	5	164	234	3				140	227	2
650°C	223	225	5	197	225	2	190	211	2	190	202	1

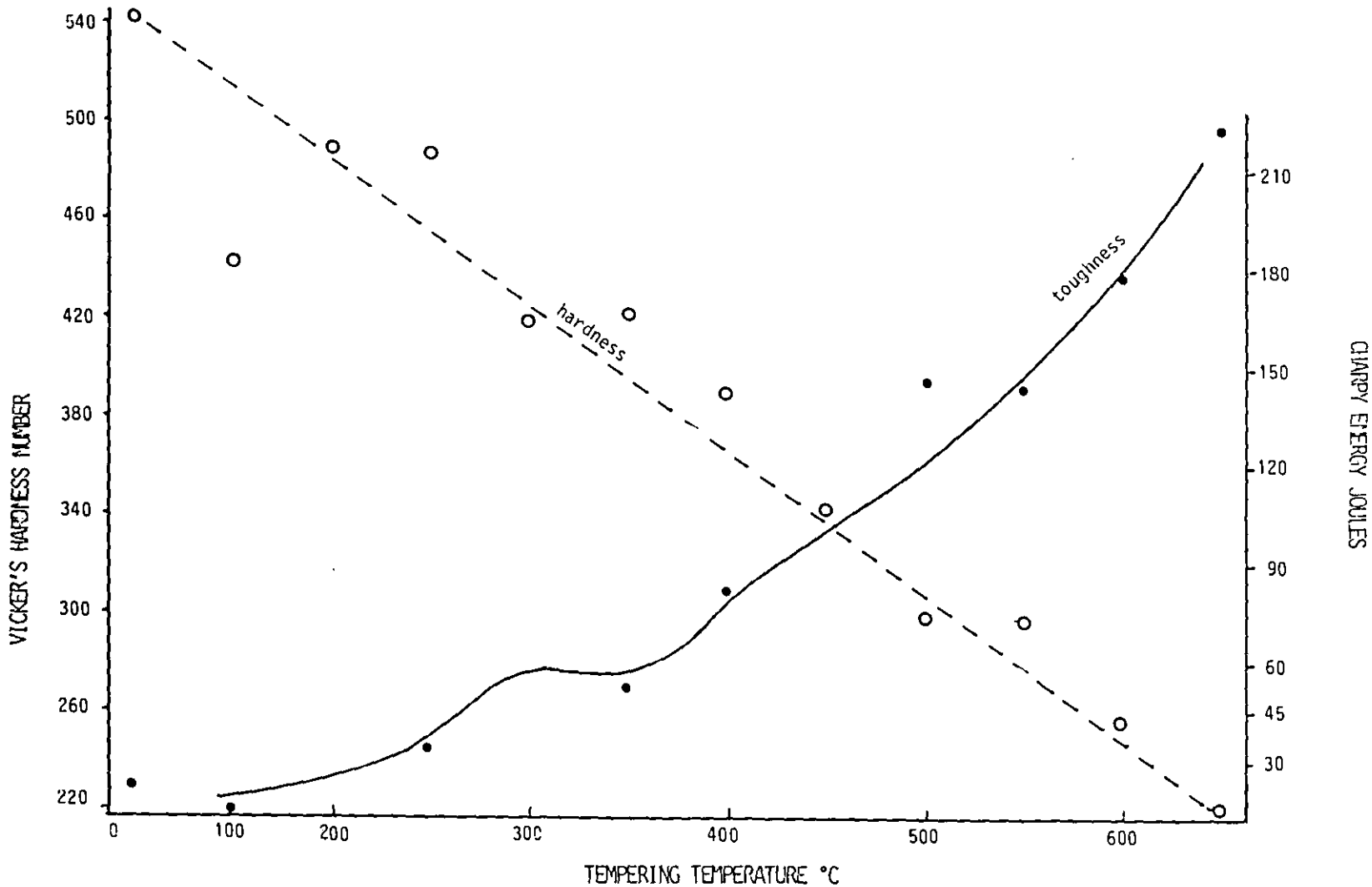

FIG. 4.16 A - EFFECT OF TEMPERING ON HARDNESS AND CHARPY ENERGY FOR EN 8 STEEL; INITIAL CONDITION: 1½H 850°C+OQ

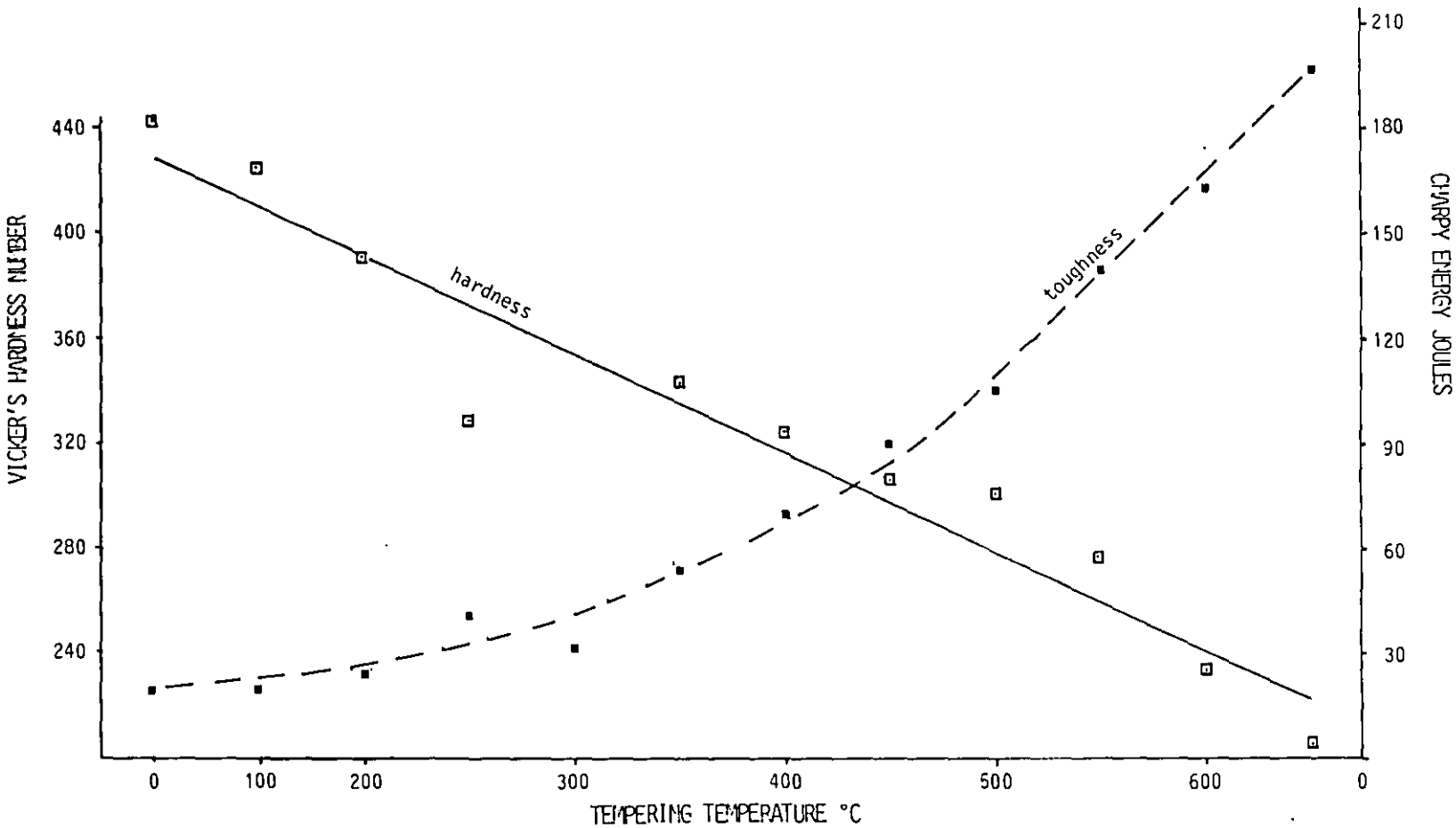

FIG. 4.16 B - EFFECT OF TEMPERING ON HARDNESS AND CHARPY ENERGY FOR EN 8 STEEL; INITIAL CONDITION: 1½H 850°C+OQ. ½H 765°C+OQ

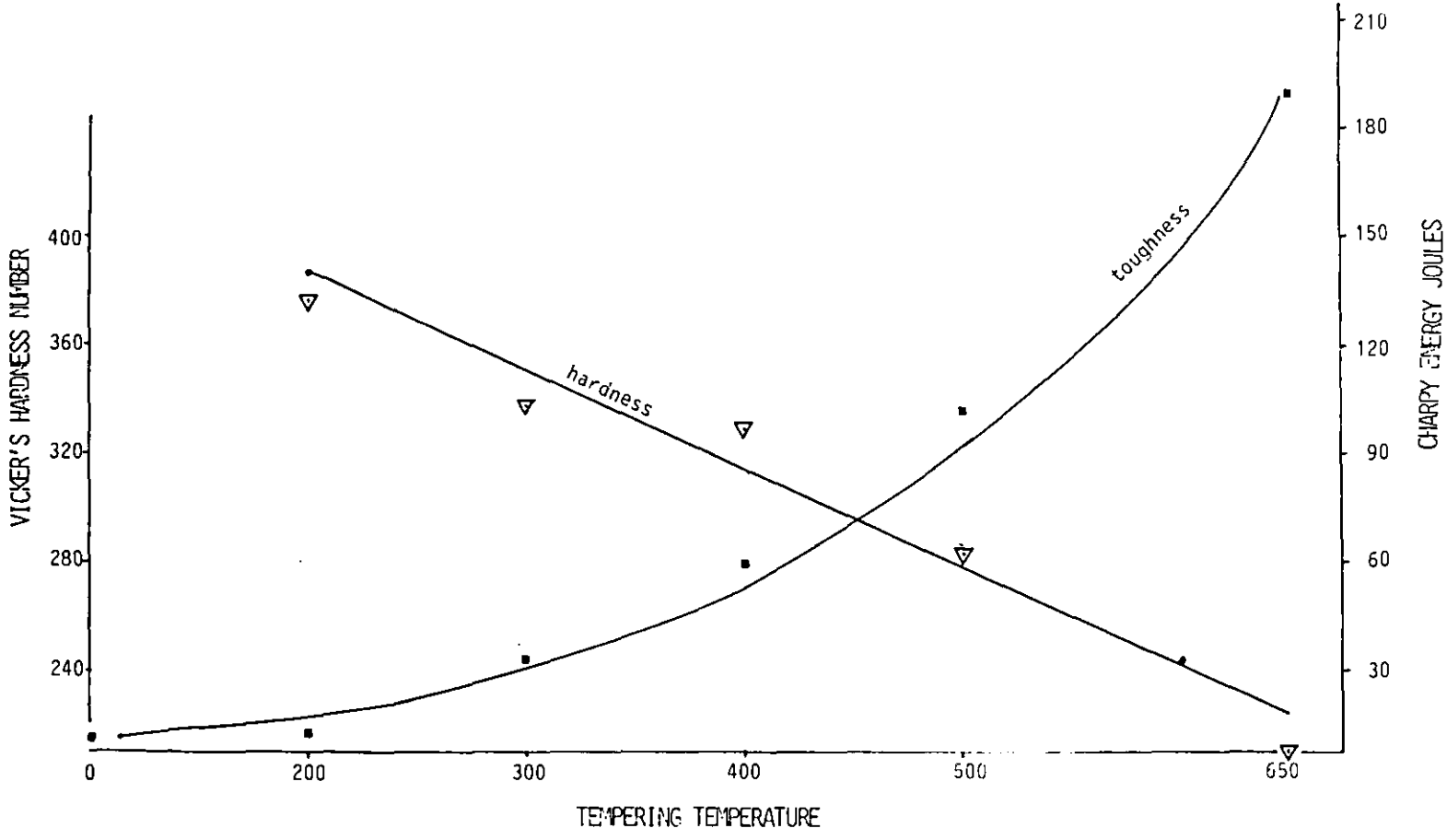

FIG. 4.15 C - EFFECT OF TEMPERING ON HARDNESS AND CHARPY ENERGY FOR EN 8 STEEL; INITIAL CONDITION: 1½H 850°C+OQ ½H 750°C+OQ

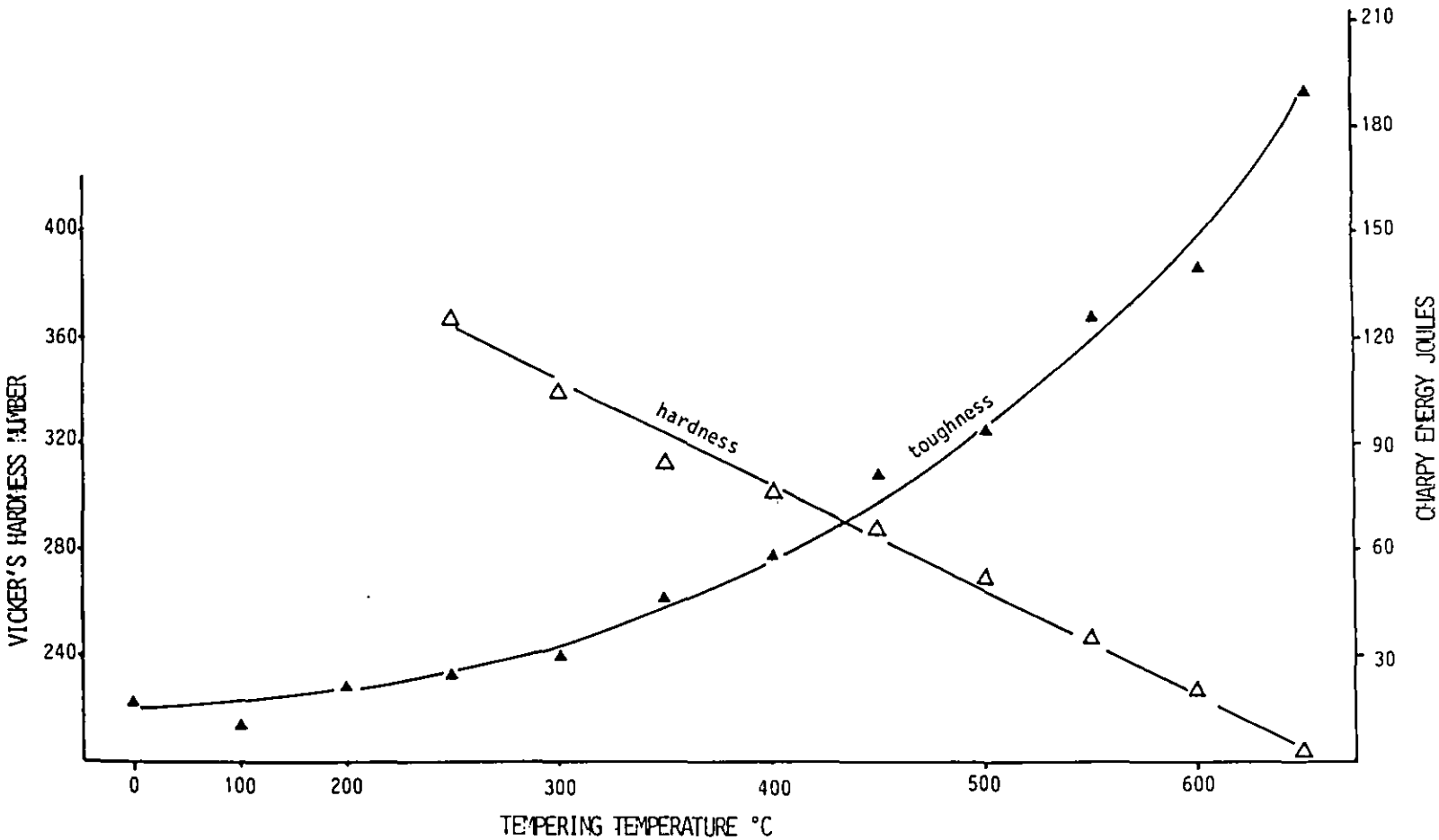

FIG. 4.16 D - EFFECT OF TEMPERING ON HARDNESS AND CHARPY ENERGY FOR EN 8 STEEL; INITIAL CONDITION 1½H 850°C+OQ ½H 735°C+OQ

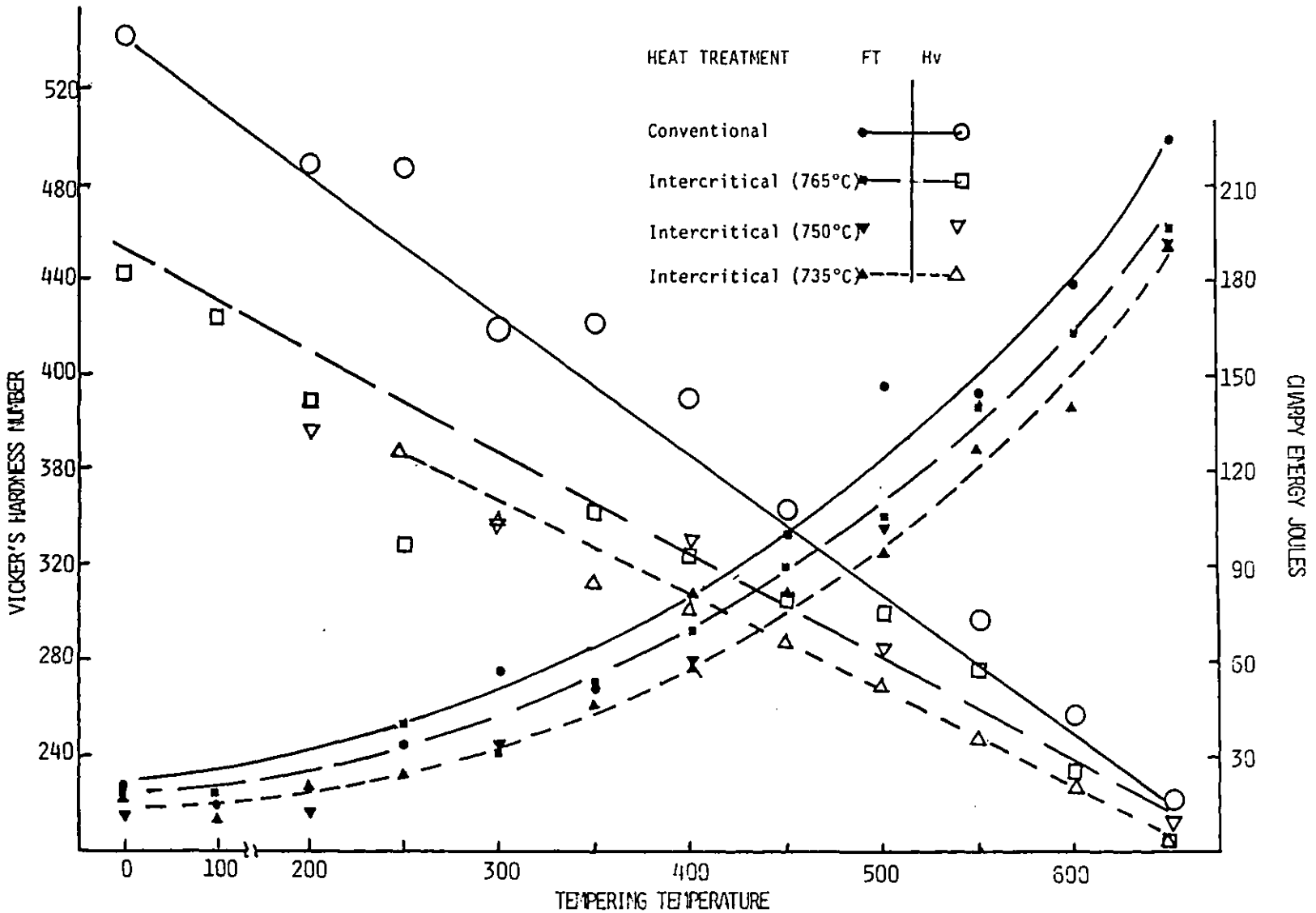

FIG. 4.17 - EFFECT OF TEMPERING ON HARDNESS AND CHARPY ENERGY FOR EN 3 STEEL WITH DIFFERENT STARTING CONDITIONS

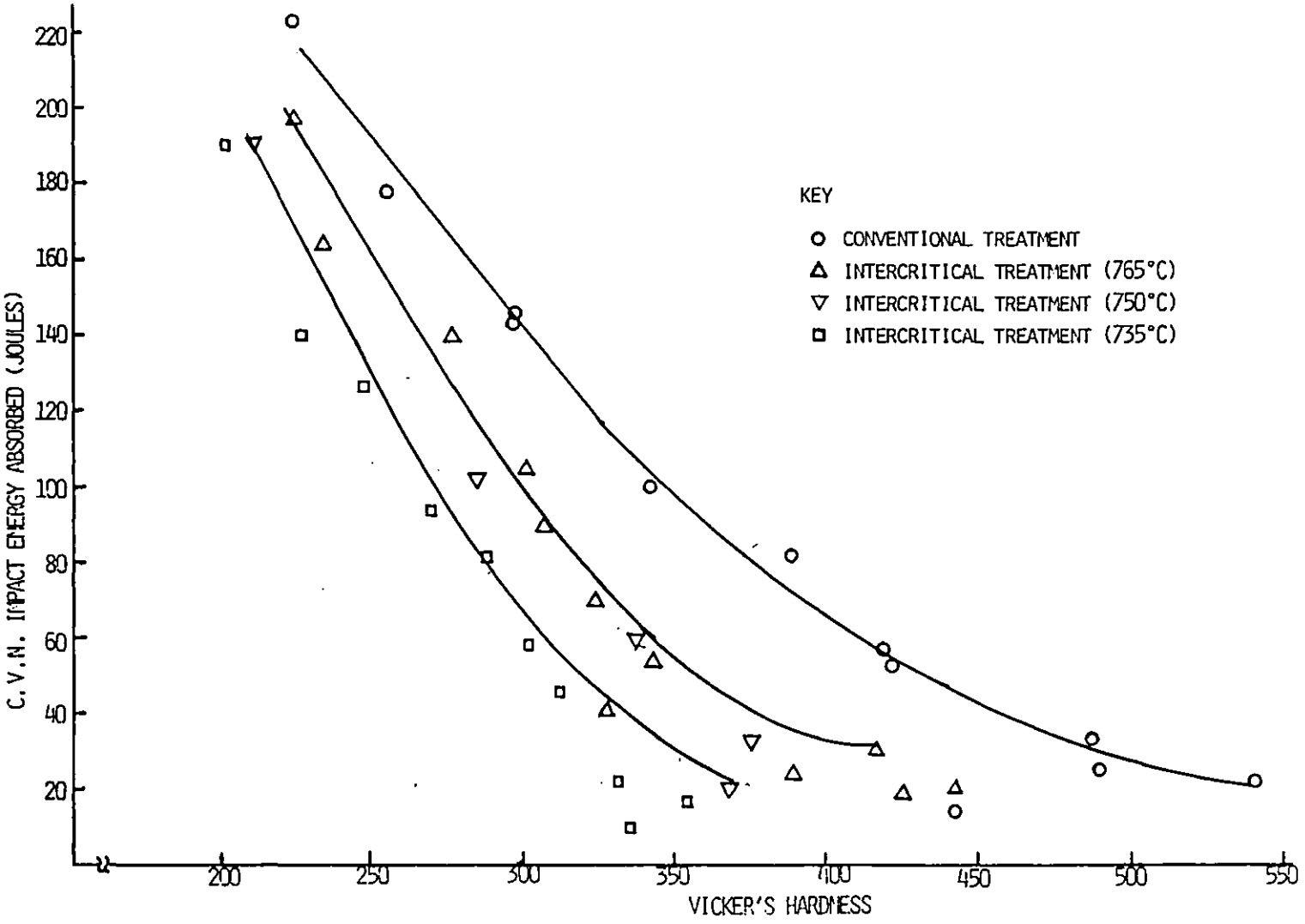

FIG. 4.18 - PLOT OF CHARPY V NOTCH ENERGY VS HARDNESS FOR EN 8 STEEL

Chapter 5

Discussion

5.1 Introductory Notes

5.1.1 The Effect of Alloy Additions on the Binary Fe-C Phase Diagram

The metallic elements commonly used in heat-treatable, low alloy steels (Mn, Si, Cr, Ni, Mo, V) alter both the eutectoid composition and the eutectoid temperature. This can affect the structure and mechanical properties of the alloys after different heat treatments. Since the assessment of the combined effects of alloying elements present in a multi-component system is complicated, one of the common approaches to the problem is to consider the effect of individual elements, assuming that the total effect is additive. This approach is not necessarily applicable in all cases and there are examples to show that the interactive effects of alloying elements cannot always be expressed in simple arithmetic terms (e.g. Ref.63). However, deviations from the actual experimental results can sometimes be explained.

5.1.2 Elements in En24 Steel

Molybdenum:

Additions of large amounts of Mo, (i.e.>~2%) are known to produce major effects as shown by the constitution of the C-Fe-Mo ternary alloy system (Ref.101); however, the effect of small additions (e.g.0.27% in En 24 steel) is not large. In fact, as it was shown in the results section, since M_3C was the only carbide detected, the major probable effect could be the formation of an "Ae_1 range of temperatures" from ~ 730 to ~ 755°C. This range can be deduced by comparing different molybdenum-constant sections of the C-Fe-Mo ternary system, Fig.5.1 a and b. It appears from these sections that while an increase in the molybdenum content results in an increase in the carbon content range of the three phase ($\alpha+\gamma+$carbide) region, the range of temperatures in which a particular type of carbide is in equilibrium with ($\alpha + \gamma$) does not depend on the molybdenum content of the alloy. For example in both sections of 2 and 4% molybdenum (and also in sections of 10 and 20% molybdenum) of the ternary system, the range of temperatures in which M_3C is in equilibrium with ($\alpha + \gamma$), appears to be between 730 and 755°C, i.e. independent of the Mo content. It seems reasonable to assume that lower concentrations of Mo can also give rise to a similar effect on the Ae_1 temperature.

FIG. 5.1 A

FIG. 5.1 B

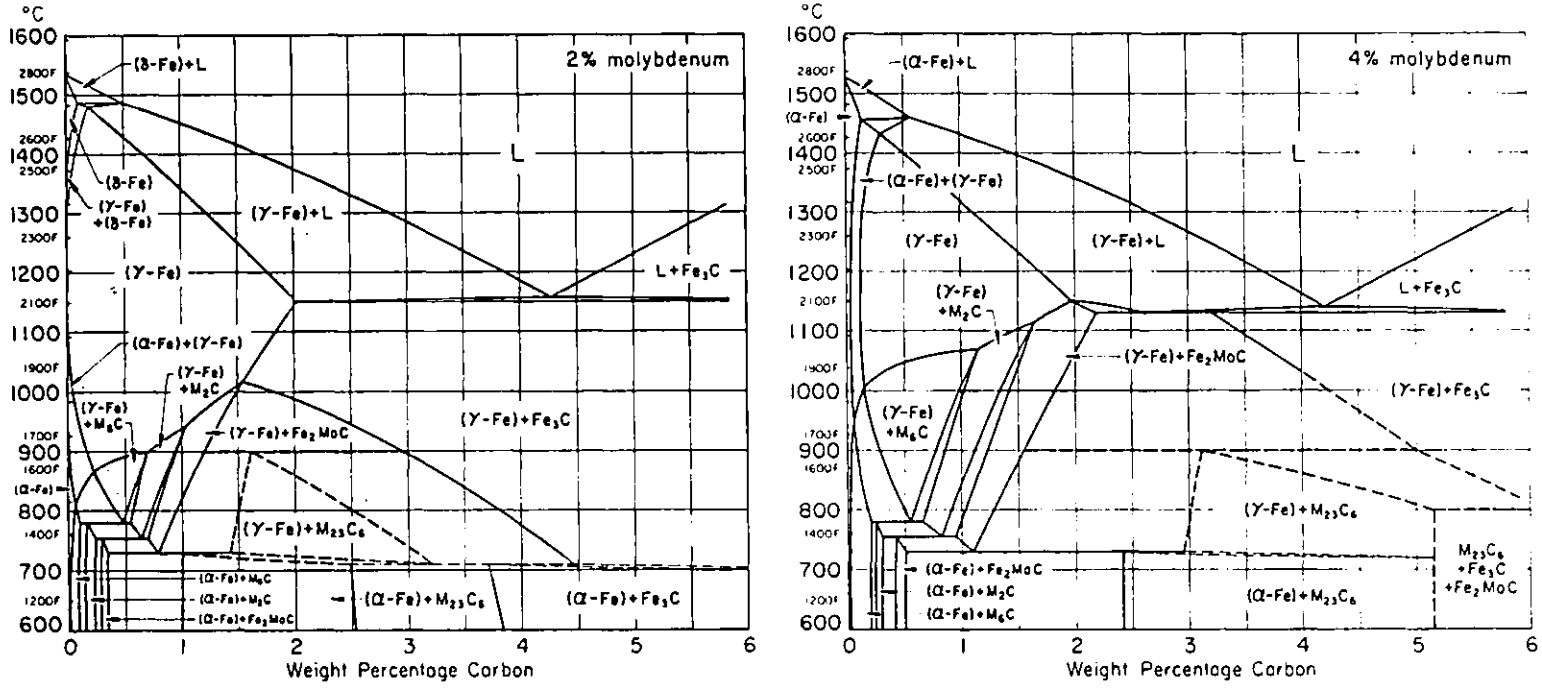

FIG. 5.1 - CONSTANT MOLYBDENUM SECTIONS FROM THE FE-MO-C PHASE DIAGRAM (REF. 101)

Since the rise in the α/γ transition temperature in the Fe-Mo binary system, for small proportions of Mo (i.e.<1%) can be considered to be linearly proportional to the molybdenum increment [101], the α/γ transition temperature at 0%C may increase ~20°C due to ~ 0.3% Mo addition. The eutectoid temperature is not affected noticeably by such a small addition and the eutectoid carbon content decreases by ~0.1 pct. If the increase in Ae_3 temperature (0.4%C) is also assumed to be linearly proportional to the Mo increment (for small additions), there would be a rise of ~ 12°C due to a 0.27% molybdenum addition. The results of all calculations are summarized in Table 5.2.

Chromium:

This element is known to be an α-former, a carbide-former and a carbide-stabilizer [102], and its addition to the Fe-C system creates a range of temperatures in which ($\alpha + \gamma$) can be in equilibrium with carbides. With the same assumptions made in the case of Mo, the Ae_1 temperature range for an alloy containing 0.4% C and 1.21% Cr can be calculated to be between ~ 735 and 740 °C. A small decrease (~10°C) will also occur in the Ae_3 temperature (0.4%C) as a result of the addition of this element (Fig.5.2). At 0%C, it can be deduced from the Fe-Cr binary diagram that the fall in the α/γ transition temperature (for Cr< ~ 5%) is linearly proportional to Cr increment. Hence there would be a decrease of ~ 20°C as a consequence of 1.21% Cr addition. The changes in the eutectoid temperature and composition are calculated from a plot [121] and together with the rest of the results appear in Table 5.2.

Manganese:

Although this element is not a strong carbide-former, it contributes to the stabilization of cementite through its higher solubility in the carbide than in the ferrite (partition coefficient = 11.4; [102]). It is known to be an austenite-former and it shows a complete solid solubility with γ-iron. When alloyed with pure iron it depresses the $\gamma/(\alpha + \gamma)$ transition temperature, this effect being proportional to the actual Mn increment for low concentrations (<~ 10% Mn). The drop for 4.5% Mn is ~120°C and hence for 0.66% Mn it is calculated to be ~ 18°C, i.e. Ae_3(0%C)=~894°C. By comparing constant manganese sections from the Fe-Mn-C alloy system (Fig.5.3) it can be deduced that there is an approximate linear relationship between the Mn concentration (Mn< 4.5%) and each of the following:

1- The decrease in the eutectoid carbon content,
2- The fall in the eutectoid temperature,
3- The drop in Ae_3 (0.4%C) temperature,and
4- The decline in both the lower and the upper limit of Ae_1 temperature range, with a higher rate in the lower limit.

Fig.5.4 is a plot of this relationship, based on data in Table 5.1 (Ref.101).

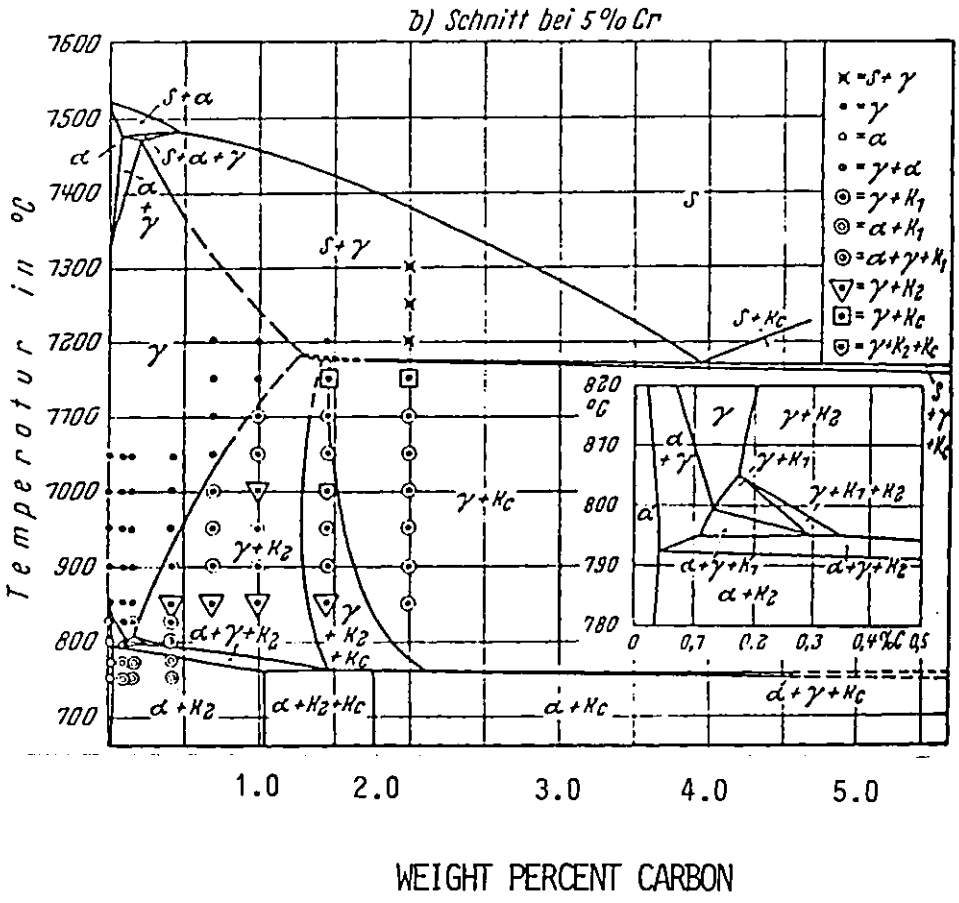

FIG. 5.2 - A CONSTANT CR SECTION FROM THE FE-CR-C PHASE DIAGRAM (AFTER V.K.BUNGARDT, E. KUNZE AND E. HORN: ARCHIVE FUER DAS EISENHUTTENWESEN, VOL.29, 1958, 193-203)

FIG. 5.3 A

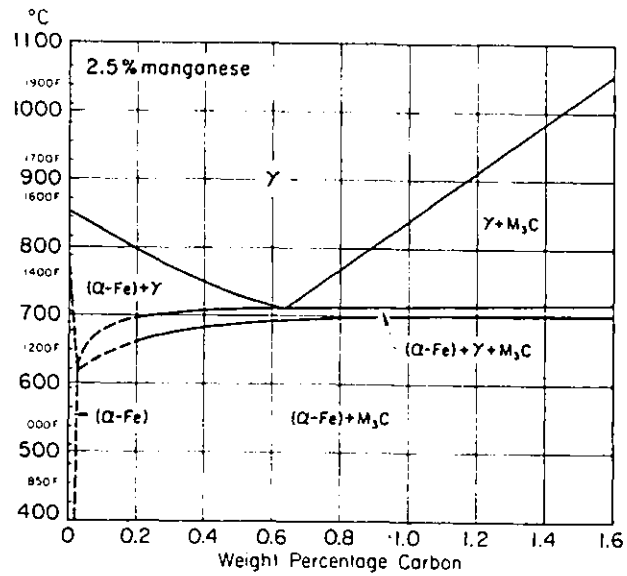

FIG. 5.3.B

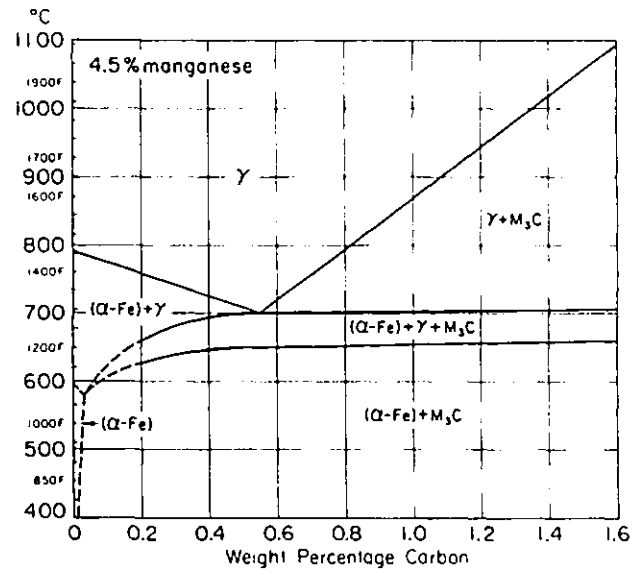

FIG. 5.3 - CONSTANT MANGANESE SECTIONS FROM THE FE-MN-C PHASE DIAGRAM (AFTER REF.101)

Table 5.1 The effect of Mn content on Fe-C phase diagram

Alloy	Eutectoid		Ae1(0.4%C),°C		Ae3 °C	
	C %	t °C	lower	higher	0 % C	0.4 % C
Fe-C-4.5%Mn	0.55	700	648	693	794	725
Fe-C-2.5% Mn	0.64	713	685	708	855	750
Fe-C-0.66% Mn	0.73	723	715	721	894	774

Table 5.2 The effects of alloying elements in En24 on Fe-C Binary system

Alloy	Eutectoid Temperature		Eutectoid C Content		Ae_1 Temper--ature °C		Ae_3 Temper--ature °C 0% C		Ae_3 Temper--ature °C 0.4%C	
	°C	Δ	%	Δ	Lower	upper	°C	Δ	°C	Δ
Fe-C	727	0	0.77	0	727	727	912	0	783	0
Fe-C+0.66%Mn	723	-4	0.73	-0.04	715	721	894	-18	774	-9
Fe-C+1.21%Cr	745	+18	0.7	-0.07	735	740	892	-20	773	-10
Fe-C+0.27%Mo			0.67	-0.1	730	755	932	+20	795	+12
Fe-C+1.43%Ni	712	-15	0.74	-0.03			822	-90		

Table 5.3 The equilibrium carbon content and weight percent phases in Fe-0.4C alloy

Temperature °C	Ferrite		Austenite	
	C Content %	wt.(pct)	C Content %	wt.(pct)
735	0.021	44	0.70	56
750	0.020	33	0.59	67
765	0.019	21	0.50	79

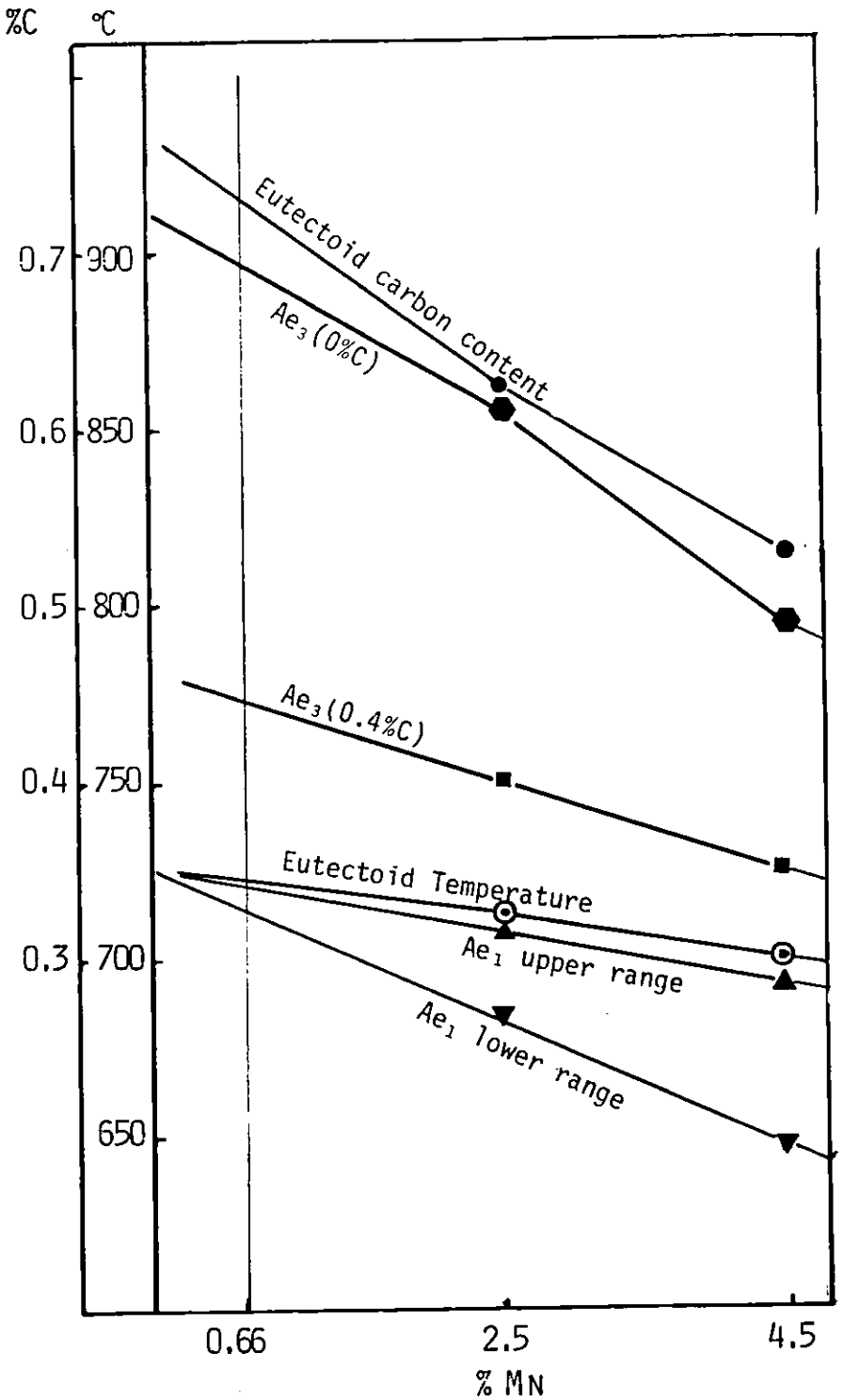

FIG. 5.4 - EFFECT OF MANGANESE ON SOME OF THE CHARACTERISTICS IN THE FE-C SYSTEM

Nickel:

This element, a strong γ-former, makes no contribution to either formation or stabilization of carbides. In fact it promotes graphitization. It is completely soluble in pure γ-Fe and acts to lower the single-phase austenite formation temperature in a manner similar to that of Mn. Hence it will decrease the Ae_3(0%C) temperature in En 24 (1.43% Ni) by ~90°C. The small decrease in the eutectoid carbon content and temperature are calculated at 1.43% Ni which can be seen in Table 5.2.

Hence, assuming the effects are additive, it can be concluded that :

a- The eutectoid temperature will remain almost unchanged.
b- The eutectoid composition will contain about 0.25% less carbon than in plain carbon steel, i.e. ~0.52 wt pct.
c- The Ae_1 temperature range could be between 720-740°C.
d- The Ae_3 temperature (0%C) will decrease by about 110°C to ~800°C.
e- The Ae_3 temperature (0.4%C) will drop to ~776°C

There are also more readily available approaches to calculating Ae_1 and Ae_3 temperatures in relatively complex systems. For example, Andrews, by examining a large amount of data, suggests empirical equations [104] which are still being used for this purpose [105]:

$$Ae_1 = 723 - 10.7\%Mn - 16.9\%Ni + 29.1\%Si + 16.9\%Cr + 290\%As + 6.38\%W$$

$$Ae_3 = 910 - 203\%\sqrt{C} - 15.2\%Ni + 44.7\%Si + 104\%V + 31.5\%Mo + 13.1\%W - (30\%Mn + 11\%Cr + 20\%Cu - 700\%P - 400\%Al - 120\%As - 400\%Ti)$$

This sort of general formulae may give some indication as to the approximate estimation of critical temperatures; however, care should be taken in their application if accurate determinations of these values are required. For example, by substitution of the actual amounts of alloying elements in En24 steel, Ae_1 and Ae_3 for this alloy would be calculated to be 720 and 765°C respectively, while as indicated earlier, from the constitution of ternary alloys, a range of temperatures is expected for Ae_1 rather than a distinct unique value. Furthermore, as can be seen in the forthcoming discussion, even after treating this alloy for long periods at 765°C, retained ferrite and carbide were still detected on quenching, which can give rise to doubts about the extent to which the general empirical equations are applicable in individual cases.

5.1.3 The Composition and Proportion of Phases in the Fe-C system

For a 0.4 pct plain carbon steel, the equilibrium composition and proportion

of phases at different intercritical temperatures can be calculated from the binary Fe-Fe_3C phase diagram (Table 5.3). The austenite in the ($\alpha + \gamma$) field transforms to b.c.t. martensite on quenching, with a specific gravity close to that of ferrite. Consequently the weight percent of the constituent phases in Table 5.3 can be regarded as almost equal to the volume fractions of ferrite and martensite in the quenched structure, assuming no carbide is present.

For the alloy steel, however, these values could be used as an approximate guideline to indicate the equilibrium conditions, since the presence of carbides (mainly M_3C) can markedly affect both the carbon content and the volume fractions of phases. The addition of alloying elements to a plain carbon steel will influence the critical range of temperatures as discussed through their effect on Ae_1 and Ae_3 ranges. Consequently a steel containing one or more alloying elements would be expected to form a different volume fraction of austenite than would a plain carbon steel of the same carbon content after intercritical annealing at the same temperature. For example, the addition of Mn to a plain carbon steel would result in the expansion of the austenite phase field and the depression of the A_1 and A_3 lines as well as reducing the eutectoid C content. This element can reduce the size of the intercritical region (Fig.5.4) and therefore the formation of more austenite would be expected than in a plain carbon steel with the same carbon content treated at the same temperature.

5.1.4 Hardness of ferrite + martensite mixtures

An approximate estimate of the overall hardness can be made when a plain carbon steel containing 0.4 pct C is held for times sufficient to attain equilibrium at different temperatures within the ($\alpha + \gamma$) field and subsequently quenched.

Assuming that the mixture rule for composites can be applied with adequate accuracy to mixtures of ferrite plus martensite obtained as above, it is possible to calculate the overall hardness of the mixture from the hardness values and volume fractions of the constituent phases. In such a calculation, the following assumptions were also made:

1- The volume fraction of martensite is close to weight fraction (i.e. weight percent $\div 100$) of austenite, derived from the Fe-Fe_3C phase diagram [101] since the density of b.c.c ferrite is close to that of b.c.t. martensites.

2- The amount of retained austenite and undissolved carbides on quenching is negligible.

3- The hardness of martensite in the mixture is estimated according to its C content [103], i.e. the C content of austenite at the equilibrium temperature. This means that any effect of the softer surrounding ferrite

on the hardness of the transformed martensite is neglected.

4- The hardness change in ferrite, due to the martensitic transformation in the neighbouring austenite, resulting from the strains introduced into ferrite on quenching is negligible and ferrite retains a low hardness of about 100Hv, regardless of the volume fraction of martensite. The calculated values (Table 5.4) are plotted in Fig.5.5.

5.1.5 An Evaluation of Alloy Diffusion Rates in Ferrite and Austenite

The diffusion coefficient (D) at different temperatures can be calculated from the relationship:

$$D = D_0 \exp(-Q/RT) \qquad (5.1)$$

where:

D = diffusion coefficient (cm^2/s)
D_0 = frequency factor (cm^2/s)
Q = energy of activation (J/mol/°K)
T = temperature (°K)
R = gas constant (8.319 J/mol)

The D_0 and Q values for different alloying elements in α and γ iron (Table 5.5) are extracted from Ref. 102.

The interparticle spacing prior to most heat treatments in En24 steel was observed to be around 0.2 μm (see Plates 4,10,14,15,17,27,29). A mean diffusion distance of 0.1 μm (10^{-5}cm) was hence assumed in order to estimate the times required for the diffusion of each element at different temperatures. According to mathematical studies of diffusion , the average distance of diffusion $\bar{x}$(cm) is equal to $\sqrt{}$(2Dt) where D is the diffusion coefficient (cm^2/s) and t is time in seconds. Table 5.7 shows the calculated times for the diffusion of the elements in ferrite and austenite at different temperatures for $\bar{x}$ = 0.1 μm.

5.2. Kinetics and Mechanism of Intercritical Transformations

5.2.1 Heat Treatment Parameters

In this section the effect of the heat treatment parameters, i.e.:

a-the heating rate
b-the heating temperature, and
c-the heating time

Table 5.4 Calculated hardness for a ferrite+martensite mixture in an Fe-0.4 pct C alloy

Temperature °C	wt% C in γ	Martensite Hardness Hv	Martensite Volume Fraction	$f\alpha' \cdot Hv\alpha'$	Mixture Hardness Hv
783	0.40	760	1.00	760	760
780	0.42	773	0.96	741	745
773	0.45	794	0.88	702	714
767	0.49	826	0.80	663	682
760	0.52	842	0.75	635	660
753	0.56	857	0.70	600	630
747	0.62	884	0.64	563	599
740	0.66	900	0.59	531	572
733	0.72	925	0.54	500	546
727	0.77	936	0.50	468	518

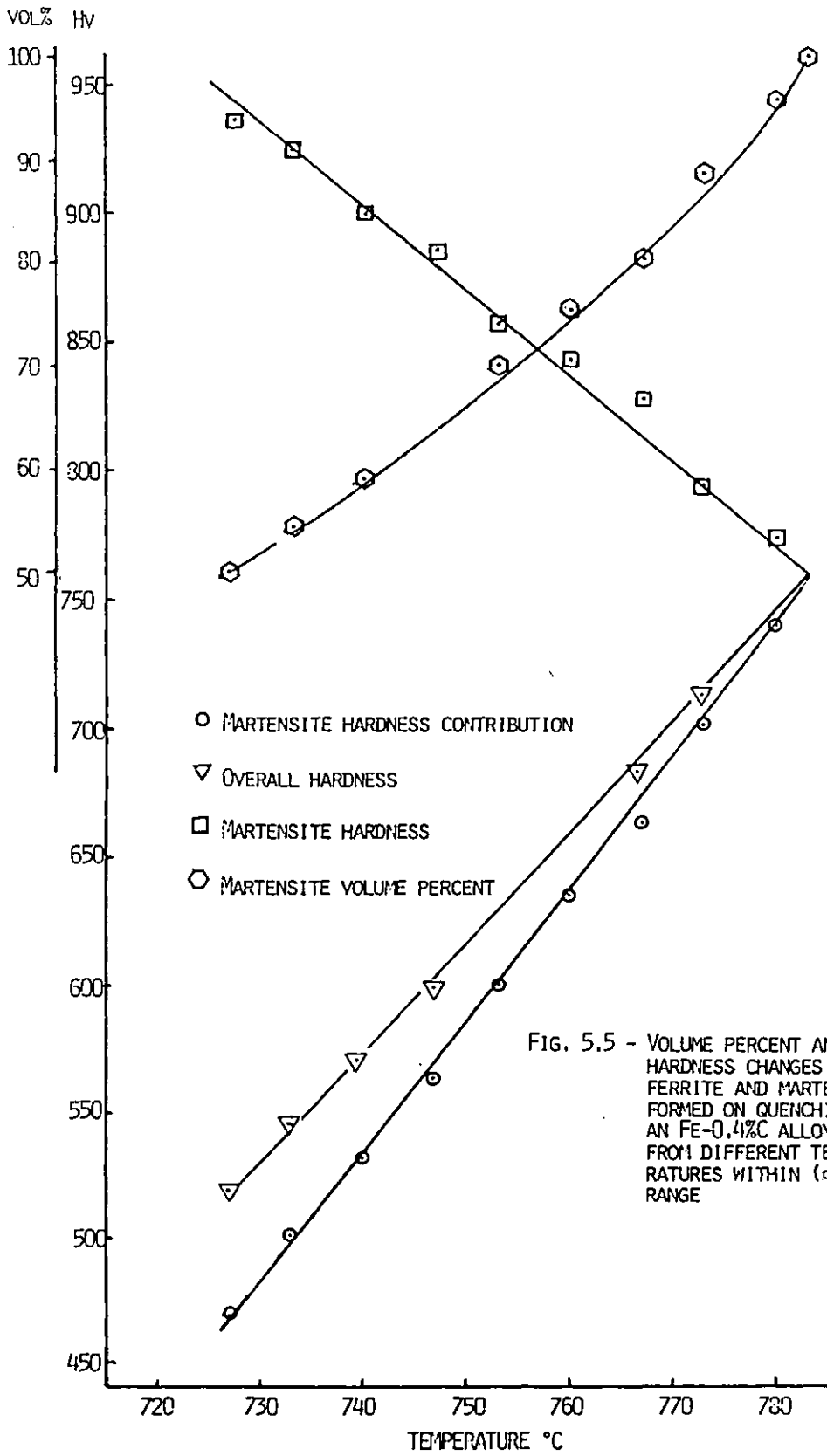

FIG. 5.5 - VOLUME PERCENT AND HARDNESS CHANGES OF FERRITE AND MARTENSITE FORMED ON QUENCHING AN Fe-0.4%C ALLOY FROM DIFFERENT TEMPERATURES WITHIN ($\alpha+\gamma$) RANGE

Table 5.5 D_o and Q values for alloying elements in ferrite and austenite [102]

Element	Matrix	D_o,cm/s	Q,J/mol
Carbon	α-iron	0.0079	75800
Carbon	γ-iron	0.21	141500
Manganese	γ-iron	0.35	280500
Chromium	α-iron	30000	343000
Chromium	γ-iron	18000	406000

Table 5.6 Diffusion Coefficients for Alloying Elements in Ferrite and Austenite at Different Temperatures

Temperature		D_C^{α}	D_C^{γ}	D_{Mn}^{γ}	D_{Cr}^{α}	D_{Cr}^{γ}
°C	°K	cm^2/s	cm^2/s	cm^2/s	cm^2/s	cm^2/s
735	1008	9.396×10^{-7}	9.846×10^{-9}	1.038×10^{-15}	4.975×10^{-14}	1.669×10^{-17}
750	1023	1.073×10^{-6}	1.261×10^{-8}	1.695×10^{-15}	9.068×10^{-14}	3.395×10^{-17}
765	1038	1.220×10^{-6}	1.604×10^{-8}	2.730×10^{-15}	1.624×10^{-13}	6.766×10^{-17}
780	1053	1.383×10^{-6}	2.025×10^{-8}	4.336×10^{-15}	2.862×10^{-13}	1.322×10^{-16}
835	1108	2.124×10^{-6}	4.516×10^{-8}	2.125×10^{-14}	2.002×10^{-12}	1.320×10^{-15}

Table 5.7 Diffusion Times for $\bar{x}$=0.1µm at Different Temperatures

Temperature		T_C^{α}	T_C^{γ}	T_{Mn}^{γ}	T_{Cr}^{α}	T_{Cr}^{γ}
°C	°K	s	s	s	s	s
735	1008	5.32×10^{-5}	5.08×10^{-3}	4.82×10^{4}	1.01×10^{3}	3.00×10^{6}
750	1023	4.66×10^{-5}	3.97×10^{-3}	2.95×10^{4}	5.51×10^{2}	1.47×10^{6}
765	1038	4.10×10^{-5}	3.12×10^{-3}	1.83×10^{4}	3.08×10^{2}	7.39×10^{5}
780	1053	3.62×10^{-5}	2.47×10^{-3}	1.15×10^{4}	1.75×10^{2}	3.78×10^{5}
835	1108	2.35×10^{-5}	1.11×10^{-3}	2.35×10^{3}	2.50×10^{1}	3.79×10^{4}

on the mode and extent of transformations will be discussed. The microstructural observations and the hardness changes resulting from the annealing of En24 steel at different intercritical temperatures for progressive periods will be explained and an attempt will be made to rationalize the effects of alloying elements on the kinetics of transformation. These effects will be compared with those anticipated in the previous section (Introductory notes).

Most of the results discussed in this section are those obtained with the higher heating rate, although the observations from the different rates of heating are compared to assess the effect of heating rate.

The lowest annealing temperature, 720°C, was chosen as being close to Ae_1. Progressive tempering was the only process observed (Fig4.4 and Plates 8-10) and it can be concluded that this temperature is, in fact, below the Ae_1. This is consistent with the first point predicted in the previous section, i.e. the eutectoid temperature should be $\sim$ 727°C.

5.2.2 Annealing at 735°C

As indicated in the previous section, this temperature can be considered to lie between the lower and the upper range of Ae_1 for En24 steel, i.e. the region in which austenite, ferrite and carbide (M_3C) can co-exist in equilibrium.

The hardness changes detected when the material was rapidly heated to (i.e.thin specimens, salt bath treatment), and held for different periods at this temperature, appeared to be complex (Fig.4.5). However, in spite of insufficient data available to provide a full explanation for the detailed mechanisms of transformation at 735°C, some of the main possible contributions will be discussed.

5.2.2.1 Initial Martensitic Structure

Kim and Thomas [106] showed that in a low carbon steel, the ($\alpha + \gamma$) microstructure depended on the heat treatment path through which it was produced. When an as-quenched martensitic structure was heated to the two phase region, the nucleation of austenite along the lath boundaries of prior martensite resulted in a distribution of fine, fibrous martensite in the ferrite matrix.

In the present study the as-quenched structure consisted of fine, partially autotempered martensite laths and plates with undissolved particles (Plates 1-5). The structure gave rise to a hardness value of about 700 Hv which is a characteristic of this grade of steel after quenching from the austenite region.

The hardness versus intercritical heating time curve at 735°C (Fig.4.5) can be divided into four successive periods as:

a. tempering on heating from the beginning of annealing, for about 20s,
b. rapid formation of austenite, from 20s to 100s,
c. constant hardness period, from 100s to 1000s and
d. the approach to equilibrium, for times longer than 1000s.

These periods and the operating mechanisms will be discussed in their respective order.

a. Tempering on heating

For times up to about 20s holding time at 735°C (involving a rapid heating rate to this temperature), the structure was tempered and a fine dispersion of carbide particles was formed. These fine particles are believed to be Fe_3C, since the tempering time was insufficient for considerable coarsening of cementite to occur and too short for any significant diffusion of the carbide forming elements like Mo and Cr. The hardness value at this stage was $\sim$ 400Hv which can be attributed partly to the fine subgrain size of ferrite (Plate 11.a) and partly to the fine, uniform distribution of Fe_3C particles.

b. Rapid formation of austenite

Upon further holding at this temperature, a distinctly sharp increase in the hardness was observed, up to about the as-quenched value for this material (Fig.4.5). This rise can be associated with a number of structural features.

The diffusion coefficient of carbon, an interstitial element, is relatively high (about 10^{-6} cm^2/s in α-Fe at 735°C) and the interparticle spacing between the fine Fe_3C precipitates is very small (of the order of 0.1μm). Thus Fe_3C can dissolve in a very short time and carbon can almost immediately go into solution producing a high volume fraction of austenite (about 60 pct is predicted from Fe-Fe_3C phase diagram considerations; the C content of the austenite is estimated to be $\sim$ 0.7pct).

Roberts and Mehl [5] showed that a finer structure can result in a more rapid ferrite to austenite transformation. The acicular growth of austenite was believed to result from preferential growth of austenite in some of the ferrite laths due to their different crystallographic orientations [1], and also a difference in the diffusion coefficient of carbon in directions parallel and perpendicular to the ferrite lath boundaries [23].

Each cementite-ferrite interface can act as a potential nucleation site for the formation of austenite [1,8-11,23] and it is anticipated that austenite grains as fine as the parent martensite laths, i.e. of sub-micron dimensions, are formed [1,15,16]. The *excess* ferrite grains are also of a similar size. Upon quenching the resultant microstructure consists of a fine intimate

mixture of acicular martensite and ferrite with an overall lamellar structure. The very fine scale of structure might be a possible explanation for the lack of resolution obtained with optical microscopy (Plates 11.b and c).

The hardness of the martensite transformed on quenching, estimated from its carbon content, is about 900 Hv [103]. Using the mixture rule, and assuming 60 pct of austenite is present, a hardness of about 400 Hv is needed for the ferrite to contribute to an overall hardness of about 710 Hv. This high value of hardness at this stage could be attributed to the following contributions:

i. Very fine grain size of the phases.
If a Hall-Petch relationship can be extrapolated for fine grains of the above order of dimensions in steels [107] a contribution of $\sim$ 400 Hv can be associated with a grain diameter of 0.2μm (e.g. Plate 14).

ii. Interactive effects
The relatively low rate of diffusion of substitutional elements in austenite at 735°C ($D<10^{-14}cm^2/s$) can give rise to a number of pre-equilibrium effects which appeared more pronounced in the lower range of intercritical annealing temperatures, i.e. 735°C:

Martensite The concentration of carbon in solution in both austenite and ferrite, can be regarded as higher-than-equilibrium, before the carbide formers and carbide stabilizers are partitioned between the metallic phases and cementite. The equilibrium carbon content of austenite for a 0.4 pct plain carbon steel at 735°C is estimated to be around 0.7 pct. This can result in a substantial amount of transformation twinning [26,27] when the material is quenched. Substitutional solid solution hardening may also participate to a small extent in further hardening of this phase since the alloying elements are assumed to be in a pre-equilibrium solution at this stage.

Ferrite The martensitic transformation strains which cause some plastic deformation can introduce high defect densities into the neighbouring ferrite, particularly in the vicinity of the martensite-ferrite interfaces, when the ($\alpha + \gamma$) mixtures are quenched [106,108]. This effect may be more pronounced in a finer grained structure with approximately alternate lamellae of ferrite and martensite. The grain boundary area per unit volume would be larger in a finer structure and transformation strains can cause substructural defects in ferrite through a wider area. Furthermore, assuming that a high density of dislocations originating from the martensite-ferrite grain boundary, can penetrate into ferrite within a certain distance from its source, the finer the grain, a higher volume fraction of ferrite will be hardened.

As discussed for martensite, a supersaturation of carbon in ferrite, due to insufficient time for the diffusion of carbide forming elements, can also lead to precipitation of fine carbides in this phase during quenching, which in

turn may participate in hardening of ferrite.

Concerning the overall hardness, since ferrite constitutes about 40 pct of the structure at this temperature, a simple mixture law indicates that a value around 400 Hv will be adequate for ferrite to bring about the measured overall hardness. This range of strength is not far from that expected from the structure discussed.

c. The constant hardness period

After the hardness value approached its peak in about 100s, a period of about 15 min (900s) was observed during which the hardness maintained this value (i.e. $\sim$ 750 Hv). This feature could be associated with simultaneous balancing effects amongst the counteracting mechanisms occurring in the microstructure. As partitioning of alloy elements from ferrite to austenite proceeds, the amount of austenite is expected to increase, because the equilibrium ($\alpha + \gamma$)/γ boundary lies at lower carbon contents than in the metastable austenite, where only carbon partitioning occurred. Speich *et al* [105] reported a continued growth of austenite into ferrite at 740°C, for times as long as 24h, after a pearlitic starting structure was transformed to ($\alpha + \gamma$) in less than 1 min, in a low carbon 1.5 pct Mn steel.

As the slow migration and partitioning of carbide forming elements proceeds, the simultaneous formation and stabilization of fine M_3C precipitates is expected to contribute, at least partly, to hardness. The effect of transformation induced strains will be increased with the increase in volume fraction of austenite.

It is interesting that similar mechanisms, can at the same time cause counteracting effects. The growth of austenite, albeit with a low rate, continues and, for example after 1000s at this temperature, some of the grains are large enough to be resolved in the optical microscope (Plate 11.d). The observation of the prior austenite grains with different shades in this micrograph may be attributable to the banding effect which is not unusual in commercial steels. The inhomogeneous distribution of alloying elements in the material can cause deviations from simultaneity in some of the kinetics of transformation in different regions. An example of the increase in banding with carbon content, in low carbon-low alloy steels, intercritically treated at 725°C, showed that a banded arrangement of carbides (similar to plates 11.b and 11.c), gave rise to a banded ($\alpha + \gamma$) morphology [23].

The progressive migration of carbide formers to Fe_3C will also result in the growth and stabilization of M_3C precipitates. This in turn can cause the *destabilization* of the metastable austenite and its decomposition to ferrite and stable austenite at 735°C. On quenching, an overall structure consisting of a lower volume fraction of martensite and a softer ferrite with coarser M_3C particles is expected to compensate for the strengthening mechanisms

discussed above.

d. The approach to equilibrium

The balancing mechanisms discussed in the previous section, will be restrained in the final period with the softening effects becoming more prominent at the beginning of this period. The diffusivity of carbon is about 10^6 times higher than that of iron or chromium [109] so when cementite is first formed, the chromium to iron atomic ratio in the carbide will be similar to that of the matrix. However, the partition ratio of chromium between cementite and ferrite at equilibrium is 28:1 [102] and if the specimen is kept at a high enough temperature, chromium will migrate from the matrix into cementite. Kuo [109] showed that in steels containing around 0.5 pct C and 1-1.5 pct Cr, (i.e. similar to En24 composition) after a 120h treatment at 700°C, the partition ratio of chromium between M_3C and ferrite was about 27:1. This process, as discussed before, can result in the growth of M_3C and at the same time, cementite can absorb carbon in solution from the austenite, causing the decomposition of austenite into ferrite and stable austenite at 735°C[20].

As a consequence of continued heating at this temperature, further coarsening in the lamellar structure of ferrite/austenite was also observed. After 65 h holding time at 735°C, the average length and width of lamellae were measured to be about 8 μm and 1.5 μm respectively (Plate 13.b). This is a coarsening of about 5 times, as compared to the structure giving rise to the peak hardness (Plate 11.d). This is consistent with a previous study reporting a low rate of growth of austenite with a fine, plate-like initial morphology, as a result of annealing in the ($\alpha + \gamma$) region [21].

The high density of dislocations generated in ferrite as a consequence of martensitic transformation in the neighbouring austenite, discussed previously, will be decreased due to both a lower volume fraction of austenite and a larger ferrite grain size.

It is believed that after 3×10^4s at 735°C, the structure approaches the equilibrium characteristics for this temperature and the slight variations noticed in hardness after this time should be attributed to minor fluctuations in the experimental instrumentation.

5.2.2.2 Tempered Structure

Most of the fore-cited discussion can be considered as valid for the structure tempered for 5h at 700°C prior to intercritical annealing. Nevertheless, there are some points of diversity to be distinguished between the kinetics of transformation in the two starting structures.

Tempering of martensite at a high temperature, is expected to cause not only the recovery and recrystallization of matrix and precipitation and growth of cementite, but also migration of Cr and Mo to these particles, at

least partially, after the 5h time allowed.

The initial *tempering on heating* period was almost absent in this case and hardness variations were negligible for times up to 30s (Fig.4.5). The particle size and spacing after this time were similar to those of the tempered parent structure (cf. plates 6d and 15a). Some of the lath-like subgrains, not restricted by the pinning action of carbides, seem, however, to have further recovered.

The second stage proceeded in a similar manner but at a lower rate. This should be associated mainly with a lower rate of M_3C dissolution as compared to that of a fine dispersion of Fe_3C. Hultgren [6] attributed the lower rate of carbide dissolution to the alloy elements segregated to cementite on tempering. Judd and Paxton [10] suggested that a local increase in alloy concentration occurs as soon as the particle starts to dissolve. This, they believe, can result in a decrease in the carbon flux through austenite. A local equilibrium model [12] anticipated that the addition of small amounts of alloying elements (e.g. 0.5 pct Mn), can decrease the solution rate of cementite substantially, particularly in the lower A_1-A_3 range of temperatures. The peak hardness was smaller and was maintained for a shorter time in the case of the initially tempered structure. In general, the extent to which the *metastable* third period was manifested, was less than the previous case. This can also be associated with the smaller amount of *fresh* cementite available and perhaps partly attributed to a larger starting subgrain size, as well as coarser particles, containing the larger proportion of alloying elements [5,6,10,12].

The fact that the hardness level of this structure remained lower than that of the martensitic starting structure, for all the times examined (Fig.4.5), can also be explained by the sluggish dissolution of larger M_3C particles, which remained coarser for similar annealing times. Carbides as large as 1μm were commonly detected in the structure after 10^4s at 735°C (Plate15.c). The carbides detected after annealing the martensitic structure for a similar time were mostly observed to be of submicron size (Plate 14).

The hardness values measured after 10^5s for the two starting microstructures were found to be approaching a constant level. This can be regarded as an indication that the structures were near-to-equilibrium.

5.2.3 The Heating Rate Effects

Experimental measurements showed that when a 1 mm thick specimen is immersed in a salt bath, preheated to a temperature in the intercritical range, it takes only a few seconds to pass through the nominal Ae_1 range of temperature (around 727°C). Similar measurements resulted in longer times (about 3 min) for Charpy specimens heated in the same medium. An even lower rate of heating was attained when Charpy-size specimens were

suspended in a pre-set vertical furnace. These specimens took up to about 15 min before passing through Ae_1 temperature.

The progressive decrease in the rate of heating is expected to cause differences in the kinetics of transformation in the intercritical range. The occurrence of different hardness curves, plotted for the three heating rates (Fig.4.9) is believed to be associated with such alterations.

As a result of comparing these curves, the following points concerning the effect of a decrease in the heating rate can be made:

a. The longer sub-critical tempering of as-quenched material causes a more extensive *tempering on heating.* The initial minimum hardness value decreases with the decrease in the rate of heating and the time corresponding to this minimum increases. This results in similar effects on structure and properties as discussed in the previous section.

b. The beginning of the *formation of austenite* period, associated with the increase in hardness, is thus postponed to longer times, and the rate at which the hardness increases in this period is also lowered. This is directly connected with the previous point. The rate of nucleation and growth of austenite is expected to be lower in a more extensively tempered alloy steel, particularly if the annealing temperature is relatively low for redistribution of alloying elements and their resolution and diffusion from carbides into the matrix.

c. The metastable hardness peak falls as a result of lowering the heating rate. The justification is the same as discussed in the previous section and in fact supports the foregoing explanation. The main criterion was that the volume fraction of the metastable austenite that forms, decreases with an increase in the extent to which the structure is tempered, prior to intercritical annealing; i.e. in an as-quenched starting structure, a lower heating rate produces a lower fraction of metastable austenite, in a longer time.

d. The characteristics of the point where the three curves converge, after about 10^5 s, can be regarded as *close-to-equilibrium.* The hardness of material water quenched after 65h at 735°C was 475 Hv. The overall morphology appears to be lamellar with a coarser average grain size than the parent martensite (cf. Plates 1 and 13b). The volume fraction of martensite, determined by automatic counting techniques (Quantimet) was about 70 pct. A simple mixture law , assuming only ferrite and austenite to be present, taking the ferrite hardness as ~100 Hv, estimates the hardness of the martensite to be about 600 Hv. This value corresponds to a martensite carbon content of about only 0.3 pct [103]. A large proportion of carbon, should thus be precipitated as M_3C particles.

The occurrence and stability of three constituents, i.e. ferrite, austenite and

carbide at 735°C (Plate 14) provides evidence for an Ae_1 range of temperatures within which the three constituents coexist in equilibrium. This is consistent with the conclusions drawn in the previous section (Introductory notes). Assuming the additive effect of alloying elements in En24 steel, it is also anticipated that the eutectoid carbon content will decrease compared to a 0.4 pct plain carbon steel. The formation of a higher amount of a *near-to-equilibrium* martensite in En24 steel (~70 vol pct) containing a lower carbon content (~0.3 wt pct) than the respective amounts for the plain carbon steel (i.e. ~56 vol pct and 0.7 wt pct at 735°C, respectively), can be regarded as further evidence to subtantiate this proposal.

5.2.4 Annealing at Higher Temperatures

Having discussed the kinetics of transformation at 735°C, the effect of higher intercritical treatments will be compared in this section. The similarities in the kinetics and mechanisms of transformation will be briefly mentioned and the emphasis will be essentially on the points of difference.

When materials are placed in contact with a hot atmosphere, the rate of heat exchange can be expressed in the form:

$$Q^\circ = h \cdot A \cdot (T_0 - T) \qquad (5.3)$$

in which Q° is the rate of heat transfer, h is the heat conductivity factor of the surface and A is the surface area, T_0 and T are the ambient and material temperatures respectively. This expression can be used to explain the behaviour of the as-quenched material, heated for short times at different intercritical temperatures in the salt bath.

As a result of a 5s holding time, it is believed that for none of the temperatures studied, was the time long enough to allow the temperature of the material to pass through Ac_1. However, a higher ambient temperature caused a higher heating rate and the material reached a higher sub-critical temperature after 5s. This resulted in a more extensive tempering and a progressive decrease in the hardness was observed with an increase in the ambient temperature from 720°C to 780°C (Fig.5.6). The as-quenched material held for 5s at 780°C revealed a hardness value of 384 Hv and the structure was more heavily tempered (Plate 28) than the same material held at 720 °C for the same period (Plate 8) showing a hardness value of 419Hv.

As can be seen from equation (5.3), the heating rate depends on the difference between the temperature of the material at each stage T, and the ambient To. In fact, with the ambient temperature assumed constant, it can be shown that the heating rate decreases with time exponentially, following an expression:

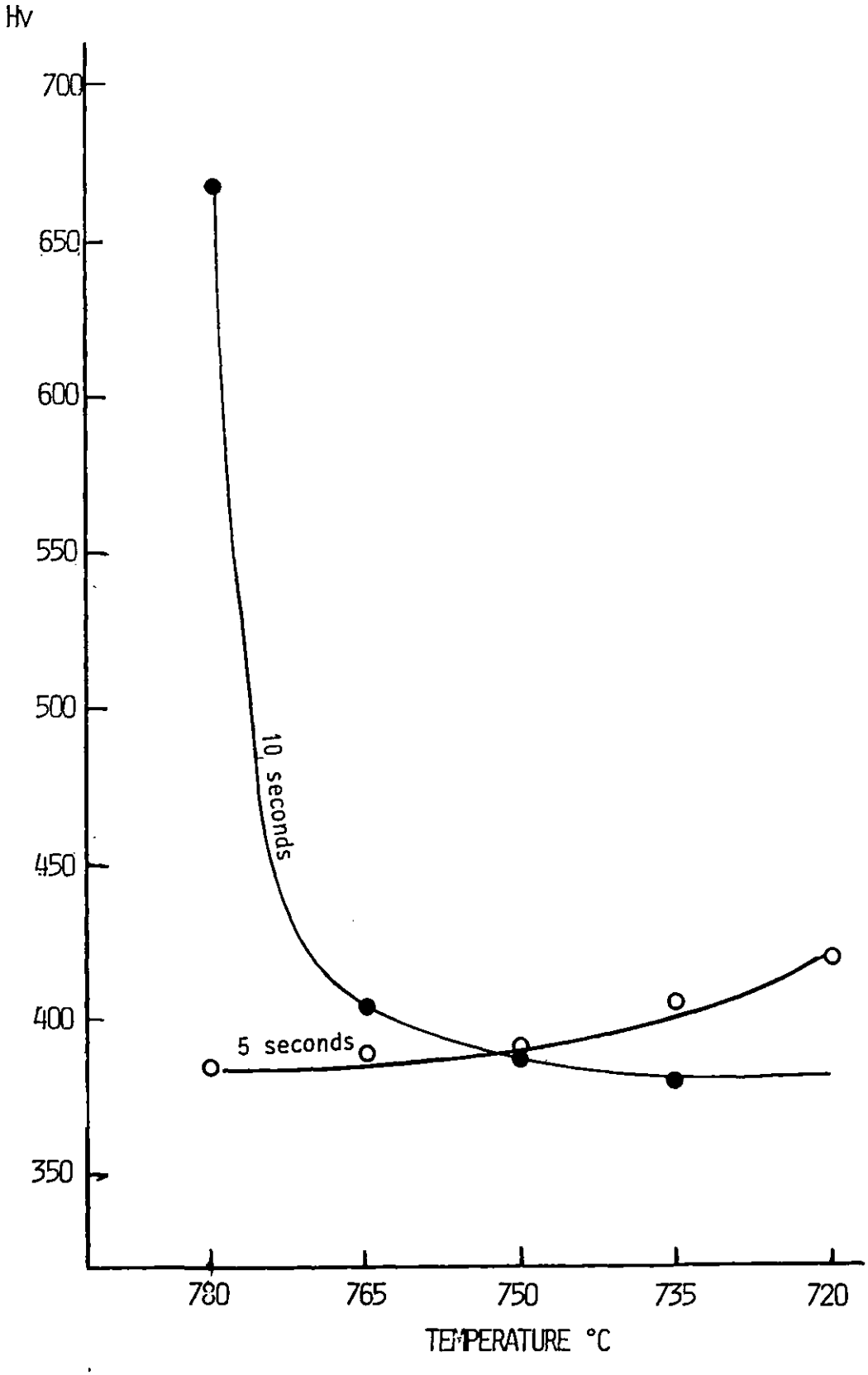

FIG. 5.6 - HARDNESS CHANGES WITH SHORT TIME RAPID HEATING OF EN 24 STEEL TO DIFFERENT TEMPERATURES

$$T - T_0 = e^{-\alpha t} \qquad (5.4)$$

in which t is time and α is a factor depending on h and A as well as the specific heat and the mass of the material; hence α could be assumed constant for the present case. This in practice means that the heating rate of material will be much lower as it approaches the ambient.

This effect is expected to accentuate the lower heating rate caused by annealing at lower intercritical temperatures. When the medium is set to temperatures closer to Ac_1, the final low heating rate may include passing through this temperature, allowing a longer time for tempering on heating. If the hardness values of the as-quenched material after 10s at different temperatures are compared, it can be seen that the material at 780°C is close to the final stage of hardness increase (second period, formation of austenite); that at 765°C appears to be in the transition from the first to the second period (see section 5.2.2; annealing at 735°C) and at 750°C and 735°C it seems to be in the earlier stages of the first period (tempering on heating) respectively.

At all temperatures studied, austenite nucleation sites are believed to be on the carbide particles. The growth of austenite is also expected to be confined within the parent martensite lath boundaries as discussed in the previous sections.

The approach to the peak hardness after 30s at 780°C is attributed to the higher rate of austenite formation at this temperature. The attainment of similar levels of hardness for the lower temperatures after 100s can be associated with the combination of strengthening contributions from ferrite and martensite. The hardness decrease from the smaller volume fraction of martensite at lower temperatures is counteracted by the increase in the actual martensite hardness, resulting from its higher carbon content.

The structure of the material, water quenched after times longer than 100s at 780°C appeared to be fully martensitic with some undissolved carbide particles, (Plates 29 and 30) and this temperature is expected to be above Ae_3 (consistent with the previous section).

A rapid rate of austenite nucleation was suggested to promote the inhibition of martensite lath boundaries from migration [19] resulting in a relatively fine and more stable acicular structure. This can be an explanation for the high level of hardness maintained after annealing at higher temperatures.

The cementite particles precipitated on heating to 765°C (Plate 25) were dissolved rapidly and the structure revealed a predominantly martensitic structure with internal twins in some areas; no ferritic area was observed in the specimens examined. This temperature was predicted to be close to Ae_3 (introductory notes).

A gradual growth of austenite was reported in the ($\alpha + \gamma$) region upon

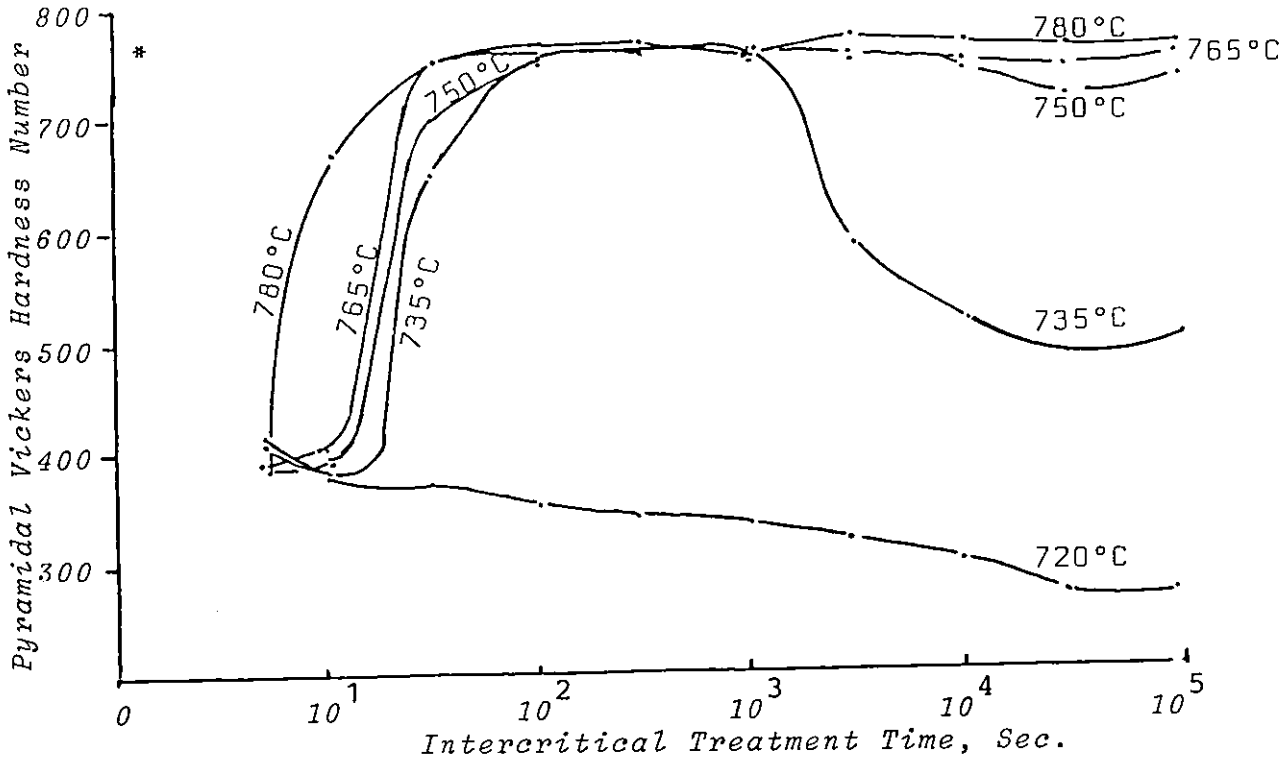

Fig.5.7 Hardness response to Intercritical Treatment Time for thin specimens, in initially Quenched Condition

*= *Initial Hardness*

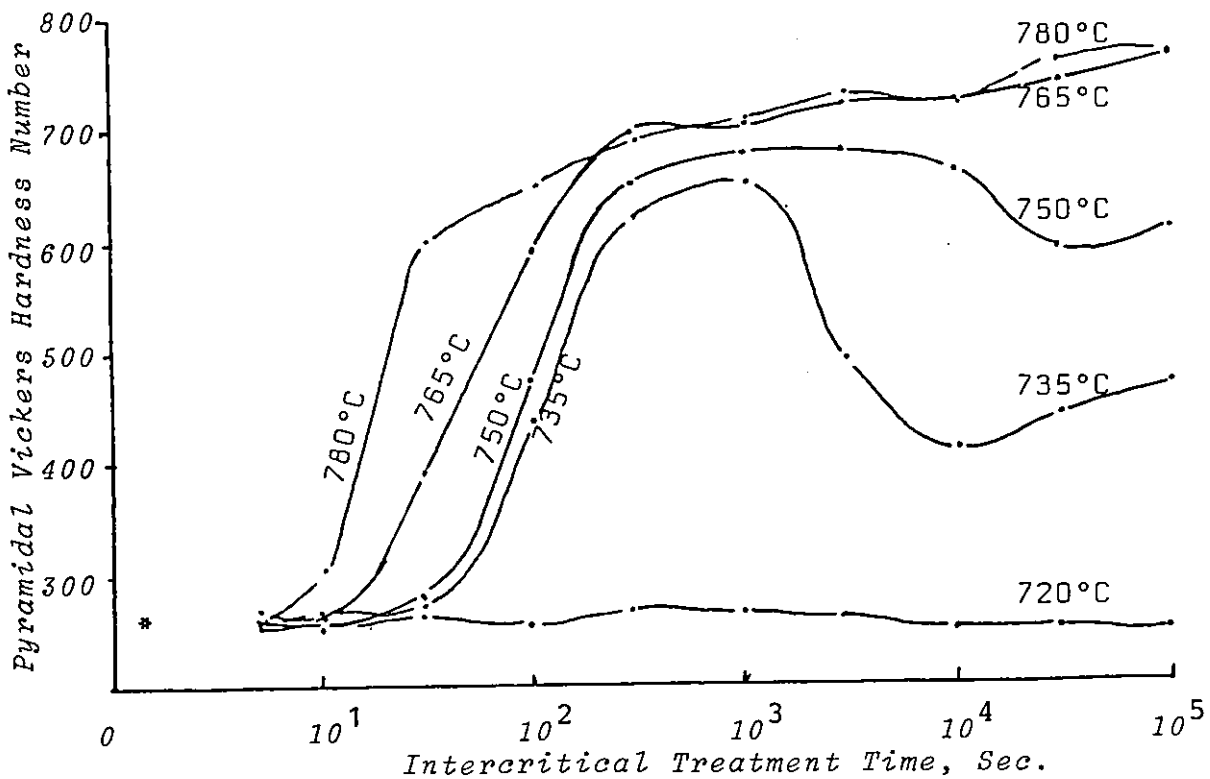

Fig.5.8 Hardness Response to Intercritical Treatment Time for Initially Quenched-and-Tempered(700°C,5hrs)Condition

prolonged annealing of a low carbon Mn steel [21]. In the present study a progressive growth of austenite was detected at 750°C which may be the cause of the slight decrease in the overall hardness (Plates 19-21). However, the ongoing dissolution of carbide particles, resulting in an increase in the volume fraction and/or carbon content of austenite appears to be the counteracting mechanism. For longer times, the spheroidized carbide particles and ferrite areas were less frequently observed in the structure; instead, fine internal twins were often detected in the martensite (Plate 17 and 18).

The previously tempered material heated to higher intercritical temperatures, resulted in a less pronounced effect of alloying elements than those discussed for similar starting structure annealed at 735°C. Judd and Paxton [10] attributed this effect to an increased carbon solubility range of austenite with annealing temperature (Fig.2.2). As indicated in the case of as-quenched material, a progressive increase in the annealing temperature from 735°C to 780°C, resulted in a rise in the rate of hardness increase (Fig.5.8) Molinder [8] in an investigation surveyed in chapter two, showed that the rate of austenite formation increases with intercritical temperature.

The shortest holding time studied, 5s, did not produce hardness increases at any of the temperatures investigated. However, some dislocation movements, associated with the starting point of carbide dissolution [18], may be speculated from a comparison of the stuctures before and after 5s at 780°C (Plates 6 and 31). A more clear example of dislocation networks, around dissolving carbide particles was observed in the water-quenched structure, after a 10s hold at 750°C (Plate 22-a).

Annealing for longer times at temperatures near to and above Ae_3, i.e. 765°C and 780°C, produced predominantly martensitic structures with some undissolved carbide particles (Plates 27 and 32). The progressive low rate of hardness increase, for times longer than 10^3s at these temperatures, should be attributed to the continuing dissolution of more stable carbides.

Prolonged annealing of pre-tempered material at medium and lower intercritical temperatures, on the other hand, produced lamellar mixtures of ferrite and martensite, with undissolved carbide particles (Plates 15b-15d-22b and 24). However, some approximately equiaxed islands of ferrite were occasionally detected (Plates 15.c and 23).

5.3 Structure-Property Relationships

5.3.1 Introduction

Strength and toughness are usually regarded as the most important properties specified for structural steels. The major difficulty in optimizing these properties arises from the fact that strength is usually inversely related

to toughness and ductility. An increase in the former is achieved at the expense of the latter and vice versa.

In recent years, metallurgical research and development have been motivated by the necessity to find materials, or composites of materials which can be substituted for those traditionally used for specific applications. Amongst the numerous attempts to improve mechanical properties in steels is the utilization of two phase microstructures through the control of solid state phase transformations. The structure is produced by annealing the material at a temperature in the two phase ($\alpha + \gamma$) region of the equilibrium diagram followed by cooling at a rate which ensures that the γ phase transforms to martensite. The process involves only thermal treatment without recourse to the expensive thermo-mechanical treatments. The solid state transformation ensures good bonding (coherency) between the constituent phases. This is a significant advantage over the artificially produced composites. The common practice is to utilize the second phase to its advantage while the less desirable features of this phase are simultaneously mitigated by the presence of the other constituent phase. The strengthening principle in a ferrite+martensite structure involves the incorporation of inherently strong martensite as the load carrying constituent in a ductile ferrite matrix. The high degree of coherency at the martensite/ferrite interface in these structures gives rise to an increased efficiency of load transfer from ferrite to martensite. The elastic constants of martensite are equal to those of ferrite; consequently there will be no localized stress concentrations in the elastic range of both phases.

In this section we are concerned with the effects of intercritical treatments, applied intermediately between quenching and tempering of medium carbon steels, on the toughness of material. As will be discussed, En24 steel, intercritically heat treated to 765°C, showed superior toughness to the conventionally heat treated material at similar hardness values between 450 and 550 Hv. This is shown to be clearly associated with a reduced susceptibility to tempered martensite embrittlement. The main parameters to be considered in intercritical treatments are as follows:

1. Composition of alloy;
2. Initial structure of alloy;
3. Temperature within the ferrite + austenite range; the heating rate to this temperature (dependent on section size and treatment medium); holding time at temperature; cooling rate; final tempering treatment (if any).

The main structural features in hypo-eutectoid steels which derive from the above parameters and which control the final properties are:

a. Volume fraction, composition, particle morphology and dispersion of the phases present at the treatment temperature (i.e.ferrite, austenite and sometimes carbides). The extent to which equilibrium is obtained during the treatment is important e.g. in relation to the partitioning of

carbon and substitutional alloy elements between the phases and also in relation to particle coarsening.

b. The nature of the decomposition process of austenite during the cooling e.g. the formation of martensite or bainite, partial retention of austenite.

c. Structural changes during tempering; these will depend particularly on the composition of the martensite and other aspects referred to in b.

5.3.2 Modes of Fracture

At ambient temperatures and under static loading conditions hardened and tempered steels may fracture by three main micro-mechanisms; fibrous fracture, cleavage and inter-granular decohesion. Fibrous fracture, or microvoid coalescence as it is also frequently described, is a strain controlled process and it is now generally accepted that the fracture toughness of a material which fails in this manner is controlled by the spacing of the void nucleating particles, (carbides and non-metallic inclusions) and by the local strain required to cause separation of the intervening matrix. The latter is related to the work hardening capacity of the material. Cleavage fracture is associated with the attainment of a critical value of tensile stress, the latter being inversely related to the size of the carbide particles which act as crack nucleating sites. Consequently cleavage is facilitated by coarse carbide sizes and by high stress. Intergranular decohesion is also thought to be a tensile stress controlled mode of fracture, However, in this case, the magnitude of the critical stress is controlled by both the size of the initiating particle and by the effective intergranular surface energy, γ_B. The latter is normally greater than the transgranular surface energy and hence cleavage is the usual micro-mechanism of brittle failure. However, the segregation of impurities such as phosphorus and antimony to the prior austenite grain boundaries during tempering can reduce γ_B to such an extent that intergranular decohesion becomes the preferred mode. In this condition the material is usually described as being temper embrittled.

5.3.3 The Objective

The present study has concentrated on two traditional medium carbon low alloy steel, En24 and En8, and has attempted to achieve an improvement in properties by a novel hardening treatment, namely quenching from within the two-phase, ferrite + austenite, or *intercritical* region. The resultant microstructure then consists of an intimate mixture of martensite and ferrite. This has several advantages. First, the presence of ferrite with its high work hardening capacity, between regions of tempered martensite might present an additional barrier to void coalescence and hence lead to increased fibrous fracture energy. Secondly, by preventing the development of a normal austenite grain structure during the ($\alpha + \gamma$) solution treatment, resistance to temper embrittlement should be increased. The embrittling elements, P

and Sb, tend to be ferrite stabilisers and consequently there is a high probability that these would remain in solution in the ferrite phase. Also with the duplex structure, the potential interface area available for segregation is very high and this should prevent damaging concentrations of impurity elements developing. As far as cleavage susceptibility is concerned, the influence of the intercritical treatment is difficult to predict. As discussed above, the cleavage failure stress is dictated by the size of the coarse carbide particles and it is not known how this might be affected by the two phase treatment.

5.3.4 Mechanical Test Results

The mechanical testing programme has relied on Vickers hardnesss testing for the assessment of strength, and room temperature Charpy impact tests for the determination of toughness. The results of tests carried out on En24 specimens furnace treated for 30min at various temperatures within the ferrite+austenite region showed that in order to achieve as-quenched hardnesses in excess of 450 Hv, it is necessary to employ treatment temperatures in excess of 750°C (Table 4.12). Also it was found that samples heat treated at low temperatures within the intercritical range tended to exhibit inferior toughness for a given strength level; Fig.4.13. Furthermore, this was also the case for all intercritical treatments carried out on En8 steel. Based on similar hardness levels, no improvement was achieved in toughness as a consequence of the intercritical treatment of the plain carbon steel at different ($\alpha + \gamma$) temperatures; Table 4.15 and Fig 4.18. For this reason most of the subsequent tests concentrated on hardening the alloy steel at 765°C.

The effects of tempering temperature on the hardness and Charpy impact energy of En24 after the conventional treatment and after a 765°C intercritical treatment are shown in Table 4.12 and plotted in Figs. 4.11a and b respectively. The conventional heat treatment shows the usual tempering response of this steel and the pronounced temper embrittlement trough is clearly apparent Fig.4.11a. After the intercritical treatment, the as-quenched hardness is somewhat lower but thereafter the steel shows similar tempering behaviour Fig.4.11b. By comparison the impact behaviour shows a much reduced embrittlement trough Fig.4.12.

Since toughness and strength tend to be inversely related, it is essential to consider identical strength conditions in order to make a meaningful comparison of toughness. To facilitate this comparison, the Charpy impact data for the conventional and intercritical heat treatments have been plotted against hardness in Fig.4.13. This shows a number of interesting features. First, at hardness levels lower than about 450 Hv, which corresponds to tempering temperatures in excess of about 450°C, the impact toughness of the two conditions appears to be identical. Secondly, in the hardness range from 450 to 550 Hv, the impact behaviour of the intercritically heat treated samples is noticeably superior to the conventional heat treatment conditions.

Finally, at hardness levels above 550 Hv, the toughness of the intercritical condition is inferior to that of the standard condition.

Scanning electron microscopy was employed to study the micromechanisms of fracture for the various heat treated conditions. This showed that for samples possessing hardness values less than 450 Hv, the micromechanism consisted of micro-void coalescence, there being no detectable difference between the conventional and intercritically heat treated conditions (e.g:cf. Plates 33b and c). By comparison there was a very marked difference between the two conditions for hardness values between 450 and 550 Hv. The conventional condition is illustrated in Plates 33-d and 33-h and it can be seen that the fracture surface is dominated by intergranular decohesion. By comparison the intercritical condition continues to display a mainly fibrous micromechanism (Plates 33-e and 33-g). At a hardness value of about 600 Hv, which is the highest hardness for which the two conditions can be compared, the situation appears to be reversed. The conventional condition then tends to exhibit a high proportion of fibrous fracture whilst the intercritical condition tends to fail mainly by quasi-cleavage mode.

5.3.5 Structural observations

The structural features of Charpy specimens as observed by light microscopy after etching with the picral/HCl/Teepol reagent are illustrated in Plates 34a-d. The specimens had been furnace heated and held for 30 minutes at an intercritical temperature, followed by oil quenching and then tempering for 1 hour at 200°C.

The boundaries of the original austenite grains produced by conventional austenitizing are shown in Plate 34a. The material treated at 735°C showed a relatively fine duplex structure with lamellar features Plate 34d; after treatment at 750 and 765°C the lamellar structure becomes coarser, and in the latter structure there were substantial areas where no lamellar features were revealed (Plates 34c and b); low magnification observations showed the presence of banding.

Transmission electron microscopical observations were made on foils prepared from Charpy sized specimens, both conventionally treated and intercritically treated at 765°C (Plates 35 and 36).

In the quenched condition after conventional (835°C) austenitizing the martensite morphology type for this composition of steel is expected to be predominantly of the lath type plus some plate type [27,65]. The observations were consistent with this and substructural features included both dislocations and twinning (Plates 2 and 3). No evidence of retained austenite was obtained; previous work on 4340 steel has shown that austenite retention is decreased with decreasing austenitizing temperatures [39]. Autotempering had occurred during oil quenching leading to the

formation of plate-like particles, interpreted as ε-carbide [63] (Plate 5). Other particles (approximately "equiaxed" in shape and up to about 0.3μm in diameter) were observed (Plate 4). The nature of these is not known with certainty but it is considered that they are carbides.

The presence of undissolved carbides in the conventionally treated (as well as intercritically quenched) specimens does not help the correlation of mechanical properties and microstructural changes. Large spherical undissolved carbide particles act as fracture nuclei even when the fracture is of the relatively ductile dimple-rupture type. Tiny cracks form locally at undissolved particles and these micro-cracks join together by local shear tearing as plastic flow proceeds. This results in a low value of fracture toughness.

The crystal structure of carbides at different stages of heat treatment was carefully examined by both electron diffraction and X-ray diffraction techniques. The only structure positively identified was M_3C (orthorhombic) and the search for other types of carbides, such as M_7C_3, $M_{23}C_6$, M_6C and Mo_2C did not result in the provision of convincing evidence for the presence of these types of precipitates.

This result agrees well with previous work on similar alloys. The formation of a chromium rich carbide, identified as $M_{23}C_6$ in En24 steel, has been reported by Walker and Honeycombe [110]; this is believed to be directly associated with the isothermal deformation of the alloy which may not necessarily lead to the same structure as the products of the quenching-and-tempering process.

Kuo in his detailed study of carbides in alloy steels [109] has shown that no Cr_7C_3 or $Cr_{23}C_6$ was detected in the chromium steels with a chromium to carbon ratio smaller than $\sim$4. In his work, during prolonged tempering, chromium replaced iron in Fe_3C up to a critical value of $\sim$20 pct, before the transformation of M_3C into M_7C_3 began. His analysis of the chemical composition of the extracted carbides precipitated in the alloy closest in C and Cr content to those in En24 (C$\sim$0.5 pct, Cr$\sim$1.5 pct), after quenching and tempering for 120 hours at 700°C, showed that the Cr content in the carbide (i.e. substituted for Fe after this treatment) was only $\sim$16 pct, which was not high enough for the M_3C to M_7C_3 transformation to occur. This fact has also been confirmed in his X-ray analysis on the extracted carbides, in which M_3C was the only structure detected.

Considering molybdenum steels, the same author has shown that as a result of tempering a quenched steel containing 0.46 pct C and 0.32 pct Mo (similar to En24), M_3C is the only structure detected for times up to 25 hours at 700°C. For much longer times (100-500h) however, $M_{23}C_6$ and eventually MoC were also formed.

The effect of combinations of alloying elements on the formation of carbides can be considered as more complex. In a later work Shaw and Quarrell

have reported a constitution for chromium-vanadium steels containing 0.2 pct carbon at 700°C [111]. A report by Woodhead and Quarrell presented a constitution by Smith for chromium-molybdenum steels containing 0.2 pct carbon at 700°C [112]. In both of these constitutions, in the regions with alloy contents similar to those in En24 steel, formation of M_7C_3 carbide is expected in addition to M_3C. However, since these observations are associated with a lower carbon concentration (0.2 % C) which results in a higher alloying element to carbon ratio, there seems to be no inconsistency between these works and Kuo's results [109].

It can be concluded that one of the crucial factors which determines the nature of carbides formed in different alloy steels after various heat treatments is the actual element to carbon ratio. The higher this ratio, the more would be the probability for the element to exploit favourable circumstances to produce carbides of higher alloy content.

Finally, it seems appropriate to point out here, that the exact composition of the carbide phase is not considered as a fundamental factor in determining the mechanical properties of tempered structures. Instead it is the size, shape, volume fraction, morphology and distribution of these particles which can have determining effects on the properties.

In the material quenched from 765°C ferrite regions of various shapes and containing dislocations were observed (Plate 36a) but the major part of the structure appeared to be martensitic. The plate-like ε carbides observed in the conventionally treated material were not detected and this may be interpreted as arising from the lower M_s temperature associated with the higher carbon martensite, and hence less autotempering. The equiaxed particles, referred to above, were observed almost as frequently as in the conventionally treated material (cf. Plates 4 and 36a).

Tempering the conventionally quenched material from the temperatures of between ~200 and 650°C produced carbide precipitation which became coarser with increasing temperature; recovery and recrystallization of the ferrite were observed at the higher temperatures (Plate 35). In the intercritically treated material, subsequently tempered, this carbide precipitation from the martensite was not detected at ~300°C and only a little was detected at 400°C (Plate 36e). This does not necessarily imply the absence of carbide precipitation but suggests possibly a finer scale dispersion not readily detected by bright field examination; such an effect suggests retardation of tempering.

5.3.6 Toughness

When this study was initiated it was hoped that the intercritical heat treatment might lead to an increase in fibrous fracture energy because of the higher work hardening capacity of the ferrite which would thus increase the void coalescence strain. The results show that there is no increase in

toughness for the fibrous failure mode and, in fact, for the lower intercritical temperatures, (i.e.735° and 750°C) there is a deterioration in toughness. A necessary consequence of the presence of low carbon ferrite is that the martensite in the intercritically heat treated samples must contain a higher carbon content than the martensite in the conventionally heat treated condition. An increase in the carbon content of austenite can promote twinning in the martensite. It has been demonstrated that the twinned martensite has a lower fracture toughness than dislocated martensite at the same strength level [41]. On tempering twinned martensite, long continuous carbides precipitate along the twin boundaries. High stress concentrations are induced in the carbide/matrix interface, leading to crack nucleation, as the dislocation movement is inhibited by carbides [58]. The observation of microcracks produced on quenching Fe-C alloys has also been associated with an increase in the carbon content of the alloy [60]. The microcracks were shown to be created at twin intersections during the martensitic transformation [61]. Although no quench cracking was detected in the present work, the deleterious effects of microtwins on the toughness are to be considered in both conditions. A direct comparison between the twin densities in the martensitic regions of two conditions was not possible; however based upon the previous work two main factors influencing the extent of twinning can be postulated. Firstly, in the material treated in the ($\alpha + \gamma$) region, the higher carbon and nickel content of austenite can lead to a lower M_s temperature. Consequently the possibility of transformation twinning may be increased [28,41-43]. However, the overall strength of ($\alpha + \gamma$) mixtures is expected to be lower than that of a fully austenitic structure at the M_s temperature. One of the most important factors determining the extent of twinning in martensite is believed to be the strength of austenite from which it forms [26]. The transformation of austenite, surrounded by a soft ferritic matrix, can lead to a partial transfer of accommodation strains to the matrix. This can result in a lowering of strength in martensite and consequently less twinning is expected. The overall effect of intercritical treatment on the extent of twinning, influenced by the above counteracting effects, will thus be difficult to anticipate. At lower annealing temperatures austenite contains a nearer to eutectoid carbon content and the first effect, i.e. an increased twin density due to a high carbon content, should be significant. However, a higher volume fraction of ferrite at these temperatures can cause the neighbouring austenite to transform to martensite with a lower twin density. An increase in the annealing temperature can result in a reverse effect on both factors.

The contribution of a relatively soft ferrite to the hardness of the duplex mixture implies that in order to achieve the same hardness in the two conditions, the martensite should be stronger in the intercritical condition. Since the major contribution to the strength in a tempered martensitic structure can be attributed to precipitation strengthening [44], the carbide spacing must be much less in the intercritical condition. Consequently if these carbides participate in the void coalescence process, the void spacing must be correspondingly less and this would be expected to lead to a deterioration in toughness.

Another factor is that in quenched and tempered steels, where carbides are the main void nuclei, the total local strain for void coalescence may be dominated by the strain required for void nucleation. This tends to be borne out by observations on plain tensile specimens where carbide initiated voids are observed only at high strains. Unlike inclusions, which are weakly bonded to the matrix, carbides tend to be strongly bonded and it is reasonable to suppose that the nucleation strain is related to the attainment of a critical dislocation pile-up density at the particle-matrix interface [113]. The latter should be proportional to the effective shear stress:

$$\tau^* = (\tau - \tau_i) \tag{5.5}$$

and inversely dependent on the effective slip distance d. In the case of a dispersion of ferrite grains,interspersed amongst the tempered martensite laths, the overall applied shear stress (τ) should be constant. However, the friction stress (τ_i) should be much less in the ferrite, due to a lower dislocation density. This can be seen from the equation:

$$\tau_i = \alpha\mu b\rho^2 \tag{5.6}$$

where: α = constant
μ = shear modulus
b = Burgers vector
ρ = dislocation density

Consequently the effective shear stress acting at a ferrite-particle interface should be greater. Also, because of the low carbide density and low dislocation density within the ferrite, the effective slip distance, d, should be greater in the ferrite.

The combination of these two factors should facilitate void nucleation at carbides which happen to be located at the boundaries of the ferrite grains. Also it would be expected that the void nucleation strain, and hence the toughness, should decrease as the ferrite volume fraction increases. This was observed for the lower temperatures within the intercritical range. It may be concluded that substantial amounts of ferrite have a deleterious effect on toughness. However, provided the ferrite volume fraction is small, as in the case of the 765°C treatment, the effect is negligible.

Within the 450 to 550 Hv range, the enhanced toughness of the intercritically heat treated material is clearly associated with its resistance to intergranular decohesion (cf. Plates 33g and h). The phenomenon of tempered martensite embrittlement and reversible temper embrittlement has been the subject of considerable research in recent years (see section 2.2.5 and Ref.72), due mainly to the recent introduction of surface analytical techniques such as Auger spectroscopy [78]. As a result of this research, it is now well established that the intergranular embrittlement is associated with the segregation of trace impurity elements, notably P, Sn and Sb to the prior austenite grain boundaries. The impurity elements lower the grain

boundary cohesive strength thus providing an energetically favorable path for fracture [114]. Alloying elements Ni, Cr, and Mn are a necessary prerequisite for temper embrittlement and enhanced embrittlement is noted when more than one alloy element is present [115] Co-segregation of specific combinations of alloy and impurity elements has been observed as a result of strong alloy-impurity interactions. Carbides also play an important role in the embrittlement process. First, the carbide precipitation may lead to rejection of alloy and impurity elements at the carbide-matrix interface, which may subsequently attract further impurity elements from the bulk [89] and secondly, the carbides may provide preferred sites for crack initiation.

In the case of the intercritically heat treated material, the identity of the original austenite grains is effectively lost [116]. Consequently there is no longer a clearly defined interface available for segregation and embrittlement. Instead the material contains an extensive network of martensite-ferrite interfaces (Plate 36a), the surface area of which is much greater than that associated with the prior austenite grains in the standard heat treated condition (cf. Plate 34a and b). It follows that the concentration of impurity elements at these boundaries must be much less than in the standard heat treated condition [116]. The second factor which may influence the embrittlement susceptibility is that the harmful impurity elements, P, Sb and Sn, are all ferrite stabilisers. Consequently during the intercritical heat treatment these elements are expected to concentrate in the ferrite phase. Similarly the Ni and Mn, which are essential co-segregants for embritlement [77] are expected to concentrate in the austenite phase. This partitioning of impurity and alloy elements between the two phases might be expected to lead to a net reduction in interface segregation. The third factor relates to the carbide precipitation characteristics. As noted above, the results of the thin foil electron microscopy suggest that the carbide precipitation is delayed in the intercritically heat treated material (cf. Plates 35d and e with Plate 36e) Consequently the carbide size and morphology may be less conducive to fracture initiation.

At the highest strength for which comparison is possible, namely 600 Hv, the toughness of the intercritically heat treated material is markedly inferior to that of the conventionally treated steel. This is readily explicable in view of the fact that in the conventionally heat treated condition, the microstructure consists of a tempered martensite whereas the intercritically heat treated material consists of a mixture of free ferrite and an as-quenched martensite. The latter is inherently brittle and this is aggravated in the present case by the increased carbon content resulting in a higher twin [41-43] density which is a necessary consequence of the intercritical heat treatment.

Chapter 6

Conclusions

The effects of intercritical heat treatments on the microstructure and mechanical properties of two medium carbon commercial steels, En24 and En8, were studied in the initially martensitic or tempered martensitic conditions. The main findings and conclusions can be summarized as follows:

1. Assuming the effects of the alloying elements Ni, Cr, Mo and Mn on the characteristics of the binary Fe-C phase diagram are additive, it is possible to estimate the transformation temperatures and eutectoid composition for a low alloy steel. With the amounts of these elements similar to those in En24 steel (Table 3.1), the following changes are expected to occur in the Fe-C diagram:

   a. The eutectoid carbon content will be decreased by about 0.25 percent.
   b. At 0.4% C an Ae_1 range of temperatures occurs between ~ 720°C and 740°C. Ferrite, austenite and M_3C carbide are the equilibrium constituent phases in this range.
   c. The Ae_3 temperature, associated with 0.4% carbon will be ~ 776°C.

   The interpretation of the structures produced as a result of different heat treatments in this study proved consistent with the above estimates.

2. Tempering occurred in the as-quenched En24 steel upon heating to the intercritical range. Heating to higher temperatures enhanced the rate of tempering for periods shorter than 5s. Both, a decrease in the intercritical treatment temperature and an increase in the specimen cross section resulted in a lower rate of heating, which thereby caused an increase in the extent of tempering on heating. Substituting a less efficient heating medium (a crusilite furnace) for a salt bath also resulted in a similar effect. When the initially as-quenched material was more heavily tempered due to a lower rate of heating, further intercritical annealing produced a lower rate of hardness increase. This was associated with a decrease in the rate of formation of austenite due to an increase in the extent of tempering in the parent martensite.

3. Rapid heating of the oil-quenched En24 steel to the lower range of the intercritical region (735°C) for 100s followed by water quenching produced a hardness level similar to that of the as-quenched material (~ 700 Hv). This is believed to be attributable mainly to the rapid formation of a large fraction of metastable austenite, transformed to martensite on quenching. Other contributing effects are considered to include the

formation of a very fine lamellar ferrite/martensite microstructure, a high carbon content, relatively strong martensite and a dislocated ferrite matrix containing carbide precipitates. The retention of the high level of hardness for times between 100 and 1000s at 735°C is connected with counteracting mechanisms discussed in chapter 5 (section 5.2.2.1.c). Annealing for longer times at 735°C resulted in a decrease in hardness. This was associated with the transformation of the metastable austenite into ferrite and stable austenite and with the formation and coarsening of stable carbides (mainly M_3C). Coarsening of the lamellar ferrite/austenite structure occurred after 1000s. The observation of ferrite+martensite+M_3C after 65h annealing at 735°C followed by water quenching suggests that this temperature is within the "Ae_1 range of temperatures".

4. An increase in the intercritical annealing temperature, enhanced the extent of hardness increase in the initially as quenched En24 steel. This was associated with a decrease in the extent of tempering on heating and the formation of a finer, more stable, acicular structure. The structure of material annealed for times longer than 100s at 765°C or 780°C, followed by water quenching was predominantly martensitic suggesting that these temperatures were close to and above the Ae_3 temperature respectively.

5. The martensite formed by quenching En24 steel from intercritical temperatures showed less autotempering than the martensite produced by quenching from the conventional austenitizing temperature of 835°C; this is attributable to its high carbon content and hence lower M_s temperature. On tempering the martensite produced by the intercritical treatment, carbide precipitation appeared to be retarded in the lower temperature range of tempering (e.g. at ~300°C). In all conditions, M_3C was the only carbide positively identified.

6. Upon heating the previously tempered En24 specimens to intercritical temperatures, the initial formation of the metastable austenite was suppressed. The formation of austenite proceeded at a lower rate due to the sluggish dissolution of larger carbide particles.

7. In order to achieve an as-quenched hardness in excess of 450 Hv (equivalent to a tensile stress of about 1500 $MNmm^{-2}$), after 30 min intercritical annealing of En24 steel in a furnace, it was necessary to employ treatment temperatures in excess of 750°C.

8. Based on similar hardness levels the En24 steel, intercritically furnace treated at 735°C and 750°C for 30 min, exhibited a deterioration in the room temperature Charpy energy, compared to the conventionally treated material.

9. Tempering the oil quenched En24 Charpy specimens to temperatures between 300°C and 450°C clearly showed the usual temper embrittlement

trough. This effect was much reduced as a consequence of an intercritical treatment, intermediate between quenching and tempering.

10. Comparing the room temperature Charpy energies, in the specimens showing similar hardness values, the effect of intercritical treatment at 765°C, prior to tempering, on the toughness of the as quenched En24 steel can be summarized as follows:

    a. At hardness levels lower than about 450 Hv, corresponding to tempering temperatures in excess of about 450°C, the impact toughness of the two conditions was identical. This was consistent with similar micro-void coalescence fracture mechanisms in both conditions.

    b. In the hardness range from 450 to 550 Hv, the intercritically treated samples exhibited a superior impact behaviour to the conventional heat treatment. The conventional treatment revealed a predominantly intergranular fracture while a mainly fibrous micromechanism was observed in the intercritical condition.

    c. At hardness levels above 550 Hv, the toughness of the intercritical condition was inferior to that of the standard condition. The latter showed a high proportion of fibrous fracture whilst the intercritical condition failed mainly by quasi-cleavage mode.

11. As a result of annealing the material at the lower intercritical temperatures (735°C and 750°C) the formation of a high carbon content martensite leading to a possible increase in twin density and a decrease in interparticle spacing on tempering are considered to counteract the advantageous effects of the ferrite phase on the toughness.

12. The enhanced toughness of the intercritically heat treated En24 steel at 765°C within the range 450 to 550 Hv is associated with a reduced susceptibility to tempered martensite embrittlement. This is believed to be due to a decrease in the segregation of alloying elements and impurities to the prior austenite grain boundaries.

    In the microduplex lamellar structure produced as a result of intercritical treatment, the alloying elements Ni and Cr are expected to concentrate in the austenite phase. Similarly the impurities are expected to concentrate in the ferrite phase and also can distribute over the extensive network of martensite/ferrite interfaces produced as a consequence of this treatment.

13. At hardness levels higher than 550 Hv, the microstructure in the conventionally heat treated condition is tempered martensite while the intercritically heat treated material consists of a mixture of ferrite and as-quenched martensite. The inherently brittle martensite containing an increased carbon content resulted in an inferior toughness in the

intercritically treated En24 steel.

14. The intercritical treatments carried out on En8 steel did not produce any improvement in the combined hardness-toughness properties. The effect was similar to that cited for En24 steel annealed at 735° and 750°C. The absence of alloying elements reduced the susceptibility to temper embrittlement and the conventional treatment maintained the superior properties over the intercritical annealing after tempering.

Acknowledgements

The work described in this thesis was performed in the Department of Metallurgy, Imperial College, under the supervision of Drs. D.R.F. West and T.J. Baker. I am very grateful to my supervisors for their interest, advice and encouragement; to Dr. H.M. Flower for his help with the electron microscopy techniques; to Miss P.R. Martins for printing the plates and to Dr. G.M. Pennock for proof reading of the thesis.

Mr. M. Sahba's assistance with the typesetting techniques is appreciated. My thanks should also go to Miss S. Hakimi and Mr. and Mrs. B. Ahmadi for typing the manuscript and their cooperation in the final stages of thesis preparation.

Finally I would like to acknowledge Professor D.W. Pashley for the provision of research facilities.

REFERENCES

1. Nehrenberg, A.E. : Trans. AIME, Journal of Metals, 188, *1950*, 162
2. Bain, E.C. and Villela, J.R. : ASM Handbook, *1948 ed.*, 399-406
3. Baeyertz, M. :Trans. ASM, 30, *1942*, 458
4. Kula, E. and Cohen, M. : Trans. ASM 46, *1962*, 727
5. Roberts, G.A. and Mehl, R.F. : Trans. ASM 31,*1943*, 613
6. Hultgren, A. : Trans. ASST, 16, *1929*, 227
7. Hillert, M. : Internal. Rep., Swedish. Inst. Metal Res., *1953*
8. Molinder, G. : Acta Metall., 4, *1956*, 565
9. Paxton, H.W. : Transformation and Hardenability in Steels , Cliamax Moly. Symp., *1967*, 3-14
10. Judd, R.R. and Paxton, H.W., Trans. Met. Soc. AIME, 242, *1968*, 206
11. Speich, G.R. and Szirmae, A. : Trans. Met. Soc. AIME, 245, *1969*, 1063
12. Hillert, M., Nilsson, K. and Torndal, L.-E. : JISI, 209, *1971*, 49
13. D'yachenko, S.S. and Fedorov, G.V. : Fiz. Metal. Metalloved., 18, *1964*, 73
14. Watanabe, S. and Kunitake, T. : Trans. ISIJ, 16, *1976*, 28
15. Matsuda, S. and Okamura, Y. : Tetsu-to-Hagane, 59, *1973*, 389
16. Watanabe, S., Ohmori, Y. and Kunitake, T. : Proc. 1st JIM Int. Symp. on New Aspects of Martensitic Transformation, Japan, *1976*, 369
17. Ohoka, H. and Suginok, K. : Nihon-Kinzoku-Gakkaishi, 30, *1966*, 435
18. Nemoto, M. : Met. Trans., 8A, *1977*, 431
19. Plichta, M.R. and Aaronson, H.I. : Met. Trans., 5A, *1974*, 2611
20. Kinsman, K.R. and Aaronson, H.I. : Transformation and Hardenability in Steels, Climax Moly. Symp., *1976*, 39
21. Gilmour, J.B., Purdy, G.R. and Kirkaldy, J.S. : Met. Trans., 3A, *1972*, 1455

22. Matsuda, S. : Proc. 1st JIM Int. Symp. on New Aspects of Martensitic Transformation, Japan, *1976*, 363

23. Gracia, C.I. and DeArdo, A.J. : Structure and Properties of Dual-Phase Steels, R.A. Kot and J.W. Morris eds., Metall. Soc. AIME, *1979*, 40

24. Owen, W.S. and Roberts, M.J. : Battelle conference on Dislocation Dynamics, *1968*, McGraw-hill, 357

25. Kelly, P.M. and Kehoe, M. : New Aspects of Martensitic Transformation, JIM Sym., Japan, *1976*, 399

26. Thomas, G. : Met. Trans. 2A, *1971*, 2373

27. Krauss, G. and Marder, A.R. : Met. Trans., 2A, *1971*, 2343

28. Kelly, P.M. and Nutting, J. : Proc. Roy. Soc., A259, *1960*, (A), 45

29. Bell, T. and Owen, W.S. : JISI, 205, *1967*, 428

30. Patterson, R.L. and Wayman, C.M. : Acta Metall., 14, *1966*, 347

31. Marder, A.R. and Krauss, G. : J. Metals, 22, *1970*,9

32. Chilton, J.M. Barton, C.J. and Speich, G.R. : JISI,208, *1970*, 184

33. Speich, G.R. and Swann, P.R. : JISI, 203, *1965*, 480

34. Marder, A.R. and Krauss, G. : Trans. ASM, 69, *1969*, 957

35. Esser, H. Eilender.W. Riedel, K. and Spenler : Arch. Eisenhuettenw, 6, *1933*, 389

36. Das, S.K. and Thomas, G. : Met. Trans., 1, *1970*, 325

37. Leslie, W.C., Stevens, D.W. and Cohen, M. : High Strength Materials, J.Wiley, New York, *1965*, 383

38. Johari, O. and Thomas, G. : Acta Metall., 12, *1964*, 1153

39. Lai, G.Y., Wood, W.E., Clark, R.A., Zackay, V.F. and Parker, E.R. : Met. Trans., 5, *1974*, 1663

40. Bhadeshia, H.K.D.H. and Edmonds, D.V. : Inst. Metall. Conf., No.11, Vol.12, *1979*, iv-9

41. Das, S.K. and Thomas, G. : Trans. ASM, 62,*1969*, 659

42. Huang, D.H. and Thomas, G. : Met. Trans., 2, *1971*, 1587

43. McMahon, J. and Thomas, G. : Third Int. Conf. on Strength of Metals and Alloys, Cambridge, England, *1973*, 180

44. Christian, J.W. : Strengthening Methods in Crystals, ed. A. Kelly and R.B. Nicholson, Elsevier Pub., London, *1971*, 261

45. Winchell, P.G. and Cohen, M. : Electron Microscopy and Strength of Crystals, Interscience, *1963*, 995

46. Winchell, P.G. and Cohen, M. : Trans. ASM, 55, *1962*, 347

47. Roberts, M.J. and Owen, W.S. : JISI, 206, *1968*, 375

48. Jackson. J.K. and Winchell, P.G. : Trans. Met. Soc. AIME, 230, *1964*, 216

49. Swartz, J.C. : Mater. Sci. Eng., 5, *1969*, 30

50. Speich, G.R. : Trans. Met. Soc. AIME, 245, *1969*, 2553

51. Kehoe, M. and Kelly, P.M. : Scripta Met., 4, *1970*, 473

52. Conrad, H., Okasaki, K., Gadgil, V. and Jon, M. : "Electron Microscopy and Structure of Materials", ed. G. Thomas, University of Calif. Press, *1972*, 438

53. Bailon, J.P. and Dorlot, J.M. : Acta Metall., 19, *1971*, 71

54. Evans, J.T. and Rawlings, R. : Mater. Sci. Eng., 4, *1969*, 297

55. Grange, R.A. : Trans. ASM, 59, *1966*, 26

56. Leslie, W.C. and Sober, R.J. : Trans. ASM, 60, *1967*, 99

57. Kelly, P.M. and Nutting, J., JISI, 197, *1961*, 199

58. Gilbert, A. Hahn, G.T., Reid, C. N. and Wilcox, B.A. : Acta Metall. 12, *1964*, 754

59. Bevis, M., Rowlands, P.C. and Acton, A.F. : Trans. TMS-AIME, 242, *1968*, 1555

60. Marder, A.R., Benscoter, A.O. and Krauss, G.: Met. Trans., 1, *1970*, 1545

61. Mazahec, K. and Sejnoha, R. : Trans. AIME, 233, *1965*, 1603

62. Bowen, D.K., Capus, J.M. and Silverstone, C.E. : Phil. Mag., 15,*1967*, 1041

63. Parker, E.R. : Met. Trans., 8A, *1977*, 1025

64. Speich, G.R. : Trans. TMS-AIME, 245, *1969*, 2553

65. Speich, G.R. and Leslie, W.C. : Met. Trans., 3, *1972*, 1043

66. Ino, H., Mouya, T., Fujita, E., Maeda, Y., Oni, Y. and Inokuti, Y: J. Phys. Soc., Japan, 25, *1968*, 88

67. Ansell, G.S., Lizunov, V.I. and Messler, R.W. : Jap. Inst. Metals Spec. Supp., 9, *1968*, 933

68. Galibois, A. and Dube, A. : Can. Met. Quart., 6, *1967*, 21

69. Speich, G.R., Dabkowski, D. and Porter, L.F. : Met. Trans., 4, *1973*, 303-315

70. Honeycombe, R.W.K., Harding, H.J. and Irani, J.T. : High Strength Materials, *1965*, John Wiley, 213

71. Chandhok, V.K., Hirth, J.P. and Dulis, E.J. : Trans. ASM, 56, *1963*, 677

72. Olefjord, I. : Int. Met. Rev., No.4, *1978*, 149

73. Low, J.R. : Fracture of Engineering Materials, ASM, *1959*, Cleveland, Ohio, 127

74. Porter, L.F. : Metallurgical Factors Affecting Toughness, ASM Seminar, *1969*, Houston, Texas

75. Steven, W. and Balajiva, K. : JISI, 193, *1959*, 141

76. Mulford, R.A., McMahon, C.J., Pope, D.P. and Feng, H.C. : Met. Trans., 5, *1974*, 516

77. Low, J.R., Stein, D.F., Turkalo, A.M. and Laforce, R.P. : Trans. AIME, 242, *1968*, 14

78. Joshi, A. and Stein, D.F. : "Temper embritlement of alloy steels", STP 499, 59, *1972*

79. Mclean, D. and Northcott, L. : JISI, 158, *1948*, 169

80. Seah, M.P. and Hondros, E. : Proc. Roy. Soc., 335A, *1973*, 191

81. Ritchie, R.O., Geniets, L.C.E. and Knott, J.F. : "The microstructure and design of alloys", Vol.1, *1973*, Inst. Met. and ISI, London, 124

82. Stephenson, E.T. : J. Met., 26, *1974*, 48,

83. Schulz, B.J. and McMahon Jr, C.J. : "Temper embritlement of alloy steels", STP499, ASTM, Philadelphia, *1972*, 104

84. Capus, J.M. : "Temper embritlement in steel", STP.407, ASTM, Philadelphia, *1968*, 3

85. Guttmann, M. : Surf. Sci., 53, *1975*, 213

86. Guttmann, M., Krahe, P.R, Abel, F., Ansel, G., Bruneaux, M. and Cohen, C. : Met. Trans. 5, *1974*, 167

87. Lement, B.S., Averbach, B.L. and Cohen, M. : Trans ASM, 46, *1954*, 851

88. Hill, R.G.C. and Martin, J.W. : Met. Treatment, 29, *1962*, 301

89. Rellick, J.R. and McMahon, Jr, C.J. : Met. Trans., 5, *1974*, 2439

90. Ohatani, H., Feng, H.C. and McMahon Jr, C.J. : Met. Trans., 5, *1974*, 516

91. Irani, J.J., May M.J. and Elliot, D. :'Temper embrittlement in steel', STP407, ASTM, Philadelphia, *1968*, 168

92. Seah, M.P. : Acta Met., 25, *1977*, 345

93. Carr, F.L., Goldman, M., Jaffe, L.D. and Buffum, D.C. : Trans AIME, 197, *1953*, 998

94. McMahon Jr, C.J., Furubayashi, E., Ohtani, H. and Feng, H.C. : Acta Met. 24, *1976*, 695

95. Pickering, F.P. : symposium by Climax Molybdenum Co. and University of Michigan , *1967*, 109

96. Speich, G.R. and Cohen, M., Trans. TMS-AIME, 218, *1960*, 1050

97. Goodenow, R.H., Matas, S.J. and Hehemann, R.F. : Trans AIME, 227, *1963*, 651

98. Oblak, J.M. and Hehemann, R.F. : Transformation and Hardenability in Steels, Climax Molybdenum Co. of Michigan Symposium, *1967*, 15

99. Irvine, R.J. and Pickering, F.B., Physical Properties of Martensite and Bainite, Iron and Steel Institute, Special Report 93, *1965*, 110

100. Matas, S.J. and Hehemann, Trans. TMS-AIME, 221, *1961*, 179

101. Metallography, Structure, and Phase Diagrams, Vol.8 of Metals Handbook, Am. Soc. for Metals, Metals Park, Ohio, *1973*

102. Thelning, K.E. : Steel and its Heat Treatment, Butterworths, London, *1975*, 7-11

103. Bain, E.C. and Paxton, H.W. : Alloying Elements in Steel, 2nd ed., ASM, *1966*

104. Andrews, K.W. J.I.S.I., 203, *1965*, 721

105. Speich, G.R., Demaresst, V.A. and Miller, R.L. : Met Trans, 12A, *1981*, 1419

106. Kim, N.J. and Thomas, G. : Met. Trans, 12A, *1981*, 483

107. Kelly, A. and Nicholson, R.B. : Strengthening Methods in Crystals; Elsevier Pub., *1971*, p 283 and 332

108. Koo, J.Y. and Thomas, G. : Met. Trans, 8A, *1977*. 525

109. Kuo, K. : JISI, 173, *1953*, 363

110. Walker D.J. and Honeycombe, R.W.K. : Met. Sc. 14, 5, *1980*, 184

111. Shaw, S.W.K. and Quarrell, A.G. : J.I.S.I., 185, *1957*, 10-22

112. Woodhead, J.H. and Quarrell, A.G. : The Role of Carbides in Low-alloy Creep-resisting Steels, Climax Molybdenum Company, P.18 from: Smith, R., Ph.D. thesis, Sheffield University, *1959*

113. Inoue, T. and Kinoshita, S. : Proc. 3rd Int. Conf. on Strength of Metals ans Alloys, Cambridge *1973*, 159

114. Kamoda, J. and McMahon, C.J. : Met. Trans., 11A, *1980*, 91

115. Mulford, R.A. McMahon, C.J. Pope, D.P. Freng, H.C. : Met. Trans., 7A, *1976*, 1269

116. Wada T. and Doane, D.V. : Met. Trans. 5, Jan *1974*, 231

117. Owen, W.S. : Fifth Harold Moore Lecture, Metals Technology, *1980*, 1

118. Marder, A.R. : Met. Trans., 13A, *1982*, 85

119. Davies, R.G. : Met. Trans., 9A, *1978*, 671

120. Bungardt, V.K., Kunze, E. and Horn, E. : Archiv. fur das Eisenhuttenwesen, 29, *1958*, 193

121. Bain, E.C. and Paxton, H.W. : Alloying Elements in Steel, 2nd. ed., ASM, *1966*, P112

122. Thomas, G. and Koo, J.Y. : Structure and Properties of Dual-Phase Steels, R.A. Kot and J.W. Morris eds., TMS-AIME symp., *1979*, 183

123. Cassel Manual, I.C.I. Ltd., 7th ed. , 164

124. Hirsch, P.B., Howie, A., Nicholson R.B., Pashley, D.W. and Whelan, M.J. : Electron Microscopy of Thin Crystals, Butterworths, London, *1965*, 31

125. Smithells, C.J. : Metals Reference Book, Vol 1, London, Butterworths, *1967*

126. Krahe, P.R. and Guttmann, M. : Metallography, 7, *1974*, 5

127. Lawson R.D., Matlock, D. K. and Krauss, G. : Metallography, 13, *1980*, 71

128. Atkinson, M. : Atlas of Continuous Cooling Diagrams for Engineering Steels. British Steel Corporation Ref.No. BBR 867 3m, 12.77 P.144 and 31

129. Bagaryatskii, Yu.A. : Dokl. Akad. Nauk. SSSR, 73, *1950*, 1161

Journal of Materials Science Letters

CHAPMAN AND HALL

Journal of Materials Science Letters is an international publication reporting recent advances in all the major fields of investigation into the properties of materials. Short communications on metallurgy, ceramics, polymers, electrical materials, biomaterials, composites, and fibres appear regularly.

Letters for submission to the *Journal of Materials Science Letters* should be sent to Professor W. Bonfield, Dept. of Materials, Queen Mary College, Mile End Road, London E1 4NS.

Journal of Materials Science Letters is published monthly by Chapman and Hall Ltd., 11 New Fetter Lane, London EC4P 4EE, from whom subscription details are available.

JOURNAL OF MATERIALS SCIENCE LETTERS 1 (1982) 316–317

The heat treatment of En24 steel in the ferrite plus austenite range

S. SABOURY-SICHANY, T. J. BAKER, D. R. F. WEST
Department of Metallurgy and Materials Science, Imperial College of Science and Technology, London SW7 2BP, UK

In recent years, extensive interest has been shown in the heat treatment of low carbon steels in the ferrite plus austenite range to obtain combinations of high strength and formability [1]. Relatively little work has been published on the "intercritical" heat treatment of medium carbon steels. Of particular interest in this context is the work of Nehrenberg [2], who found that fine acicular austenite grains form on heating martensitic or bainitic structures. Subsequently it has been found [3] in a 0.25% C alloy steel that intercritical treatments as compared with conventional hardening treatments can reduce temper embrittlement.

The results reported here form part of an investigation seeking to improve the combinations of strength and toughness of a medium carbon low alloy steel, En24, through the production of an acicular ferrite/martensite duplex structure. The composition of the steel (wt%) was C 0.38, Ni 1.43, Cr 1.21, Mo 0.27, Si 0.26, Mn 0.66, P 0.025, S 0.028, Cu 0.19, Sn 0.006, and V 0.013. Charpy specimens (slightly oversize) were austenitized at 835° C for 1 h in argon and oil quenched. Intercritical treatments, using furnace heating, were then given at temperatures of 735, 750 and 765° C, respectively, with a holding time of 30 min. Specimens were oil quenched and tempering treatments of 1 h were given in the range 200 to 650° C. Machining to final size and notching of the specimens was carried out prior to Charpy testing at room temperature and hardness testing.

Preliminary tests indicated that specimens heat treated at low temperatures in the intercritical range tended to show inferior toughness for a given strength level. However, for the highest intercritical temperature studies (namely 765° C) the data showed a reduced embrittlement trough for tempering in the range ~300 to 450° C. This effect is illustrated in Fig. 1 which represents the Charpy impact data plotted against hardness for conventional and intercritical treatments.

At hardness levels below ~450 H_V, which corresponds to tempering at temperatures greater than about 450° C, the impact values for the conventionally and 765° C intercritically treated conditions appear to be identical. Scanning electron microscopy showed that for both conditions the micromechanism of fracture consisted of microvoid coalescence. For hardness levels between 450 and 550 H_V, the superior toughness of the intercritically treated material is associated with a mainly fibrous fracture mechanism. In the conventionally treated material, the fracture behaviour was dominated by intergranular decohesion. At hardness levels greater than 550 H_V, the toughness of the intercritically treated material is inferior to that of the conventional condition; comparing the fracture mechanisms at a hardness level of about 600 H_V, the intercritically treated material shows mainly a quasi-cleavage mode whereas the conventionally treated material shows a high proportion of fibrous fracture.

The results and their interpretation in relation to kinetics and structural observations are to be reported elsewhere and only a brief summary is given here. As reported above, for a given hardness level, the intercritical treatments studied do not increase the fibrous fracture energy; with treatment in the lower part of the intercritical range toughness is decreased, indicating a deleterious effect of a large volume fraction of ferrite. Various factors contribute to these observed properties; for example, the higher carbon content of the martensite in the intercritically treated material and the finer carbide spacing for a given hardness may lead to a decrease in microvoid spacing and hence reduce the toughness. At the high strength level (H_V 600), the 765° C intercritically material consists of ferrite plus as-quenched, twinned

0261–8028/82/070316–02$02.74/0

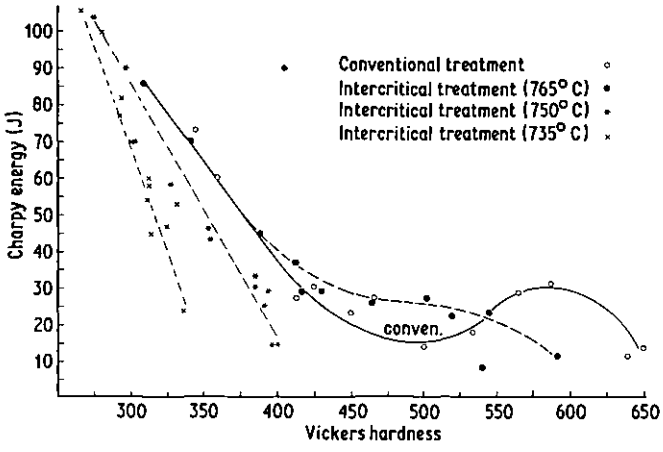

Figure 1 Charpy energy plotted against hardness for En24 steel in the tempered condition after conventional or intercritical treatment.

martensite, which is inherently brittle compared with the tempered, lower carbon content martensite in the conventional condition. Within the 450 to 550 H_V range, the enhanced toughness of intercritically treated material is associated with its resistance to intergranular decohesion. This may be attributed to two main features. Firstly, the presence of the extensive network of martensite–ferrite interfaces and the partitioning of embrittling impurities to the ferrite reduces the concentration of such impurities at prior austenite grain boundaries [3]. Secondly, structural studies made in the present work suggest that carbide precipitation on tempering is delayed in intercritically treated material; thus the carbide size and morphology may be less conducive to fracture initiation.

Acknowledgements

This work was carried out with the support of Procurement Executive, Ministry of Defence.

References

1. W. S. OWEN, *Met. Technol.* 7 (1980) 1.
2. A. E. NEHRENBERG, *Trans. AIME* 188 (1950) 162.
3. T. WADA and D. V. DOANE, *Met. Trans.* 5 (1974) 231.

Received 16 April
and accepted 23 April 1982